Landslide Susceptibility Modeling Using a Machine Learning Algorithm in Halila Catchment, Gamo Zone, Southern Ethiopia.

Mihret Teshome Yami

A Thesis submitted To the Department of Applied Geology

School of Applied Natural Science

Office of Graduate Studies

Adama Science and Technology University

October, 2024

Adama, Ethiopia

Landslide Susceptibility Modeling Using a Machine Learning Algorithm in Halila Catchment, Gamo Zone, Southern Ethiopia.

Mihret Teshome Yami

Advisor: - Shankar Karuppannan (PhD)

A Thesis submitted To the Department of Applied Geology

School of Applied Natural Science

Office of Graduate Studies

Adama Science and Technology University

October, 2024

Adama, Ethiopia

DECLARATION

I hereby declare that this Master Thesis entitled "**Landslide Susceptibility Modeling Using a Machine Learning Algorithm in Halila Catchment, Gamo Zone, and Southern Ethiopia**." is my original work. That is, it has not been submitted for the award of any academic degree, diploma or certificate in any other university. All sources of materials that are used for this thesis have been duly acknowledged through citation.

Mihret Teshome _____ _____

Name of student Signature Date

RECOMMENDATION

I, the advisor of this thesis, hereby certify that I have read the revised version of the thesis entitled "**Landslide Susceptibility Modeling Using a Machine Learning Algorithm in Halila Catchment, Gamo Zone, and Southern Ethiopia.**" prepared under my guidance by **Mihret Teshome Yami**. Submitted in partial fulfillment of the requirements for the degree of Masters of Science in **Engineering Geology.** Therefore, I recommend the submission of a revised version of the thesis to the department following the applicable procedures.

Shankar Karuppannan (PhD) _____ _____

Major Advisor Signature Date

APPROVAL PAGE

I, the advisor of the thesis entitled "**Landslide Susceptibility Modeling Using a Machine Learning Algorithm in Halila Catchment, Gamo Zone, and Southern Ethiopia.**" developed by Mihret Teshome Yami hereby certify that the recommendation and suggestions made by the board of examiners are appropriately incorporated into the final version of the thesis.

Shankar Karuppannan (PhD) _____ _____

Major Advisor Signature Date

We, the undersigned, members of the Board of Examiners of the thesis by **Mihret Teshome Yami** have read and evaluated the thesis entitled "**Landslide Susceptibility Modeling Using a Machine Learning Algorithm in Halila Catchment, Gamo Zone, Southern Ethiopia.**" and examined the candidate during open defense. This is, therefore, to certify that the thesis is accepted for partial fulfillment of the requirement of the degree of Master of Science in Engineering Geology.

_____	_____	_____
Chairperson	**Signature**	**Date**
_____	_____	_____
Internal Examiner	**Signature**	**Date**
_____	_____	_____
External Examiner	**Signature**	**Date**

Final approval and acceptance of the thesis is contingent upon submission of its final copy to the Office of Postgraduate Studies (OPGS) through the Department Graduate Council (DGC) and School Graduate Committee (SGC).

_____	_____	_____
Department Head	**Signature**	**Date**
_____	_____	_____
School Dean	**Signature**	**Date**
_____	_____	_____
Office of Postgraduate Studies, Dean	**Signature**	**Date**

ACKNOWLEDGMENT

First and foremost, I express my deepest gratitude to the Almighty God for guiding me through every step of this journey. I extend my sincere appreciation to my esteemed advisor, Dr. Shankar Karuppanan, Associate Professor at Department of Applied Geology (SoANS), Adama Science and Technology University (ASTU), for his invaluable guidance, and insightful feedback throughout the research process. His expertise and encouragement have been instrumental in shaping this thesis. I am particularly grateful to him for providing me with an online course that significantly enhanced my understanding and skills, further contributing to the success of this research.

I am profoundly grateful to Mr. Teshome Yami, my father, for his unwavering financial support from the inception to the culmination of this endeavor. His beliefs in my abilities and his constant encouragement have been my pillars of strength.

I extend my heartfelt thanks to the National Meteorological Agency of Ethiopia (NMAE), and the Geological Institute of Ethiopia (GIE), for their generous provision of meteorological data, geological maps, and soil maps, respectively.

I extend my deepest gratitude to my family, whose unwavering love, understanding, and encouragement have fueled my motivation. In particular, I am profoundly thankful to my families, Aberash Kefyalew, Nazrawit Teshome, and, Kaleb Melkamu, for their constant encouragement. I want to take a moment to express gratitude towards myself for the dedication, and hard work I have invested in this thesis.

Lastly, I extend my heartfelt appreciation to all my friends and staff of the Geology department. This thesis would not have been possible without the collective support and encouragement of these individuals and organizations. Thank you all for being an integral part of this experience.

TABLE OF CONTENTS

Contents **Pages**

LIST OF TABLES ..... **viii**
LIST OF FIGURES ..... **ix**
LIST OF ACRONYMS AND ABBREVIATIONS ..... **x**
ABSTRACT ..... **xi**
CHAPTER ONE **1**
1. INTRODUCTION **1**
1.1 Background of the study 1
1.2 Statement of the problem 3
1.3 Objective 4
1.3.1 General objective 4
1.3.2 Specific objectives 4
1.4 Significance of the study 4
1.5 Scope of the study 5
1.6 Limitations 5
1.7 Organization of the Thesis 6
CHAPTER TWO **7**
2. LITERATURE REVIEW **7**
2.1 Landslide 7
2.2 Types of landslides 8
2.3 Landslide Factors 9
2.3.1 Topographic factors 9
2.3.2 Geological Factors 10
2.3.3 Hydrological Factors 11
2.3.4 Environmental (Human use factor) 11
2.4 Landslide in Ethiopia Highlands 12
2.5 Landslides and its triggering factors in Gamo Highland, South Ethiopia 14
2.6 Landslide analysis technique by using Machine learning Algorithms 14
2.7 Common Machine Learning Algorithms for Landslide Analysis 15
CHAPTER THREE **17**
3. STUDY AREA **17**
3.1 Description of the study area 17

3.2 Physiography 18
3.3 Rainfall Pattern and Climatic Condition 18
3.4 Drainage pattern of the study area 20
3.5 Geology of the Study Area 21
3.5.1 Southern Ethiopian Shield 22
3.5.2 Pre-rift volcanic and sedimentary units 24
3.5.3 Early-Rift volcanic deposits 25
3.4.4 Late-Rift volcanic deposits 26
3.6 Soil types of the study area 26
3.7 Seismicity of the Study Area 29
CHAPTER FOUR 31
4. METHODOLOGY 31
4.1 Softwares 31
4.2 Data collection 31
4.2.1 Primary data 31
4.2.2 Secondary data 31
4.3 Data analysis 32
4.4 Methods 33
4.4.1 Random Forest 33
4.4.2 Support Vector Machine 34
CHAPTER FIVE 37
5. RESULTS AND DISCUSSION 37
5.1 Landslide Inventory map 37
5.2 Landslide causative factor maps 38
5.2.1 Aspect 39
5.2.2 Curvature 39
5.2.3 Elevation 41
5.2.4 Slope 41
5.2.5 Distance to Lineament 43
5.2.6 Distance to Stream 43
5.2.7 Lithology 45
5.2.8 Rainfall 45
5.2.9 Soil type 45

5.2.10 Land Use Land Cover 48
5.3 Multicollinearity analysis 49
5.3.1 Tolerance 49
5.3.2 Variance Inflation Factor (VIF) 49
5.4 Rating Landslide Factors Using Information Value Method 51
5.4.1 Information value 51
5.5 Relationship between landslide and causative factor 55
5.6 Landslide Susceptibility Mapping 58
5.6.1 Landslide Susceptibility Mapping Using SVM 59
5.6.2 Landslide Susceptibility Mapping Using RF 60
5.7 Validation of the models 62
5.8 Area under the Curve (AUC) 62
5.8.1 Success and Predictive Rate Curve 62
CHAPTER SIX 64
6. CONCLUSIONS AND RECOMMENDATION 64
6.1 Conclusions 64
6.2 Recommendations 64
APPENDIX **72**

LIST OF TABLES

Table 1: Slope movement classification 8
Table 2: Data type and sources 32
Table 3: Collinearity diagnostic results of influence factors 51
Table 4: Landslide susceptibility class of SVM and RF model..... 52
Table 5: Rating of factor classes from a spatial relationship between each factor class and landslide using information value model..... 54
Table 6: Factors influencing rank based on their mean information values……..…… 61

LIST OF FIGURES

Figure 1: Locations of landslide-affected areas in the highlands of Ethiopia Ayalew. 13
Figure 2: Location map of the study area 17
Figure 3: Physiographic map of the study area 18
Figure 4: Annual rainfall distribution and maximum rainy months of the study area..... 19
Figure 5: Drainage Map of the study area 21
Figure 6: Geology map of the study area 22
Figure 7: Soil map of the study area 27
Figure 8: Seismic zone map of Ethiopia 30
Figure 9: Flow chart of the research methodology 36
Figure 10: Landslide inventory map of the study area with landslide and non-landslide events. 38
Figure 11: Landslide causative factor maps: (a) Aspect, (b) Curvature Map. 40
Figure 12: Landslide causative factor maps: (a) Elevation, (b) Slope Map 42
Figure 13: Landslide causative factor maps: (a) Distance to lineament, (b) Distance to Stream Map 44
Figure 14: Landslide causative factor maps: (a) Lithology, (b) Annual Rainfall, (c) Soil Map 47
Figure 15: Landslide causative factor map: (A) Land Use Land Cover 48
Figure 16: Landslide susceptibility map using SVM 56
Figure 17: Landslide susceptibility map using RF 60
Figure 18: Success and predictive rate of SVM and RF 61
Figure 19: Relationship of landslide occurrence with the causative factors 63

LIST OF ACRONYMS AND ABBREVIATIONS

MER - Main Ethiopian Rift

GIS - Geographical Information System

ML - Machine Learning

SVM - Support Vector Machine

RF - Random Forest

LULC - Land Use Land Cover

LSM - Landslide Susceptibility Map

EBCS - Ethiopian Building Code Standard

DEM - Digital Elevation Model

ASTER - Advanced Spaceborne Thermal Emission and Reflection Radiometer

NASA - National Aeronautics and Space Administration

NMAE - National Meteorological Agency of Ethiopia

IDW - Inverse Distance Weighted Interpolation

GIE - Geological Institute of Ethiopia

DTS - Distance to Stream

DTL - Distance to Lineament

AUC - Area under Curve

ROC - Curve Receiver Operating Characteristic Curve

VIF - Variance Inflation Factor

TOL – Tolerance

IV- Information value

ABSTRACT

Landslides are major disasters causing significant property damage and loss of life. This study focuses on identifying the areas most vulnerable to landslides and the key factors contributing to landslides in the Halila catchment of the Gamo zone using machine learning algorithms. The primary goal was to determine the causative factors and develop landslide susceptibility maps using support vector machine (SVM) and random forest (RF) algorithms. Based on Google Earth imagery, approximately 302 landslides were identified and randomly divided into training (70%) and validation (30%) datasets within the ArcGIS environment. Ten landslide-related factors were selected: slope, aspect, curvature, distance from streams, and distance from lineaments, lithology, land use/land cover, soil type, elevation, and rainfall. The resulting landslide susceptibility maps were classified into very low, low, moderate, high, and very high susceptibility classes using both support vector machine and random forest. These maps were validated using the receiver operating characteristic (ROC) curve; with the area under the curve (AUC), the results indicate that the SVM model achieved a success rate of 0.816 and a predictive rate of 0.809. In comparison, the Random Forest (RF) model demonstrated slightly better performance with a success rate of 0.821 and a predictive rate of 0.811. To mitigate the impact of landslides, recommendations include implementing strict land-use planning and zoning regulations, enforcing and updating building codes, stabilizing vegetation and slopes, and installing effective drainage systems.

***Keywords**: landslide susceptibility, machine learning, support vector machine, random forest, Halila catchment.*

CHAPTER ONE

1. INTRODUCTION

1.1 Background of the study

Professionals such as geologists and engineers frequently have different definitions of landslides. The diversity of terminology reflects the multiplicity of disciplines involved in the study of landslide phenomena. "landslide" refers to the general phrase for the downslope movement of soil, rock, and organic materials caused by gravity as well as the resulting land shape (Highland and Bobrowsky, 2008). Moreover, it represents a constant threat to infrastructures and the lives of people, drawing attention on a global scale because of its considerable socioeconomic effects and the difficulties it creates for urbanization and development projects in hilly areas (Varnes, 1978). Communities living in mountainous areas could be vulnerable to a range of geo-environmental drives such as geological, meteorological, and human conditions. The primary causes affecting landslides. most significant inherent elements are the bedrock geology (slope gradient, aspect, relative relief), soil (depth, structure, permeability, and porosity), land use/cover, and hydrologic conditions. Local factors that affect landslide triggers include relative relief, closeness to drainage, and proximity to a lineament. Moreover, numerous extrinsic factors, including earthquakes, drilling and blasting, storms and sudden floods can cause landslides (Anbalagan et al., 2015).

In Africa, particularly in Ethiopia, landslides have emerged as a critical environmental challenge, hindering urbanization, infrastructure projects and activities conducted on or near slopes. The adverse effects have been notably felt in various regions including the northern, northwestern, central, southern, southwestern and rift escarpments of Ethiopia (Woldearegay et al., 2006).

Ethiopia has experienced substantial losses due to landslides, with documented instances; such as the period from 1993 to 1998, witnessing the destruction of homes, interruptions in road networks, and loss of lives (Ayalew, 1999). The complex interplay of geomorphological, hydrological, geological factors, active geodynamic processes, and unplanned land use practices in these regions contributes to the heightened susceptibility to landslides (Woldearegay, 2014).

Recently, a series of devastating landslides have occurred, causing widespread destruction and loss of life. In Kafa Deche, a family tragically lost their lives when a landslide struck, also blocking the vital asphalt road connecting Telo to Bonga. In Sidama Wensho, another deadly landslide claimed the lives of nine people and injured six others. In Dese Arada, a landslide destroyed a mosque and severely disrupted daily life by blocking critical roads. The Bonga to Kontana Road was rendered impassable due to a landslide, while a massive landslide in Sekota blocked a major artery connecting the city to neighboring areas. In Northern Gondar, Telemt, a sudden landslide killed more than ten people, injured eight others, and caused significant agricultural and livestock losses, with over 35 domestic animals perishing, crops on more than 30 hectares being destroyed, and over 2,400 people displaced.

The southern Ethiopian highland, has witnessed a concerning rise in landslide incidents in recent years, necessitating focused research and investigation. The south Ethiopia region's vulnerability to landslides is exacerbated by its topography, characterized by steep slopes formed on highly weathered basalts and ignimbrites. Intrinsic factors, such as slope geometry, material, structural discontinuities, land use, and groundwater conditions, along with external influences like rainfall and human activities, contribute to the heightened risk of slope instability in this area (Oyda et al., 2023).

For instance recently, in the Gofa Zone, Geze Gofa Woreda, Kencho Shacha Gozdi Kebele, a sudden and devastating landslide tragically claimed the lives of approximately 250 people. In the context of the Gamo Zone in southern Ethiopia, a comprehensive understanding of landslide triggers and susceptibility is vital for effective risk reduction and environmental management. This research focuses on employing remote sensing technology to assess and monitor critical factors influencing landslide hazards in the region. The study aims to evaluate and delineate landslide hazard-prone areas through susceptibility mapping techniques, considering factors such as slope, aspect, curvature, elevation, geological units, groundwater, land use/cover, stream erosion, and proximity to lineaments. The primary trigger identified is heavy rainfall, with recorded monthly and yearly rainfall ranges providing critical data for the assessment (Fisiche and Laterina, 2018; Oyda et al., 2023).

A pivotal aspect of landslide research involves pre- and post-disaster studies, specifically focusing on pre-disaster activities such as landslide susceptibility mapping. This spatial

prediction technique enables the identification of probable landslide zones and assesses the safety levels of current habitations. The effectiveness of maps lies in their ability to inform strategic planning and development initiatives in hilly areas, offering valuable insights into the environmental stability of a region (Kanungo et al., 2011).

It is essential to identify and map the areas that are prone to landslides to reduce the impact of the hazard (Girma et al., 2015). It is possible to prevent at least 90% of landslide losses if the issue is identified before the occurrence. Furthermore, the research and mapping of landslide-prone can provide valuable evidence for reducing catastrophic damage and help with feasible land-use planning (Chen and Wang, 2007). This may suggest that mapping landslide susceptibility is a crucial stage in landslide research and risk mitigation.

By generating a landslide inventory map from historical and current records, analyzing causative factors, and utilizing machine learning algorithms, this research aims to provide a comprehensive susceptibility assessment. Ultimately, the findings are intended to guide remedial and mitigation efforts, contributing to the reduction of landslide risks and supporting safer land-use planning in the region.

1.2 Statement of the problem

Landslides pose a serious and frequent threat to the south Ethiopia region, especially in the Gamo Zone and the Main Ethiopian Rift (MER). The region's geological features—which are impacted by tectonics, active continental rifting, lithology, and geomorphology—raise the possibility of slope instability. This risk is further increased by creating and reactivating faults caused by shifting stress fields. Due to the region's difficult topography, flimsy geological formations, and twice-yearly heavy precipitation, landslides can occur often and have a detrimental effect on infrastructure and agriculture (Martínek et al., 2021; Shano et al., 2021; Addis, 2023).

In southern Ethiopia, landslides have disastrous effects that include damage to infrastructure, buildings and agricultural land in addition to deaths and the burial of homes, roads and villages. Furthermore, the heightened seasonality of precipitation patterns is a common initiator of landslides, resulting in the evacuation of residents from their houses. There is still much to learn

about and do to fully address these landslide-related challenges, even with the research done in the study area and other highland parts of Ethiopia.

It is critically necessary to generate essential data through landslide susceptibility mapping, forecasting, and monitoring to inform both the government and the local population about the geographic likelihood of landslides since there is an absence of studies utilizing machine learning methods to comprehend and map factors contributing to landslide susceptibility in the study area. Machine learning techniques offer a more dynamic and nuanced approach unlike traditional statistical methods, which may fall short of capturing complex relationships. It is especially important to incorporate machine learning techniques into landslide susceptibility mapping to evaluate varied datasets and find intricate patterns and linkages.

1.3 Objective

1.3.1 General objective

The general objective of this study is to identify the causative factors and prepare the landslide susceptibility maps of the study area using a support vector machine and random forest methods with GIS techniques.

1.3.2 Specific objectives

- ✓ Generating landslide inventory map by using historical and current landslide records.
- ✓ To prepare a landslide susceptibility map of the study area using a Machine learning algorithm.
- ✓ To suggest remedial actions to reduce the risk of landslides.

1.4 Significance of the study

Landslides present serious threats to project infrastructure, particularly to newly constructed roads and railways situated on steep hills. The resulting delays may result in serious hold-ups, financial damage and in some instances, death of individuals. Furthermore, houses, bridges, and utility networks could sustain significant damage as a result of landslides. Repairing such damaged infrastructure is expensive and time-consuming, and it also leads to environmental changes such as soil erosion and sedimentation in rivers. The identification of landslide-prone areas is made easier by a susceptibility map unique to the research area. This map provides vital

information for early danger alerts which can reduce the number of casualties, injuries, suffering and environmental damage.

Susceptibility mapping is an important method for reducing the hazards associated with landslides since it gives important information about regions vulnerable to these types of natural disasters. Authorities can reduce potential damage and protect people and property by identifying landslide-prone areas and implementing targeted preventive measures such as early warning systems, infrastructure reinforcement and land-use planning. Susceptibility maps are also essential for strategically planning next-generation development initiatives, such as determining where to put towns, farms and roads. With the use of this data, administrations at the local, zonal, regional, and federal levels can prioritize environmental sustainability and the safety of people living in high-risk locations when making decisions about land use.

Additionally, since machine learning algorithms (SVM and RF) have not been applied in the region, this research can provide information about applying machine learning algorithms for landslide susceptibility mapping. Researchers' capacity to identify and map the area's landslide susceptibility will also be strengthened.

1.5 Scope of the study

The present study was conducted in the Halila catchment at Gamo Zone of the south Ethiopia Region. An analysis of landslide susceptibility was carried out utilizing GIS techniques in conjunction with support vector machines and random forests and developed for local scale by considering ten parameters for the landslide susceptibility mapping.

1.6 Limitations

The main challenge of this research was the limited time available for field observation of landslides due to the lengthy duration of an online machine-learning class. The winter season exacerbated the difficulty of fieldwork with intense rainfall, making it nearly impossible, and there were safety concerns due to recent landslide incidents in the Gamo zone. Moreover, acquiring time-series images to pinpoint the timing and causes of the landslides proved to be quite difficult. The discontinuous data obtained from the National Meteorological Agency of Ethiopia (NMAE) further complicated the task as finding stations near the study area was a significant hurdle.

1.7 Organization of the Thesis

The study is structured into six comprehensive chapters. Chapter One introduces the topic of landslides, presenting the study's problem statement, objectives, significance, scope and limitations. Chapter Two reviews the literature, examining general factors contributing to landslides, their impact in Ethiopia and in Gamo and the application of machine learning algorithms in landslide analysis. Chapter Three provides an overview of the study area, describing its location, accessibility, physiography, climate, geology, soil types and seismic activity. Chapter Four details the methodology, encompassing methods, data collection procedures and data analysis techniques. Chapter Five presents the results and discussion, including the relationship between triggering factors and landslides, analyzing correlation relationships, and preparing the final landslide susceptibility maps. The final chapter, Chapter Six, summarizes the research findings, presents conclusions and recommendations based on the study's outcomes.

CHAPTER TWO

2. LITERATURE REVIEW

2.1 Landslide

A landslide is a broad term that refers to the movement of soil, rock and organic materials downslope due to gravity that results in a unique landform. Different classifications of landslides are associated with specific mechanisms of slope failure and characteristics of various failure types. geologists and engineers often define landslides in slightly different ways. The variety of definitions reflects the multitude of disciplines involved in the study of landslip occurrences (Highland and Bobrowsky, 2008).

Landslides are complex events driven by friction, water, and gravity. Materials are pushed downward by gravity by overcoming its internal strength and friction. Water increases the likelihood of landslides by weakening material strength, reducing friction and increasing gravitational force, especially during wet seasons (Washington State Dept of Natural Resources, 2017). Landslides can happen in places with typically low relief, even though they are usually connected to steep slopes. Friction is important and is affected by surface changes and slope steepness. Because steeper slopes produce less friction, the risk of a landslide increases. River cutting and human activity are two examples of changes that might worsen slope dynamics and demonstrate how complex landslides can be (USGS, 2004).

According to Agrawal and Dixit (2023), landslides are one of the most common geological risks, particularly in mountainous areas. These events change the landscape and pose significant risks to critical infrastructure, including gas or oil pipelines, transportation networks, and electricity transmission lines. In this process, surface water penetration, river erosion, seismic activity, human activity, and other variables cause the rock-soil mass on a side slope to slide down the weak surface as a whole or dispersedly under the effect of gravity.

Landslide susceptibility is the likelihood of a landslide event occurring based only on the problem's spatial size. Predicting the spatial distribution of landslides is, by far, the most researched topic, according to Agrawal and Dixit (2023) the international scientific community

has spent the last thirty years working to create practical methods for anticipating and reducing the harmful consequences of landslides (Ajayi et al., 2016).

2.2 Types of landslides

According to Varnes (1978), Landslides are categorized according to the types of material (rock, earth, soil, mud, and debris), how they move (fall, topple, slide, spread, flow), and the complicated classes of movements, which entail two or more separate modes of movement acting on the landslide mass's downslope movement as shown in Table 1. Falls occur when large rocks break away from cliffs due to gravity and other factors. Toppling involves the forward rotation of units influenced by gravity and adjacent forces. Slides, like landslides, involve clear zones of weakness separating materials. Lateral spreads result from the liquefaction of sediments during earthquakes, causing abrupt movements. Flows include debris flows, avalanches, earth flows, mudflows, and creep, driven by friction, water, and gravity. Complex landslides combine multiple processes, posing challenges for assessment and mitigation strategies, which are crucial for risk management (Cruden and Varnes, 1996).

Table 1: Slope movement classification (Varnes, 1978).

<table>
<tr><th colspan="2" rowspan="3">Types of Movement</th><th colspan="3">Types of Material</th></tr>
<tr><th rowspan="2">BEDROCK</th><th colspan="2">ENGINEERING SOILS</th></tr>
<tr><th>Predominantly Coarse</th><th>Predominantly Fine</th></tr>
<tr><td colspan="2">FALLS</td><td>Rockfall</td><td>Debris fall</td><td>Earth fall</td></tr>
<tr><td colspan="2">TOPPLES</td><td>Rock topples</td><td>Debris topple</td><td>Earth topples</td></tr>
<tr><td rowspan="2">SLIDES</td><td>ROTATIONAL</td><td rowspan="2">Rock slide</td><td rowspan="2">Debris slide</td><td rowspan="2">Earth slide</td></tr>
<tr><td>TRANSLATIONAL</td></tr>
<tr><td colspan="2">LATERAL SPREADS</td><td>Rock spread</td><td>Debris spread</td><td>Earth spread</td></tr>
<tr><td colspan="2" rowspan="2">FLOWS</td><td rowspan="2">Rock flow (Deep creep)</td><td>Debris flow</td><td>Earth flow</td></tr>
<tr><td colspan="2">(Soil creep)</td></tr>
<tr><td colspan="2">COMPLEX</td><td colspan="3">Combination of two or more types of movement</td></tr>
</table>

2.3 Landslide Factors

There must be an external factor that changes the natural nature of the land in some way for landslides to happen. The parameters that cause the landslide are referred to as causative factors, and they may be intrinsic or extrinsic. Changes in the environment brought on by humans as well as natural causes can cause landslides (Varnes and IAEG, 1984). It's crucial to differentiate between triggering and causal elements in slope instability. Causative elements, which include slope geometry, soil characteristics, geological features, vegetation cover, water content, and human activities like excavation or construction, predispose a slope to movement by establishing conditions that make it prone to instability. However, slope movement is brought about by triggers, which cause the slope to transition from a slightly stable to an actively unstable state. These elements include significant precipitation, seismic activity, vibrations caused by people, shifting groundwater levels, and erosion some of the elements that contribute to landslides are as follows (Popescu, 2002; Highland and Bobrowsky, 2008).

2.3.1 Topographic factors

2.3.1.1 Slope

The passage of water and the formation of soil is significantly impacted by slope, which refers to the steepness or angle of the land. Shear stress occurs in the material on steeper slopes, increasing the material's vulnerability to failure and the likelihood of landslide incidents. Because of the increasing gravitational forces acting on the slope material, an area is essentially more vulnerable to collapse and landslide disasters the larger the slope angle (Yuan et al., 2022).

2.3.1.2 Elevation

Elevation has a significant impact on weathering processes and the formation of the landscape. Higher elevations are frequently subjected to harsher weather, accelerating erosion and eventually deteriorating slope material. Because of this increased weathering, slopes may become less stable and more vulnerable to failure and landslide incidents. Elevation also affects the topography of a region, which influences drainage patterns and the distribution of stresses in the ground, increasing the risk of slope failure. Elevation is a major causal component in defining a landscape's vulnerability to slope instability and the ensuing landslide events (Hammad Khaliq et al., 2023).

2.3.1.3 Aspect

The term "aspect" describes the compass direction that a slope faces and has a major impact on the distribution of solar radiation and climatic fluctuations. Varied slope aspects see varied levels of sunlight and variations in temperature and moisture content during the day. Variations in temperature and moisture content can cause varying rates of expansion, contraction, and weathering within the slope material, which can impact the slope stability. As a result, slopes with opposing features could show varying vulnerabilities to collapse and landslides, with slopes facing particular directions being more unstable based on the weather at the time (Raghuvanshi et al., 2014).

2.3.1.4 Curvature

The shape or geometry of the slope surface is referred to as curvature, and it plays a crucial role in the occurrence of landslides. Negative curvature values indicate concave slopes, and convex slopes are shown by positive values. Concave slopes tend to gather material, whereas convex slopes may shed material more rapidly. The curvature of the slope surface affects how pressures are distributed across the terrain. Hill stability may also be impacted by how water flows off the hill due to the surface curvature. Because of the way the terrain is shaped, effects like erosion and gravity pulling on the slope material can be amplified, making pronouncedly curved slopes more prone to landslides. As a result, determining a slope's curvature is crucial to determining its instability and reducing the likelihood of landslides (Khaliq et al., 2023).

2.3.2 Geological Factors

2.3.2.1 Lithology

The geological structure of the rock and soil that makes up a slope and determines its susceptibility to landslides and slope failure is known as lithology. Different reactions to external factors like gravity, water infiltration, and seismic activity are caused by variations in lithology. In contrast to firmer, more resistant rock or cohesive soil, softer, weathered rock or loose soil may show lower shear strengths, increasing the danger of collapse. An understanding of lithological factors is essential to determine slope stability and landslide susceptibility and inform efficient risk assessment and mitigation techniques (Hussain et al., 2022).

2.3.2.2 Distance to Fault

Slope stability is greatly impacted by geological features such as bedding planes, shear zones, joints, faults, and folds. These features are referred to as the slope's "distance to the fault." Due to the increased risk of structural weaknesses and geological instability, slopes closer to these characteristics are more prone to landslides. A slope's instability may be made worse by faults or lineaments nearby, which can provide weak spots where rocks are more likely to fracture or slide. Slope collapse risk can be further increased by reducing a rock's overall strength due to the number of joints in the rock. To evaluate the risk of landslides, it is necessary to know how far away faults and other geological formations are (Manderso, 2021).

2.3.3 Hydrological Factors

Long-term, intense rainfall is a major cause of landslides and a major trigger component in dynamic landslide susceptibility models. Different earth minerals respond differently to water. For example, surface tension causes dry sand to become more stable when water is introduced, increasing cohesiveness and the angle of repose. On the other hand, too much water can saturate the soil, which weakens its shear strength and allows the material to flow. In mountainous terrain, groundwater movement usually follows discontinuities in the rock, making consistent assessment difficult. Therefore, surface indicators such as moisture, wetness, and flow are essential for quickly assessing groundwater behavior and slope stability for susceptibility mapping (Anbalagan, 2008).

2.3.4 Environmental (Human use factor)

2.3.4.1 Land use Land cover

Slopes become unstable due to changes in their hydrological state brought about by changes in land cover. The spatial distribution of landslides is influenced by changes in land cover in addition to other conditioning factors. In addition to its effects on surface runoff, soil moisture, groundwater behavior, and slope stability for susceptibility mapping, the type of land use also indirectly affects the development of landslides and collapses (Manderso, 2021).

2.3.4.2 Seismicity

One of the environmental factors that causes landslides to occur is seismicity. Previously stable slopes could fall due to the vibrations produced by earthquakes. The ground's shaking, not the earthquake's actual magnitude, determines the likelihood that a landslide event would be caused.

Water can be discharged when an earthquake causes the soil skeleton to shift, which then causes vibrations to be released. The water's increased pressure carries a portion of the soil skeleton at that point. We call this phenomenon liquefaction (Raghuvanshi et al., 2014).

2.3.4.3 Man-made Factors

Slope instability in mountainous areas can be caused by human activities such as farming, construction, and development projects that change the moisture content and structure of the soil. Construction-related operations, including terracing, building roads, and mining, can alter slope angles and decrease support, while groundwater changes and irrigation impact erosion and drainage. Slopes can be weakened by increases in pore-water pressure caused by groundwater variations, such as reservoir drawdowns or lawn irrigation. On the other hand, because of decreased buoyancy, quick groundwater drawdowns can potentially cause failure (Long, 2008).

2.4 Landslide in Ethiopia Highlands

Ethiopia's landmass is divided mostly into lowlands and highlands. According to the Food and Agriculture Organization of the United Nations (1986), the highlands of Ethiopia, which include areas higher than 1500 meters above sea level, make up around 44% of the nation's entire land area. These highlands are the most heavily populated areas, home to over 60% of the population. Figure 1shows locations of landslide-affected regions of the highlands of Ethiopia.

The hilly terrains of the Ethiopian landmass has been affected by both new and reactivated ancient landslides due to its complex and rugged topography and a variety of contributing factors, including clayey horizons, tectonic fractures, faults, volcanic outcrops and colluvial-alluvial deposits geomorphological, hydrological and geological setting (Ayalew, 1999; Abebe et al., 2010).

In Ethiopia, landslide susceptibility, hazard, and risk have received little attention despite the obvious danger. This highlights the need for greater awareness and action in potentially unstable locations. Over the previous 50 years, historical data showed that there have been about 106 landslide incidences in Ethiopia's highlands. Significantly, disastrous occurrences occurred in 1977, 1979, 1988 and 1994 highlighting the serious and ongoing landslide problems in the area. These events have resulted in considerable losses in people and infrastructure, underscoring the

urgent need for preventative actions to address and lessen the effects of landslides in this geographically sensitive area (Woldearegay, 2013; Vařilová et al., 2015).

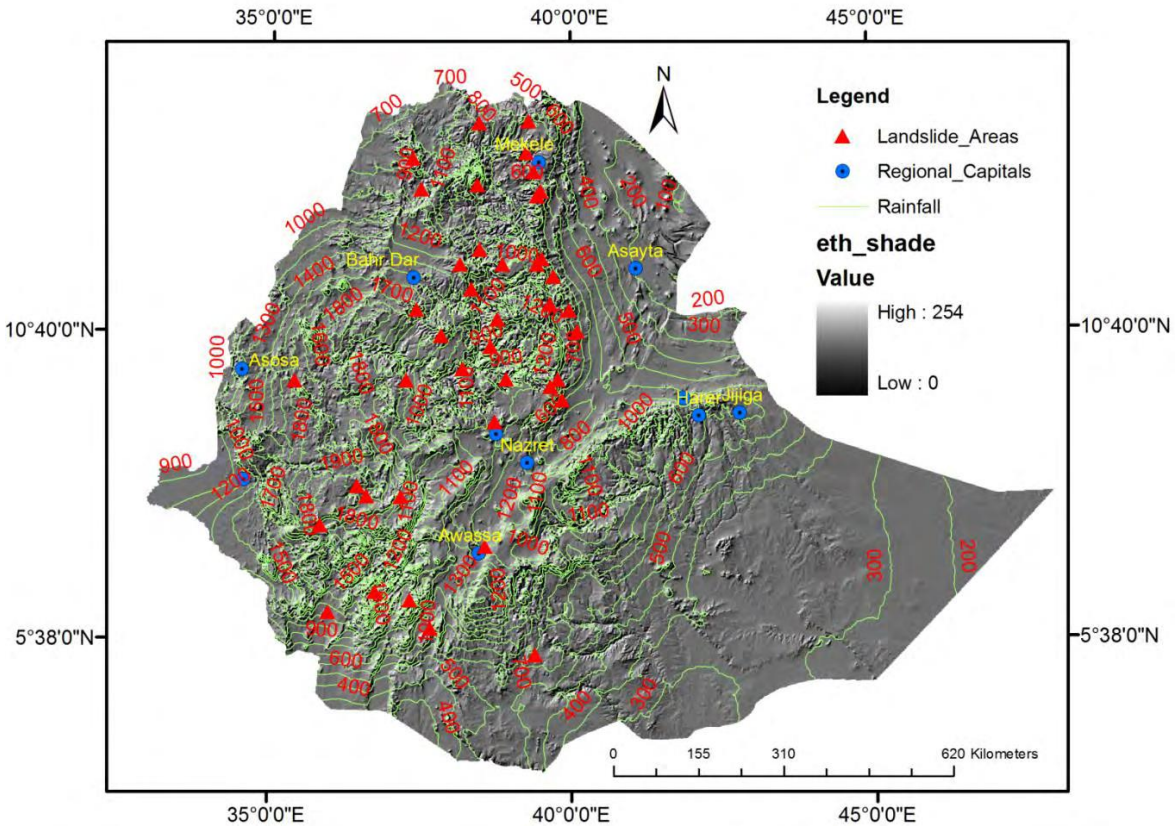

Figure 1: Locations of landslide-affected areas in the highlands of Ethiopia (Woldearegay, 2003).

In many parts of Ethiopia, landslides are a common geohazard with distinct consequences and concerns. Diverse mass movements in the northern region, particularly in places like the Blue Nile Gorge, pose serious risks to infrastructure and human life, including rock falls and earth slides. Significant events have also occurred in the Eastern region, such as the flooding and landslides in East Wollega in 2020, highlighting the dynamic character of landslides and the necessity of ongoing monitoring. In the western portion, landslides are caused by steep erosional slopes and heavy precipitation, especially along the Blue Nile River and its tributaries. Rugged terrain and dense population increase the risk of landslides in the Central Highlands, where few safe places are present despite the catastrophic effects on infrastructure and human lives. Steep

slopes, active fault escarpments and deforestation increase the susceptibility of landslides in the southern part of Ethiopia. This highlights the complex relationship between natural and human factors in landslide occurrence and mitigation measures in Ethiopia (Abebe et al., 2010; Ajayi et al., 2016; Amare et al., 2018; OCHA, 2020; Mebrahtu et al., 2021; Martínek et al., 2021).

2.5 Landslides and its triggering factors in Gamo Highland, South Ethiopia

Landslide susceptibility mapping is crucial for environmental planning and risk mitigation in the Gamo Zone of southern Ethiopia. Conditioning factors include slope, aspect, curvature, elevation, geological units, groundwater, land use/cover, stream erosion, and proximity to lineaments. Heavy rainfall is the primary trigger, with recorded monthly and yearly rainfall ranging from 35 to 180 mm and 580 to 2400 mm, respectively. This understanding will help in effective strategies for risk reduction and environmental management in the Gamo Zone. Steep slopes on weathered basalts and ignimbrites in the area result in frequent landslides driven by intrinsic factors like slope geometry, material, structural discontinuities, land use and groundwater conditions. External influences include rainfall and human activities such as deforestation and road construction. Landslide hazards are categorized into high, moderate, and low zones in the Gamo Zone of southern Ethiopia. The central and northeast parts are high-hazard zones due to agriculture and human interventions, while the southern area pose moderate risks. The west and northwest regions are labeled low-hazard zones (Fisiche and Laterina, 2018; Shano et al., 2021; Sci et al., 2023).

2.6 Landslide analysis technique by using Machine learning Algorithms

The study of pattern recognition and computational learning theory is included in machine learning, a subset of artificial intelligence. It includes techniques and algorithms designed to let computer systems learn from given data to draw conclusions and make forecasts (Hertzmann and Fleet, 2012). Machine learning is one of the many innovations people have created throughout history to make activities easier (Mahesh, 2019). Certain Algorithms for Machine Learning language implementation tools include Rapidminer, Matlab, Python, and R (Shanthamallu and Spanias, 2022).

Machine learning systems can be divided into multiple types based on their training approaches. While classification places data into pre-determined categories and regression predicts

continuous values, supervised learning trains a model to predict a target variable by identifying patterns in labeled data (Honavar and De La Higuera, 2001). Unsupervised learning, which is frequently applied to clustering or dimensionality reduction tasks, on the other hand, seeks to find patterns or structures in data without labeled results (Abdi, 2016). When there is a shortage of labeled data, semi-supervised learning is advantageous as it makes use of both labeled and unlabeled data. In addition, reinforcement learning is crucial for jobs requiring sequential decision-making processes like gaming or robotics. It trains agents to make decisions in a given environment by optimizing rewards. Depending on the nature of the problem and the availability of labeled data, many types of machine learning systems are deployed, each with its own advantages (Shanthamallu and Spanias, 2022).

Landslide susceptibility mapping (LSM) relies heavily on machine learning (ML) to manage the risks and complexity of landslide prediction. To determine whether the excellence of a model originates from its intrinsic quality or its tuning inputs, rigorous tuning methods are necessary. By using landslide maps to build large geographic databases for training and assessment, adjusting ML models is crucial in improving their efficacy (Merghadi et al., 2020). Owing to its flexibility, machine learning is perfect for solving non-linear geoenvironmental issues in large-scale mining (LSM), as it can establish connections between the causes of landslides and their frequency without requiring structural models. Requiring careful model selection, comparison, tuning, and geographic data integration for accurate susceptibility mapping, spatial data integration is a crucial component of the learning process (Nikparvar and Thill, 2021).

2.7 Common Machine Learning Algorithms for Landslide Analysis

A variety of machine learning techniques, such as Logistic Regression (LR), Support Vector Machine (SVM), Random Forest (RF), K Nearest Neighbor (KNN), and Artificial Neural Network (ANN), have been utilized to forecast slope failures. While SVM converts the original space into a higher-dimensional one to construct hyperplanes for classification, LR uses binary response variables to forecast the incidence of landslides (Parra et al., 2023).Model precision and nonlinearity are influenced by parameters such as C and gamma. While KNN assigns class membership likelihood based on the k closest training cases, RF uses voting among decision trees created from bootstrap samples to determine classifications (Yuan et al., 2022). Pattern recognition in complicated datasets is made possible by ANNs, whose performance is dependent

on elements such as hidden layers, activation functions and weight modifications. These approaches use various input criteria to anticipate collapse occurrences, including terrain relief, slope, aspect, curvature and others. This helps assess and reduce landslide risk (Agrawal and Dixit, 2023).

CHAPTER THREE

3. STUDY AREA

3.1 Description of the study area

The study area is located in the Gamo Zone of the South Ethiopia Region which is situated approximately 500 kilometers south of Addis Ababa; the area extends from 5°58'8.26"N to 6°10'58"N and 37°11'7.968"E to 37°21'24.8"E, covering an approximate area of 296 km^2. The highest elevations in the region reach a maximum of 3385 m, as shown in Figure 2. The local showcases challenging topography, mountainous scenery, varied geomorphic attributes, soil compositions, ecological zones, and steep to very steep slopes. Positioned in the Main Ethiopian Rift Valley, at the foothills of the western Ethiopian volcanic plateau, accessibility is facilitated by a road connecting Addis Ababa to Arba Minch, followed by a 40km southwest journey from Arba Minch.

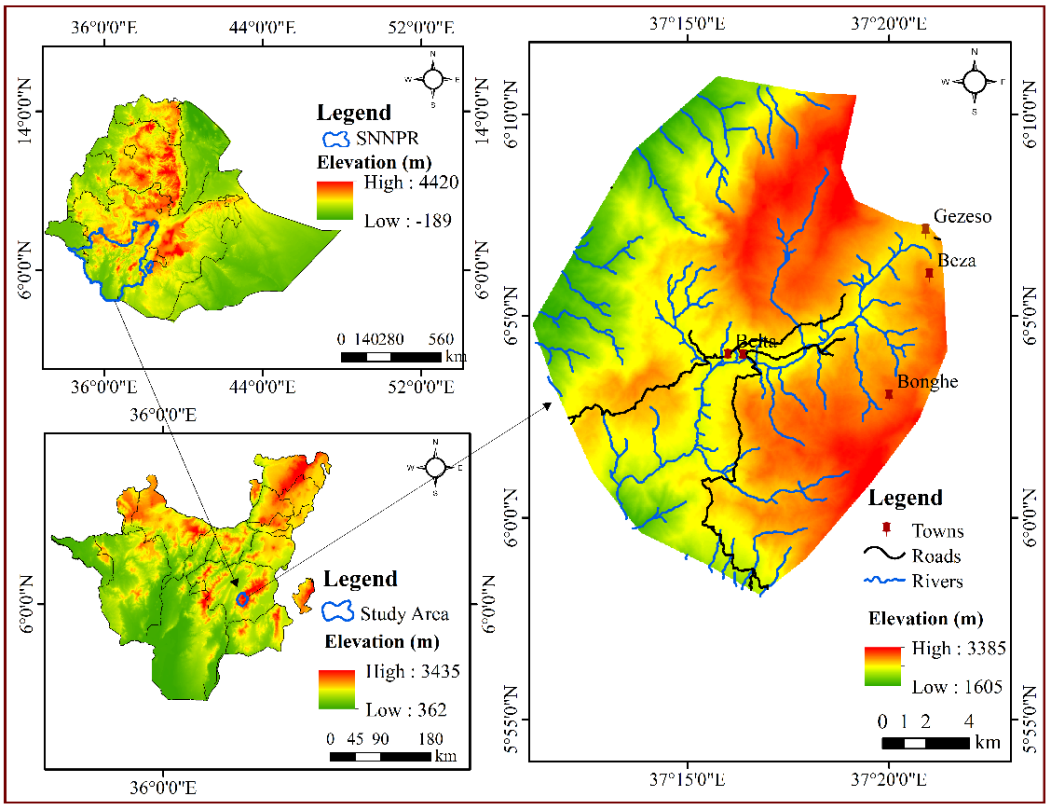

Figure 2: Location map of the study area

3.2 Physiography

The research area's topography is characterized by its rough terrain and mountainous environment which display a variety of ecological zones, steep to extremely steep slopes and different geomorphic features as shown in Figure 3. The study area is part of the western Ethiopian plateau with a deep river. A region is generally seen to be susceptible to landslide activity and active surface processes if it has deep gorges, valleys, steep scarps, cliffs, sharp ridges and rocky slope faces.

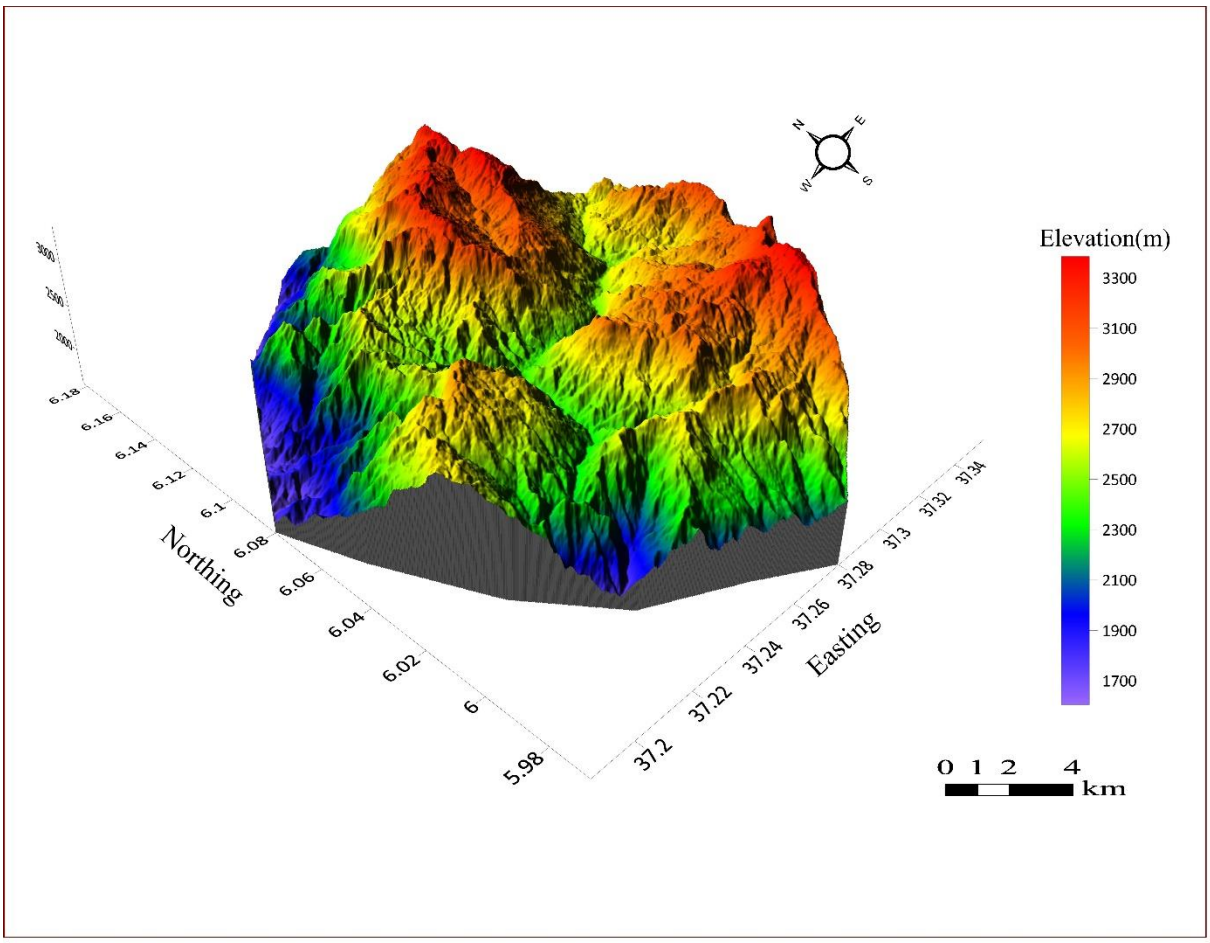

Figure 3: Physiographic map of the study area

3.3 Rainfall Pattern and Climatic Condition

In rainfall zone C, the Gamo Zone experiences bimodal precipitation patterns with distinct seasons: April-May and September-October, interspersed with drier intervals. Annual rainfall

averages 1,118 mm, ranging from 643 to 1510 mm (appendix 1a and 1b). Despite minor variations in long-term data, 1118 mm is considered a reliable average, blending observations from networks and satellite estimates provided by reputable international organizations and the National Meteorology Agency of Ethiopia. The region's topography influences the climate around Lake Abaya and Chamo in the eastern Gamo Zone. The area experiences a subtropical climate on the rift floor, with warm temperatures and moderate humidity. The climate ranges from temperate to humid and sub-alpine in the highlands to the west of the rift escarpment. Along the western highlands, warm tropical conditions prevail in deeply incised valleys. Average temperatures around Lake Abaya and Chamo cover around 21 ºC annually, with highs exceeding 30 ºC in March and April and lows dropping to around 18 ºC in July. Daily temperature variations range from 16 to 32 ºC.

The data from Ethiopian Meteorological agency institute indicates that July and August are the main wet seasons as shown in Figure 4. The area around Kemba gets moderate to high rainfall. Belta also has high precipitation records records as can be seen from 2013 up to 2023.

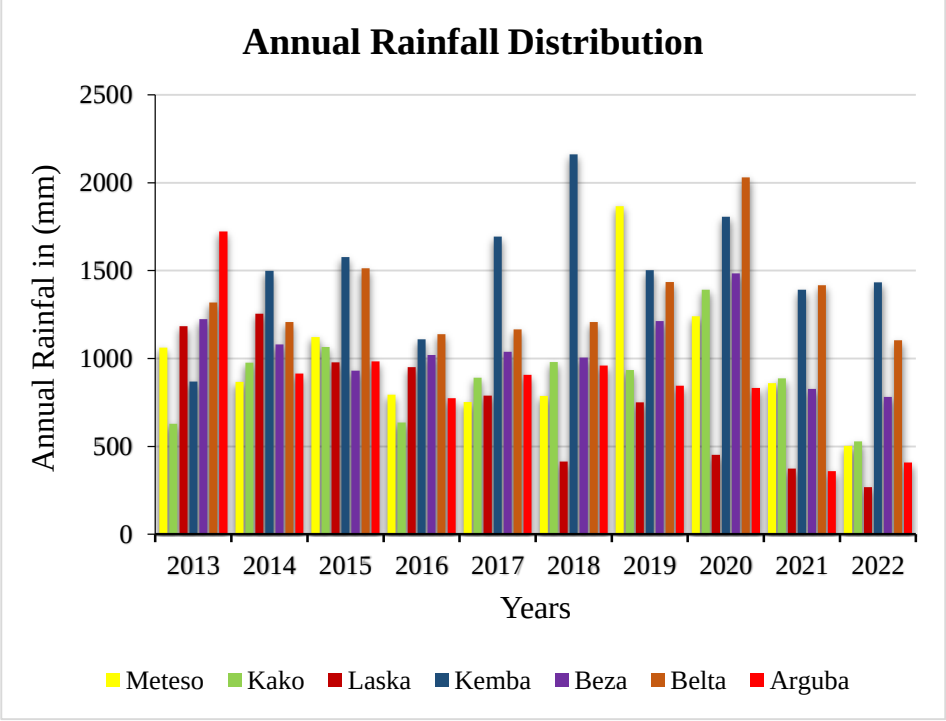

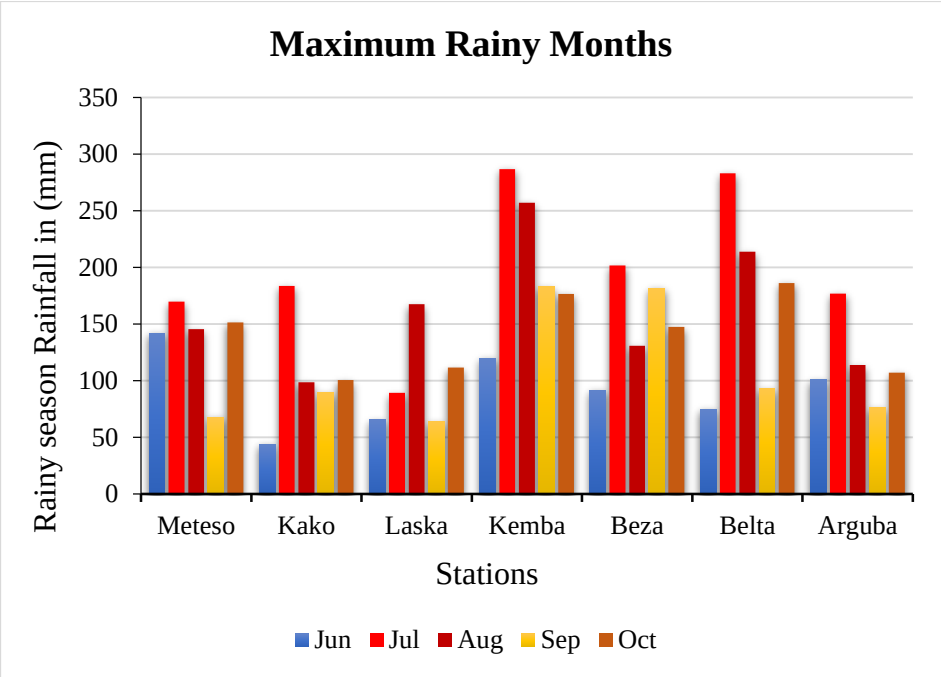

Figure 4: Average Annual rainfall distribution and maximum rainy months of the study area

3.4 Drainage pattern of the study area

The drainage patterns in the region exhibit a dendritic configuration as illustrated in Figure 5. In a dendritic drainage pattern, the river channels create a network of interlinked streams that resemble the branches of a tree. This type of drainage system is prevalent in the study area due to the presence of uniform rock or soil types which offer minimal variation in its resistance to erosion.

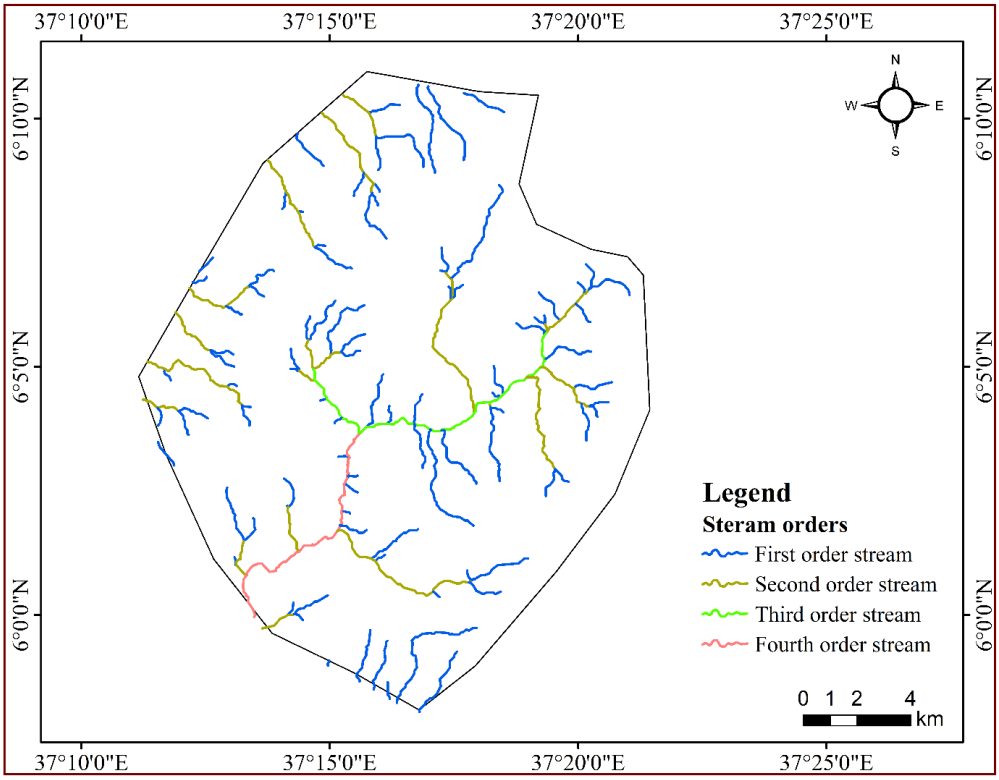

Figure 5: Drainage Map of the study area

3.5 Geology of the Study Area

The earliest metamorphic terrains in the southwest, the Tertiary volcanic plateau in the middle (known as the Gidole-Gamo Ridge), the Main Ethiopian Rift in the east, and the Gofa "broadly rifted" province in the west are the four main geological provinces creating up the Gamo Zone.

The Arabian-Nubian Shield's low-grade met volcano-sedimentary stages and the Mozambique Belt's high-grade gneissic units result in the southwestern Ethiopian metamorphic terrain (Davidson, 1983). The Lower, Middle and Upper complexes are the traditional divisions of the Precambrian basement (Kazmin et al., 1978). There are parts of the Lower Complex in the east, west, south and southwest. It is primarily granitic (Davidson, 1983). Three domains are used to classify further the crystalline basement rocks: Hammar, Akobo and Surma (Davidson, 1983). Sandstone, conglomerate and siltstone make up the majority of the Paleozoic deposits found in the northwest (Davidson, 1983).

Pliocene-Pleistocene strata of the Omo Group, encompassing the Mursi. Nkalabong, Usno, and Shungura Formations are abundant in the rift basins of southern and southwest Ethiopia (Davidson, 1983). The research region includes 11 different lithological units as shown in Figure 6. Including pegmatite, amphibolite, magnetite, and migmatized biotite paragneiss, as well as granite, aplite, and musscovite-biotite, sandstones trachy basalt to basalt lava with layers of secondary basaltic volcaniclastic rocks, subordinate rhyolite lava accompanied by rhyolitic ignimbritelava ranging from trachyte to trachybasalt with minor volcaniclastic deposits, basaltic volcaniclastic deposits, and trachybasalt to alkali basalt lava, ignimbrite and secondary volcanic breccia with rhyolite lava, trachyte with secondary trachyte volcaniclastic deposits, trachyte to trachybasalt, separating fluvial and colluvial sediments.

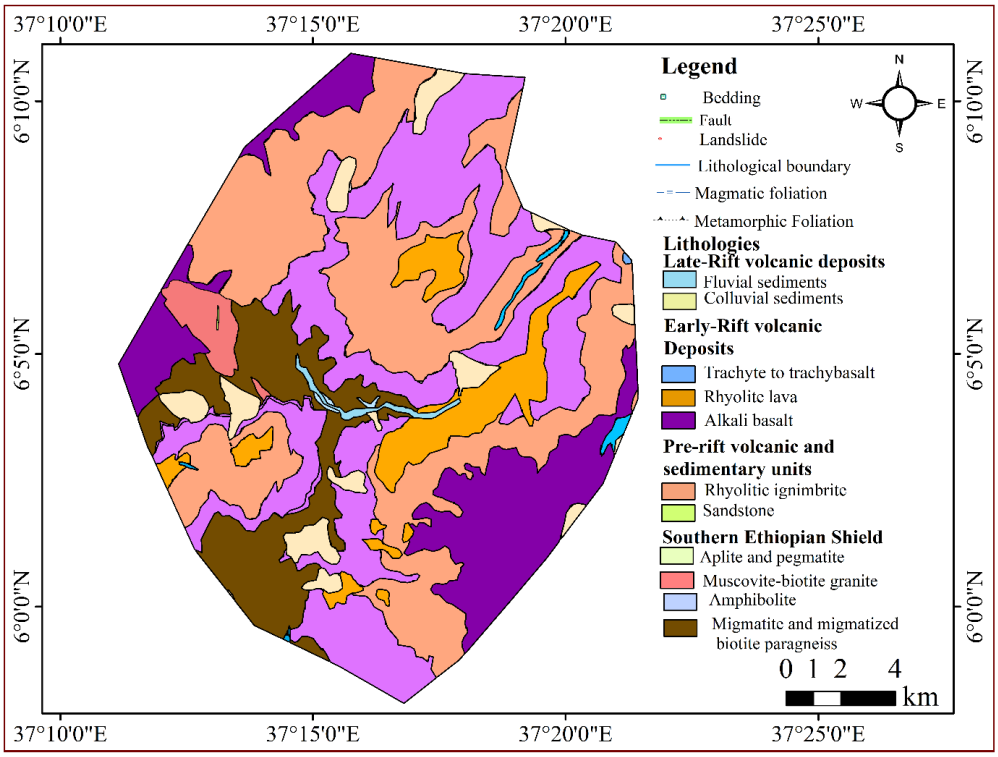

Figure 6: Geology map of the study area (GIE, 2023).

3.5.1 Southern Ethiopian Shield

Amphibolite

Amphibolite bodies are discovered in the meta-sedimentary sequence close to Dimele village, mostly in the SW and NW belts. They are usually elongated and can reach lengths of up to 1 km and widths of 1-6 m. These enormous, deeply broken, dark gray rocks have a texture that ranges from equigranular to porphyroblastic. Amphibole (41–75%) and plagioclase (21–48%) make up the majority of them, with smaller amounts of quartz, biotite, epidote–clinozoisite, and accessory minerals such titanite, ilmenite, zircon, and apatite. Locally banded amphibolite with alternating layers of leucocratic and amphibole-rich rock can be seen in some places.

Migmatite and Migmatized Biotite Paragneiss

The main exposed areas of magnetite and migmatized biotite paragneiss are in the valleys southwest and south of Gerese town (between the villages of Bonke Beza, Gerda, and Dimele). It is a dark grey, medium- to fine-grained rock with varied leucosome content.

Muscovite-Biotite Granite

In the region southwest of Gerese town, gneisses and migmatites meet to form muscovite-biotite granite. Quartz (39–41 mod. %), K-feldspar (20–31 mod. %), plagioclase (18–25 mod. %), biotite (3–14 mod. %), and muscovite (0–5 mod. %) make up the fine- to medium-grained, equigranular, frequently leucocratic granite (Fig. 4-4). While the perthitic K-feldspar, which has an average size of 0.5 to 3 mm, produces subhedral to euhedral grains, the quartz primarily forms anhedral to subhedral crystals with undulose extinction. The plagioclase is locally holeiitic and subhedral, frequently exhibiting polysynthetic twinning. Apatite, zircon, and monazite are the most frequently occurring accessory minerals.

Aplite and Pegmatite

Dykes of aplite and pegmatite up to 1.5 meters thick are haphazardly scattered over the Gamo Zone's southwest border. Massive muscovite applite and muscovite, garnet-muscovite, and beryl-garnet-muscovite pegmatites make up the dykes. Along with the accessory minerals biotite, zircon, and apatite, all albite-rich plagioclase, quartz, K-feldspar, and varying amounts of muscovite, garnet, and beryl are often found in all applite and pegmatites. Pegmatite dykes' margins have a medium-to coarse-grained granitic structure. Along the dyke's length, further pegmatite units are haphazardly scattered. They include locally existent quartz core with beryl

crystals and blocky K-feldspar that progressively evolves from graphic K-feldspar + quartz intergrowths.

3.5.2 Pre-rift volcanic and sedimentary units

Sandstones

Sandstones are found beneath pre-rift volcanic and volcaniclastic deposits in irregular, several-meter-thick layers. In certain places, the mostly red to reddish sandstones transition into breccia strata up to 1 m thick, hematite or strata up to 0.3 m thick, and in the top portion of the series, angular volcanic clasts or layers of epiclastic rocks. The framework angular quartz grains (average 78 mod. %), diagenetic cement (20 mod. %), and a trace amount of clay-rich matrix make up the majority of the sandstone composition. Angular to subangular monocrystalline and polycrystalline quartz grains range in grain size from medium to extremely coarse and in sorting quality from very bad to very poor. The quantities of muscovite and chlorite are negligible.

Rhyolitic ignimbrite with subordinate lava

Rhyolitic ignimbrite with subordinate lava can be found west of Arba Minch and along the western margin of Lake Abaya. The ignimbrite is firmly fused with brecciated lava containing pieces of fine-grained rhyolite and quartz and feldspar phenocrysts. Thin ash fall deposits alternate with welded to non-welded ignimbrites in the acid pyroclastic series, which is 10–200 m thick. 1–35% of the ignimbrite is made up of crystal pieces, primarily quartz, sanidine, and plagioclase phenocrysts. Yellowish, porous pumice fragments are common in weakly welded ignimbrites and are frequently linked to greyish-white to yellowish fall deposits.

Trachyte to trachybasalt lava with volcaniclastic deposits

West of Selam Ber and in the vicinity of Bonke Beza are deposits of volcaniclastic rock mixed with trachyte to trachybasalt lava. These rocks have a fine-grained, porphyritic structure and range in color from light grey to dark grey. Subhedral to euhedral plagioclase, sanidine, and/or anorthoclase make up trachyte and trachyandesite, whereas feldspar crystal interstices are filled with clinopyroxene or modified glass. Dark trachyte typically weathers into white, clay-rich rocks. Ash and agglomerate/lapillistone beds supported by clasts can be up to 2 mm thick. Lahar's deposit is subrounded to angular clasts locally in a fine-grained muddy matrix, with clast sizes varying.

3.5.3 Early-Rift volcanic deposits

Alkali basalt to trachybasalt lava and basaltic volcaniclastic deposits

A varied geological terrain may be found in the central Gamo Zone, which is situated between Selam Ber and Shele. The predominant rock type is dark alkali basalt, which creates columnar joints. Occasionally, lava flows up to three meters thick are interspersed with thin layers of basaltic scoria and paleosol horizons. These basalts frequently acquire reddish-brown tints from weathering. Their estimated age ranges from 19 to 11 million years. Known as Getra-Kele basalts, they come from a mantle source that is rich in incompatible elements but lacking in garnet. As one moves south, these basalts give way to trachybasalts, which have porphyritic textures and phenocrysts like olivine, clinopyroxene, and plagioclase. The groundmass is made up of volcanic glass, Fe–Ti–oxides, olivine, and clinopyroxene.

Rhyolite lava with subordinate volcanic breccia and ignimbrite

A variety of volcanic characteristics, including ignimbrite, volcanic breccia, and rhyolite lava, may be found to the west and southwest of Arba Minch. Lava flows, domes, necks, and strata are produced by them. The light grey to red rhyolites exhibit fluidal textures and flow banding, and they are home to quartz and K-feldspar phenocrysts as well as sporadic clinopyroxene or amphibole. The groundmass frequently devitrifies into spherulites, containing quartz, K-feldspar, plagioclase, and volcanic glass. The majority are welded yellowish rhyolitic to trachytic ignimbrites, which occasionally include artifacts made of petrified wood. Furthermore, far-off regions have porous pumice flow deposits that are mostly found in pyroclastic flows and contain ash matrix and pumice clasts that range in size from millimeters to centimeters.

Trachyte to trachybasalt

Dykes of trachyte to trachybasalt are sporadically dispersed throughout the whole mapped region, usually measuring less than 3 m in thickness and up to 500 m in length. The main unit is trachyte, which has an aphanitic or porphyritic texture and is light grey and finely-grained. With a trachytic or intersertal groundmass, the trachybasalts are subordinate, large, porphyritic, and dark grey. Plagioclase and clinopyroxene are the most common representations of phenocrysts. Dykes frequently exhibit moderate to severe alteration (argilitization), and their interface with the host rock is acute.

3.4.4 Late-Rift volcanic deposits

Colluvial sediments

The content and size of the colluvial sediments of the Gamo Zone, which are primarily from landslides and rockfalls, vary. Boulders up to several meters in diameter are found in unsorted, matrix-supported sediments resulting from large ancient landslides. Near unweathered rock outcrops, sharp cobbles and boulders make up rockfall accumulations. The middle portion of the zone is dominated by fine-grained sediments that have crept into sections of worn rock. Substantial accumulations with deposits over 10 meters thick are found beneath fault scarps west of Abaya Lake and Chamo Lake, north of Gerese town, and near Selam Ber.

Fluvial sediments

River dynamics and sediment sources influence the types of fluvial sediments found in the Gamo Zone, which are connected to river channels and floodplains. The majority of rivers exhibit a braided structure, distributing coarse sands and unconsolidated gravels into channels and bars. There are meandering waterways in several places, particularly toward the west. Two primary types of sediments are identified: cross-bedded sand and gravel sediments within channels, and floodplain deposits, which are primarily silts and clays with sporadic sand or gravel layers. The thickness of these sediments usually reaches several meters.

3.6 Soil types of the study area

The boundary separating geological, hydrological, atmospheric, and biological processes is represented by soil. A wide range of soil characteristics are produced by five main variables, which can be combined in different ways: climate, geography, parent material, time, and creatures. The interaction of these five elements determines the kind of soil development and its distribution in a given area. Particularly in regions with a high diversity of soil-forming elements, the relative importance of each factor changes from place to place. The study area has six types of soils including regosols, nitisols, lucisols, fluvisols, and alisols, as shown in Figure 7.

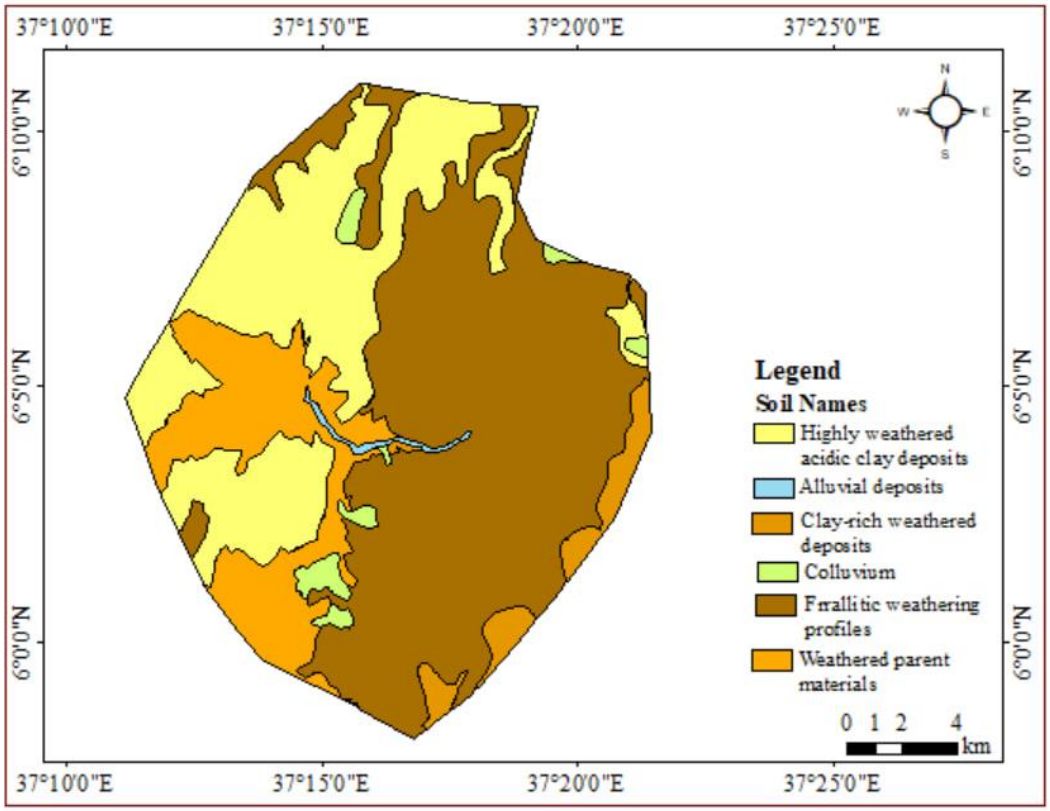

Figure 7: Soil map of the study area (GIE, 2023).

Alisols

Alisols are extremely acidic soils that have a characteristic A-Bt-C profile. They are defined by the buildup of high-activity clays in the subsoil, mostly due to clay migration processes. They have a low base saturation but a CEC of at least 24 cmolc per kg clay in the argic horizon. Alisols are usually found in hilly or undulating terrain, and in farmed regions in particular, they frequently have the "A" horizons truncated by erosion. These soils exhibit low productivity in subsistence agriculture and frequently call for acid-tolerant crops like sugar cane and coffee because of their fragile surface layer, which makes them prone to erosion. With the right liming and fertilization, they can become more productive and even turn into lucisols with comparable soil profile features.

Cambisols

A developing cambic horizon and an A, Bw, and C soil profile are characteristics of cambisols, which show varying degrees of pedogenetic modification. Typically identified by deeper colors resulting from organic matter enrichment in the mineral horizons above or by increased oxide and/or clay concentration in the cambic horizon relative to surrounding layers. Due to faster weathering rates, they form more quickly in humid tropical regions but are less prevalent overall. Cambisols are used for a variety of crops and grazing because they grow well in environments that are inappropriate for other soil processes, frequently on steep slopes. They are mostly found on metamorphic rocks in the southwest of the mapped area, with low-lying areas being dominated by alluvial and lacustrine deposits.

Fluvisol

Apart from farmed topsoil layers, fluvisols are relatively young soils made up of lacustrine and fluviatile sediments. They do not exhibit clear horizon separation. Texture, color, and differences in the amount of organic carbon show stratification in parent material, which differs between riverbanks, lagoons, and basins. Although they are utilized for grazing, orchards, and food crops, their fertility varies widely depending on their source materials. Flood risks are frequent, especially in regions with seasonal rainfall patterns, which causes significant erosion and deterioration of the soil. Leptosols and regosols frequently emerge from heavily eroded regions and slopes with thin, stony soils.

Luvisols

The argic horizon of luvisols is characterized by a robust cation exchange capability throughout. Their usual profile is A - Bt - C, with a prismatic or subangular blocky structure frequently visible at the Bt horizon. These somewhat worn soils are rich and versatile for a range of agricultural applications. However, poor agricultural techniques can cause structural deterioration in high-silt Luvisols, especially on steep slopes requiring erosion management. On slopes, they typically coexist with nitisols and alesoles, with vertisols seen in low-lying areas of the mapped region.

Nitisols

The tropical soils known as nitisols have a clayey nitic horizon and are deep and permeable. When wet, the angular, blocky structures in this at least 30% clay horizon disintegrate into shiny-

faced polyhedral or nut-shaped pieces. These shiny faces' precise cause is unknown; however, it has been connected to processes that alternate between micro swelling and shrinking. Usually, nitisols are found in flat, gently sloping places on plain bedrock. Food crops and coffee plantations in humid tropical regions can benefit from their high productivity and resilience to erosion.

Regosols

The colluvial sediments at the foot of steep slopes contain regulated soils or Regosols. These soils are characterized by a lack of diagnostic horizons, poor development, and scant indications of soil formation. The only sign of any development is usually a darker topsoil due to the buildup of organic materials. When material is carried downslope by erosion, wash, or soil creep, it results in deteriorated and eroded surfaces linked to regosols. Despite not having the usual stratification, this colluvial material is somewhat fresh and diverse, frequently moderately sorted. A common cover of trees and shrubs is seen on regosols, which are severely eroded.

3.7 Seismicity of the Study Area

The seismic hazard map of the country provided by EBCS (1995) was used in this study to estimate the study area's seismic hazard rating. It categorizes different seismic risk zones based on historical data of destructive earthquakes. These zones range from earthquake-free (zone 0) to zones with varying degrees of damage potential (zones 1, 2, 3 and 4). Each zone is associated with a fixed bedrock acceleration ratio: 0.03 for zone 1, 0.05 for zone 2, 0.07 for zone 3, and 0.1 for zone 4. Zone 0 is considered free from seismic activity. The study area falls within Zone 3, as shown in Figure 8. It indicates a considerable risk of damage. Therefore, the occurrence of seismic hazards in the study area could potentially lead to or exacerbate landslide hazards.

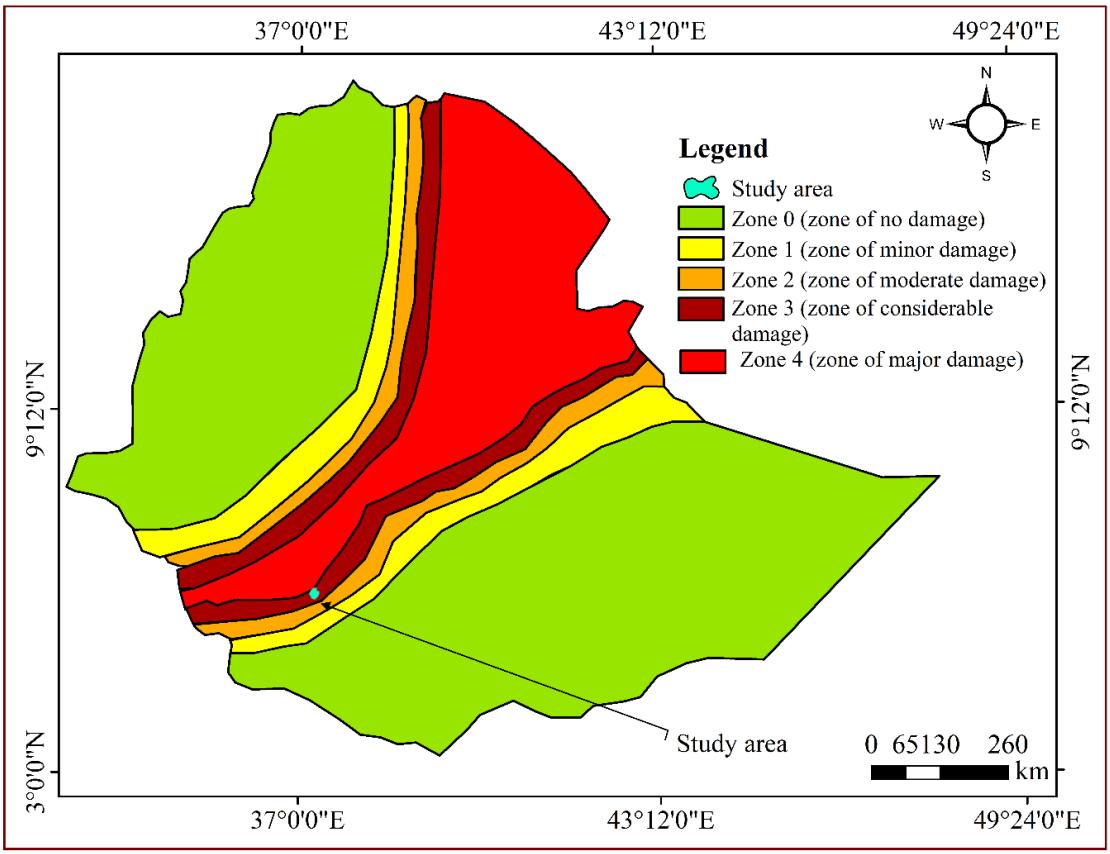

Figure 8: Seismic zone map of Ethiopia

CHAPTER FOUR

4. METHODOLOGY

4.1 Softwares

Data management and report generation were conducted utilizing Microsoft Office Word 2013 and Microsoft Office Excel 2013. Various thematic maps were produced using ArcGIS version 10.8.1 and a physiography map was generated using Global Mapper and Surfer software. QGIS and Rstudio were employed to analyze data using machine learning algorithms. SPSS software facilitated ROC analysis, while Google Earth Pro was utilized to create landslide inventory and lineament maps.

4.2 Data collection

4.2.1 Primary data

Slope, curvature, distance to stream, elevation and aspect maps were derived from the Digital Elevation Model (DEM) sourced from ASTER DEM, with a resolution of 30m x 30m. A land use and land cover map was created using Sentinel imagery from 2022, also at a resolution of 30m x 30m. High-resolution imagery from Google Earth was utilized to develop the landslide inventory map and distance to lineament map. This dataset played a crucial role in validating the causative factor maps and landslide inventory maps for the respective areas. Google Earth Pro imagery served as the primary source for generating landslide inventory data. Relevant information about the locations, modes of failure and sizes of previous landslides was collected from Google Earth Pro, as well as the identification of lineaments.

4.2.2 Secondary data

Secondary data were collected from various institutions and organizations, encompassing a comprehensive literature review of published and unpublished papers from diverse online and journal repositories. A regional geological map was acquired from the Geological Institute of Ethiopia. Meteorological data was obtained from the National Meteorological Agency of Ethiopia and NASA power larc as shown in Table 2.

Table 2: Data type and sources

Input Data	Source	Purpose
Literature	Published and unpublished papers from Google Scholar	To provide an overview and conceptual foundation for the study.
Geological and soil map	Geological Institute of Ethiopia	To digitize Lithology, structures, and soil type
Metrology data	National Meteorological Agency of Ethiopia and NASA Power larc	To generate a Rainfall map
STRM DEM with a resolution of 30m*30m	USGS	To generate slope, aspect, curvature, distance to stream, and elevation maps
Google Earth image	Google earth pro	To digitize landslide inventory and distance to lineament
Sentinel imagery from 2022 with a resolution of 30m*30m	Sentinel imagery	To generate a Land Use Land Cover map

4.3 Data analysis

Data analysis incorporated both primary and secondary sources through a series of systematic procedures. Slope, curvature, distance to streams, elevation and aspect maps were derived from the ASTER DEM with a resolution of 30m x 30m. Landslide inventory polygons and distance to lineament maps were created using Google Earth imagery while land use/land cover maps were developed from 2022 Sentinel imagery. Thematic map layers of causative factors were prepared in ArcGIS 10.8.1 using both primary and secondary data including annual rainfall and geological data sourced from the Geological Institute of Ethiopia as well as meteorological data from the National Meteorological Agency of Ethiopia and NASA Power Larc. These maps were transformed into raster format with a uniform cell size of 30m x 30m. The Raster Calculator in ArcGIS was used to compute landslide susceptibility index maps using random forest and support vector machine models. These indices were then classified into five susceptibility

classes: very low, low, moderate, high and very high. The landslide susceptibility maps were validated using ROC curve to ensure accuracy.

4.4 Methods

4.4.1 Random Forest

The term "Random Forest" refers to an ensemble of decision trees collectively known as the "Forest." Each tree in the Random Forest contributes to the classification process by assigning a vote based on its properties when classifying a new item—a concept known as the tree's "voting" for that class (Oladipupo, 2010). This unique approach highlights the versatility and effectiveness of the Random Forest model in machine-learning applications (Merghadi et al., 2020), Initially proposed by Breiman (Jin et al., 2020)., Random Forest (RF) stands as a powerful integrated classification and regression model grounded in ensemble learning and the bagging concept.

Random Forest (RF) excels in handling large datasets with both numerical and categorical variables, employing a non-parametric multivariate regression and classification approach. By aggregating decisions from individual decision trees (Agrawal and Dixit, 2023). The decision-making process involves a random selection of entry characteristics at each node, leading to optimal node partitions based on the Gini standard. The ensemble of K trees forms the RF model with the final classification determined through majority voting based on the K classification results. RF's inherent randomness, from both the training set and the selection of optimal attributes for node splitting, prevents overfitting, enhancing model stability. RF also provides the Gini index for each input variable, offering insights into their relative importance (Shahzad et al., 2022; Yuan et al., 2022).

Gini= 1-$\sum_{i=1}^{2} pi2$……(eq.1)

Where *pi* represents the probability that the observed sample falls in category i.

The landslide susceptibility mapping process began with the download and installation of QGIS, where spatial data layers, including the DEM and a landslide inventory map, were imported. Raster layers were generated by converting vector data, then normalized and reclassified. Raster values at landslide points were extracted and exported into a CSV file for model training.

In RStudio, the CSV data was prepared by converting landslide occurrence data into a categorical variable and splitting the dataset into training and testing sets. A Random Forest model was trained on this data to predict landslide susceptibility.

The model's performance was evaluated using accuracy, precision, and recall metrics. Finally, the trained model was applied to raster layers of the study area to create a susceptibility map, which was exported as a TIFF file and visualized in ArcGIS. A color gradient and additional contextual data were added to enhance map interpretation.

4.4.2 Support Vector Machine

SVM stands out as a formidable algorithm, leveraging multiple kernels to gauge the similarity of observations in feature space. Renowned for its high performance, SVM employs various kernels such as linear, polynomial, radial-based function, and sigmoid, each exerting a substantial influence on the modeling process and its outcomes (Shahzad et al., 2022). The conceptualization of SVM can be attributed to marking it as a widely adopted supervised machine-learning technique in the field of landslide susceptibility Mapping (Chen et al., 2017).

SVM's prowess lies in its dual role as a supervised model for both regression and classification. Facilitated by the "kernel trick," SVMs seamlessly navigate between linear and non-linear classification by delineating boundaries between different classes. This involves a strategic transformation of inputs into high-dimensional feature spaces, enabling the creation of margins that effectively minimize classification errors. The specific context of landslide susceptibility mapping utilizing SVMs, the algorithm undergoes training on input features and landslide occurrence labels. The Objective is to identify the optimal decision boundary, or hyperplane, that adeptly distinguishes susceptible areas from their non-susceptible counterparts, showcasing SVM's applicability in geospatial predictive modeling (Thiruvengadam et al., 2022).

$F(x)=(w|x) +b= \sum (wixi) +b=0$……(eq.2)

Where the x presents the independent variables, vector w represents the vector of weights which has to be estimated by the model, and b is a constant

(RBF Gaussian kernel) $K(x_{i,}x_{j)} = \exp(-y \| x_i-x_j \|^2$Where x_i and x_j are the input vectors, and y is the gama parameter……(eq.3)

Landslide occurrence data and environmental factors, including slope, aspect, and elevation, were gathered. The data was then cleaned in ArcGIS to ensure it was ready for analysis. Once processed, the data was exported in TIFF format and saved as CSV files for further use in RStudio.

For model training, RStudio was set up with necessary R packages, including e1071 for SVM analysis, and the prepared data was imported. Using the SVM algorithm, a predictive model was developed based on the training dataset to assess landslide susceptibility.

Model evaluation was performed by testing the SVM model on a separate dataset to assess its accuracy and reliability. After testing, the trained model was used to predict landslide susceptibility on new data. These predictions were saved as a CSV file, imported into ArcGIS, and visualized in a susceptibility map to support further analysis.

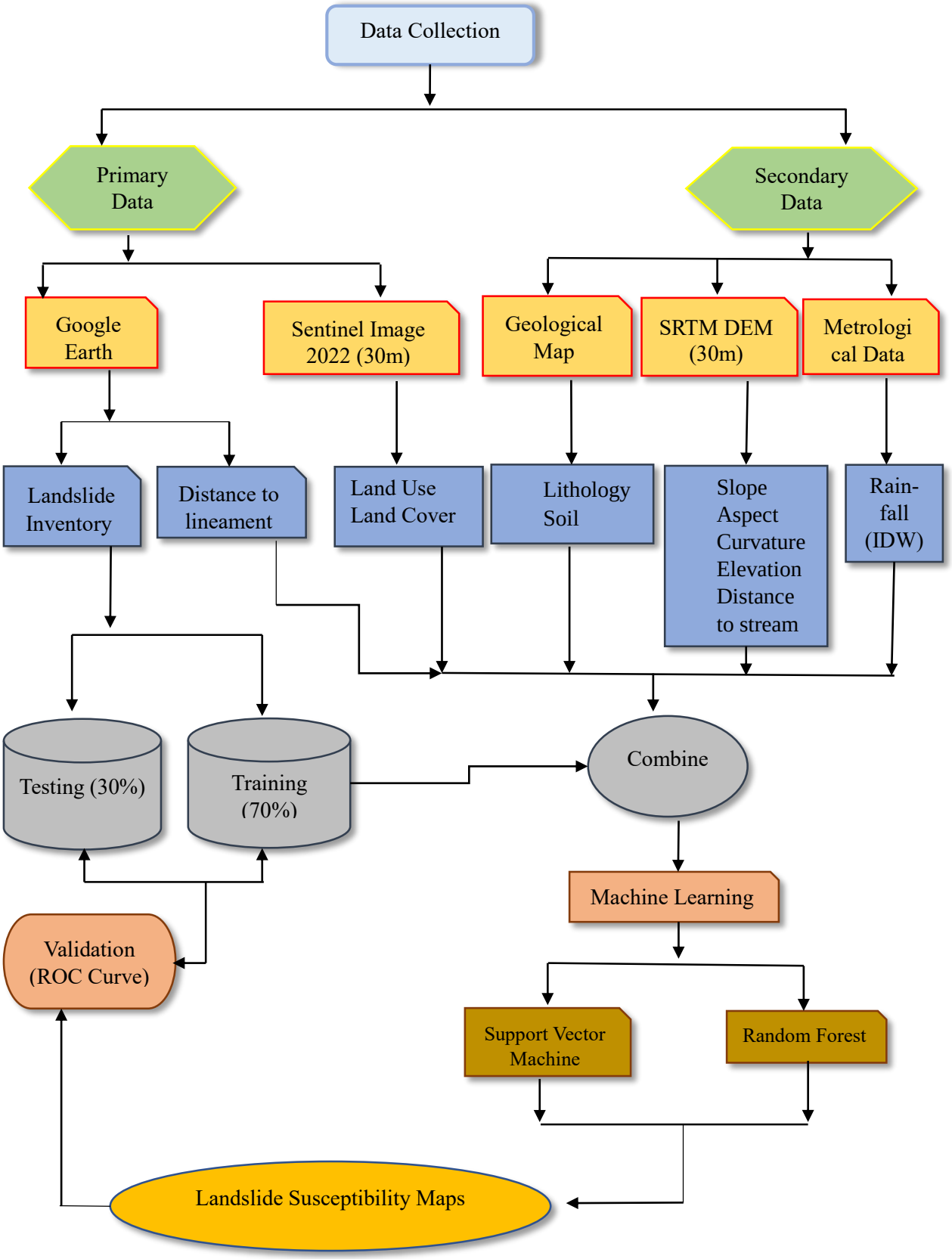

Figure 9: Flow chart of the research methodology

CHAPTER FIVE

5. RESULTS AND DISCUSSION

5.1 Landslide Inventory map

Landslide inventory maps serve as a crucial foundation for comprehending future landslide potential because they offer important information on the locations and characteristics of historical landslides, even though they do not specifically detail the triggers of those events (Dai et al., 2002). These maps are the foundation of most susceptibility mapping methods, providing prospective risk evaluations with information gleaned from historical geology, topographic, and climatic circumstances. A detailed understanding of landslide circumstances is required to construct a systematic inventory. This understanding can be attained by the investigation of aerial photographs, technical documents, historical records, and other sources of information about past failures (Westen et al., 2006).

Field surveys are often utilized in conjunction with remote sensing techniques to create inventory maps. Field surveys are used to find evidence of past and present landslides based on factors including deformed trees, sedimentary deposits, and slope morphology. Field data has been dated using a variety of relative and absolute dating techniques, which have shed light on the temporal dynamics of landslide occurrences (Bull, 1996; Lang et al., 1999).

For the landslide inventorymap, 302 landslides were generated vector-based polygons through Google Earth image interpretation. The vector data was converted to raster format using ArcGIS with a pixel size of 30m by 30m as shown in Figure 10. This study utilizes classification-dependent landslide susceptibility mapping by integrating binary data. A total of 302 landslide locations were digitally recorded using Google Earth imagery (appendix 3). An equal number of 302 non-landslide locations were selected to ensure unbiased and accurate results. These non-landslide sites were identified using QGIS with the K-means clustering algorithm, ensuring they matched the positive landslide samples.

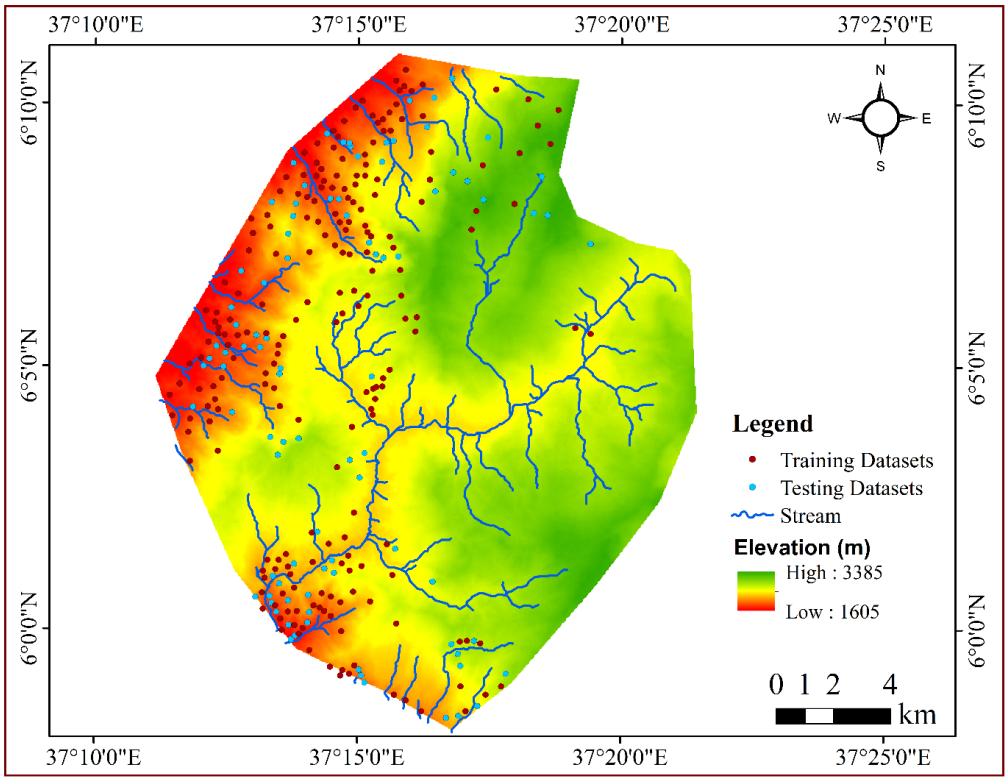

Figure 10: Landslide inventory map of the study area with landslide points.

5.2 Landslide causative factor maps

This paper uses aspect, curvature, and distance to stream, elevation, geology, land use, land cover, slope, and rainfall as landslide factors. As of now, there are no established standards for choosing landslide factors. The landslide factor maps were created and then sub-classified to determine the contribution of each factor class to landslide occurrences. With a resolution of 30 m x 30 m, the Digital Elevation Model (DEM) obtained from ASTER DEM was used to calculate the slope, curvature, aspect, and distance to streams. The DEM was then divided into several classes. The Geological Institute of Ethiopia's regional map of Gamo Gofa served as the basis for the updated geology map. The distances to the lineament and stream were calculated using buffering analysis. Sentinel imagery from 2022 was used to create a land use and land cover map with a resolution of 30 meters by 30 meters. The rainfall map was created by using the IDW interpolation technique of the spatial analyst tool in GIS to interpolate the 10-year rainfall data of ten rain gauge stations located within and adjacent to the study area.

5.2.1 Aspect

Aspect, or slope orientation, influences how exposed a slope is to wind, sunshine, and precipitation; as a result, it indirectly affects other landslide-causing elements such as soil moisture, vegetation cover, and soil thickness (Meten et al., 2015). The area aspects were divided into classes that face the north, northeast, east, southeast, south, southwest, west, and northwest as shown in Figure 11 (a) below using the Natural Breaks (Jenks) method.

5.2.2 Curvature

One important component that contributes to the topography variation of hill slopes and influences the process of surficial erosion is curvature. It is described as the rate at which the gradient of a slope changes in a direction that directs the flow down a slope toward lower elevations (Ismail et al., 2018). Values close to zero indicate a flat terrain, high positive values indicate convex curvature, and large negative values show concave curvature. Concave curvature is linked to a higher likelihood of groundwater presence, and groundwater affects slope instability in and around the concave slope. On the other hand, slope erosion is encouraged when the slope curvature is convex (Shano et al., 2021b). The area is divided into class's flat, concave and convex as shown in Figure 11 (b) below using the Natural Breaks (Jenks) method. Compared to concave and convex curvatures, flat curvature is the most dominant and spans a larger area overall. Therefore, compared to a flat curvature, landslide occurrence is greatly influenced by concave and convex aspect classes.

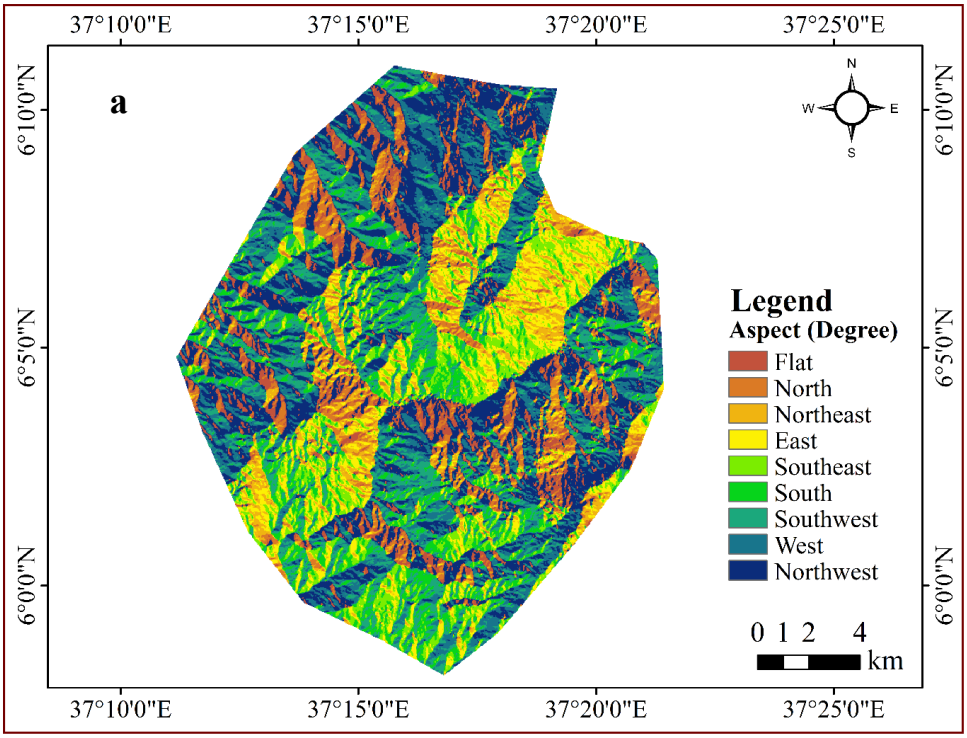

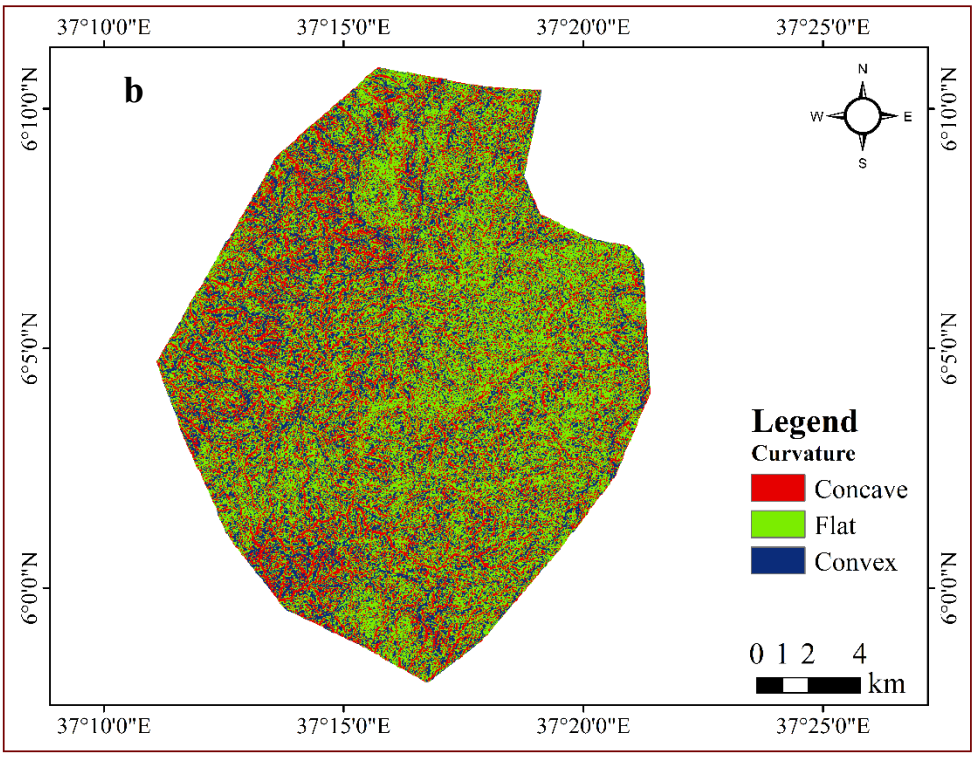

Figure 11: Landslide causative factor maps: (a) Aspect, (b) Curvature Map.

5.2.3 Elevation

The influence of elevation is attributed to the degree of weathering, variation in humidity, erosion process, and depth of weathering. The higher the elevation, the higher the intensity of weathering and erosion will be. Thus, it is quite reasonable to consider elevation as one of the causative factors for controlling the landslide process (Firomsa and Abay, 2018).

It is manually classified into nine classes using the Natural Breaks (Jenks) method to represent the relationship between elevation and landslides in a realistic way as shown in Figure 12 (b): (1600–1900 m), (1900–2200 m), (2200–2300 m), (2300–2500 m), and (2500–2700 m), (2700–2800 m), (2800–3000 m), (3000–3100 m), and (> 3100 m).

5.2.4 Slope

The slope angle has a big impact on landslide investigation. The shear stress in the soil or unconsolidated material increases as the slope angle increases. Because gentle slopes have lower shear loads related to low gradients, landslides are likely to occur less frequently. In contrast to moderate and gentle slopes, steep slopes frequently experience landslides. A downslope migration of large masses following steep terrain is favored by the disintegration of rocks caused by weathering, river erosion, incision, groundwater infiltration, or percolation from intense rainfall events along cracks (Meten et al., 2015). The results indicated that landslides occur less frequently at lower slope angles, but more frequently as the slope angle increases. Steepness of the slope is thought to be the primary cause of landslides in the majority of landslide studies (Asmelash and Barbieri, 2012). In contrast to gentle slopes, steeper slopes are more prone to instability. Because gentle slopes have lower shear loads related to low slopes, landslides are predicted to occur less frequently (Raghuvanshi et al., 2015). In this study, slopes were classified into five categories using the Natural Breaks (Jenks) method (0-10, 10-17, 17-24, 24-33, and >33) as shown in Figure 12 (b) below based on the natural break breaks method.

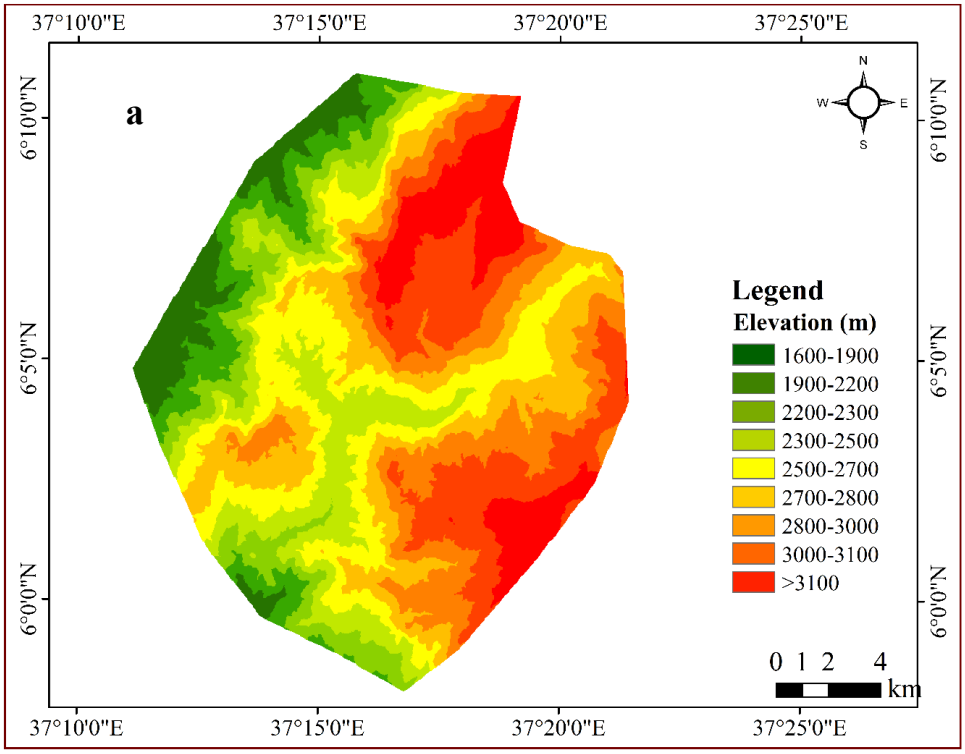

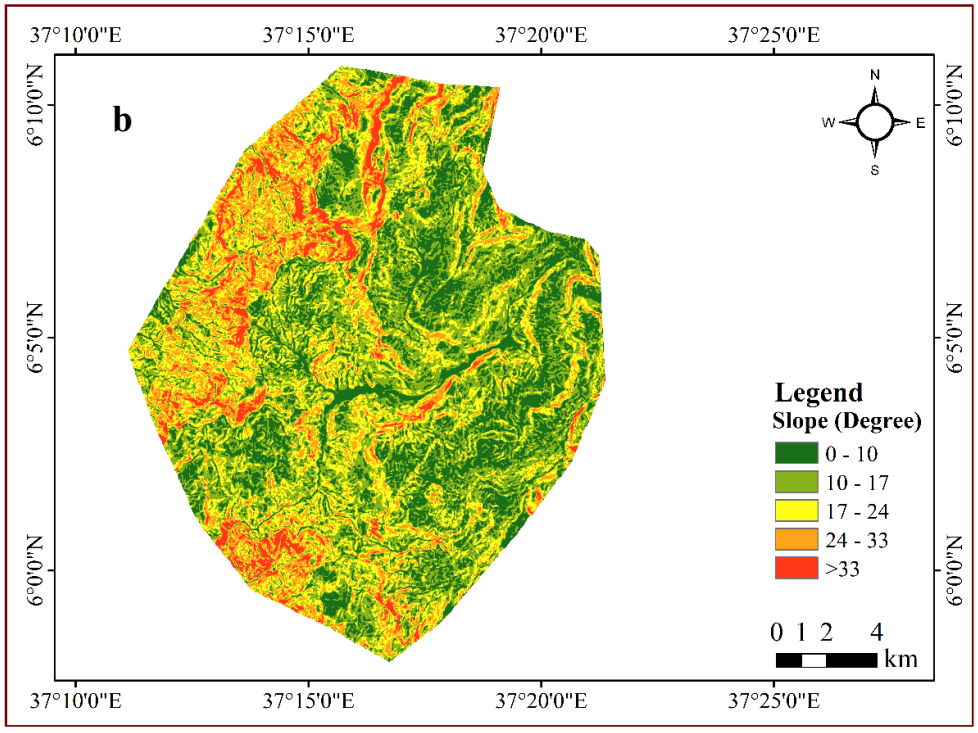

Figure 12: Landslide causative factor maps: (a) Elevation, (b) Slope Map

5.2.5 Distance to Lineament

Lineament has an impact on the structures of surface materials and has a major effect on topographic permeability and, consequently, slope stability. A slope's stability is impacted by its closeness to certain characteristics, making landslides more likely to occur (Samanta 2016).

The distance to the lineament factor was divided into five classes using the Natural Breaks (Jenks) method: 0-380m, 380-834m, 834-1400m, 1400-2300m, and > 2300m as shown in Figure 13 (a) below.The lineament factor was characterized by proximity analysis using the Euclidian distance buffering tool.

5.2.6 Distance to Stream

The slope's closeness to the stream course is a crucial element that determines how the landscape changes in the region and indicates landslides and associated erosional features. Because several drainage networks degrade the slope base and saturate the underwater portion of the slope-forming material, rivers with multiple drainage networks have a high risk of causing landslides (Getachew & Meten, 2021).

Five subclasses were used to categorize this map, as shown in Figure 13 (b) below.using the Natural Breaks (Jenks) method: 0–240, 240–510, 510–810, 810–1200, and > 1200 meters.

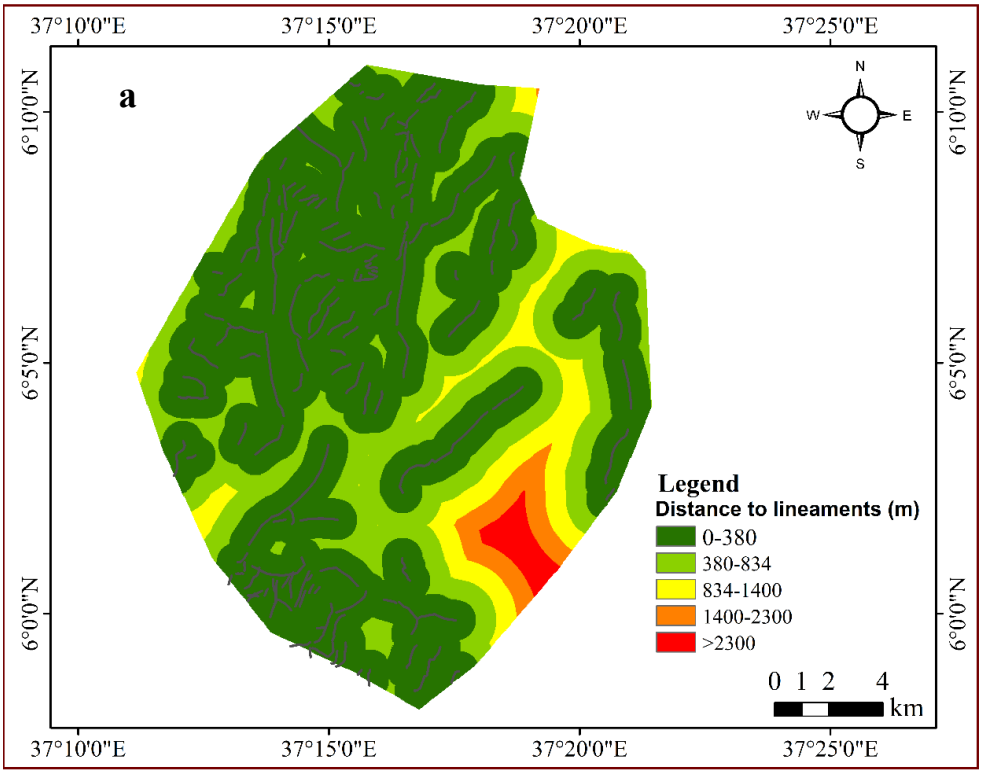

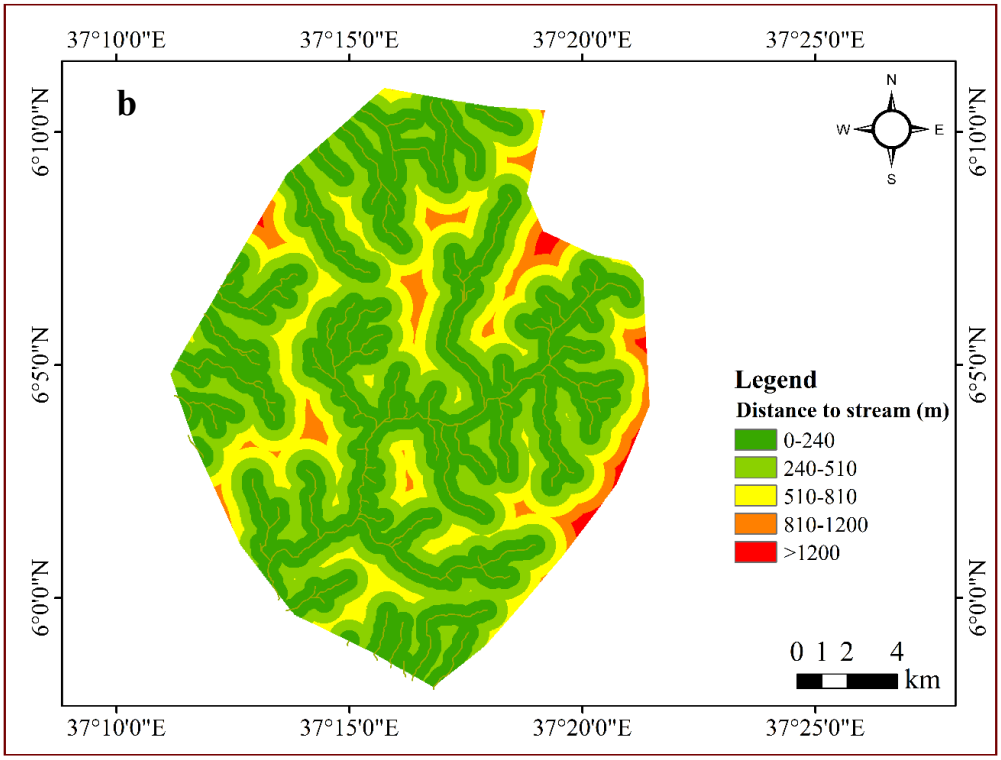

Figure 13: Landslide causative factor maps: (a) Distance to lineament, (b) Distance to Stream Map

5.2.7 Lithology

The physical and chemical characteristics of rocks or lithology largely determine the stability of slopes. Rocks differing in strength and cohesiveness react differently to external forces, affecting their resistance to landslides. This includes the rock mass's strength and structure, among other things. To comprehend and evaluate the stability of slopes, it is essential to consider the relationship between lithology and slope-forming materials. Slope vulnerability to instability and possible landslides is mostly determined by the characteristics of the rock mass such as its strength and structure (Bai et al., 2014). The results of lithology from the existing map showed that the study area contains eleven lithological units as shown in Figure 14 (a) below. The result showed that trachybasalt, Aplite, and pegmatite cover the highest and lowest areas.

5.2.8 Rainfall

Slope failures are mostly caused by heavy rain (Ayalew, 1999; Getachew and Meten, 2021). It is difficult to assess the significance of rainfall considering the other variables that might also have an impact on the process of landslide formation. While in some areas, considerably lower hills with moderate relief may fail after relatively small amounts of rain over several days, very irregular chains of mountains with steep slope angles may maintain their stability regardless of the amount of precipitation (Ayalew, 1999). The Rainfall factor map, extracted from the interpolated data of seven rain gauge stations (Meteso, Kako, Laska, Kemba, Beza, Belta and Arguba) using the extract by mask tool in ArcGIS, it was manually classified into seven classes to represent the relationship between rainfall and landslides in a realistic way. The rainfall data analysis showed that the maximum monthly rainfall occurs in June, July, August, September, and October, coinciding with the landslide occurrence in this area.

The rainfall map of the study area was divided into seven annual rainfall classes Figure 14 (b) using the Natural Breaks (Jenks) method: 1100-1200, 1200-1300, 1300-1400, 1400-1500, 1500-1600, 1600-1800, and > 1800millimeters.

5.2.9 Soil type

Various factors including soil type, composition and stability, influence the susceptibility of a slope to landslides. The type and properties of soil underlying a slope play a significant role in its stability, with slopes containing clay soils or soils with high water content being more prone

to failure. A critical factor for landslides is the clay percentage in the soil, which should be higher than 2.5% for landslides to occur, as fine particle migration can lead to pore blockage, affecting slope stability (Makonyo and Zahor, 2023). In addition to soil type, Soil texture indicates the relative proportion of sand, silt, and clay, which affects soil stability. Soils high in clay form stable aggregates resistant to detachment, while sandy or coarse loams, with low organic matter, are easily detached. Consequently, soils with more sand, high slopes and intensive rainfall are prone to severe landslides (Sharma et al., 2012).

The results of soil types from the existing map showed that the study area contains six soil types as shown in Figure 14 (C). The result showed that Nitiols and Fluviols cover the highest and lowest area, respectively.

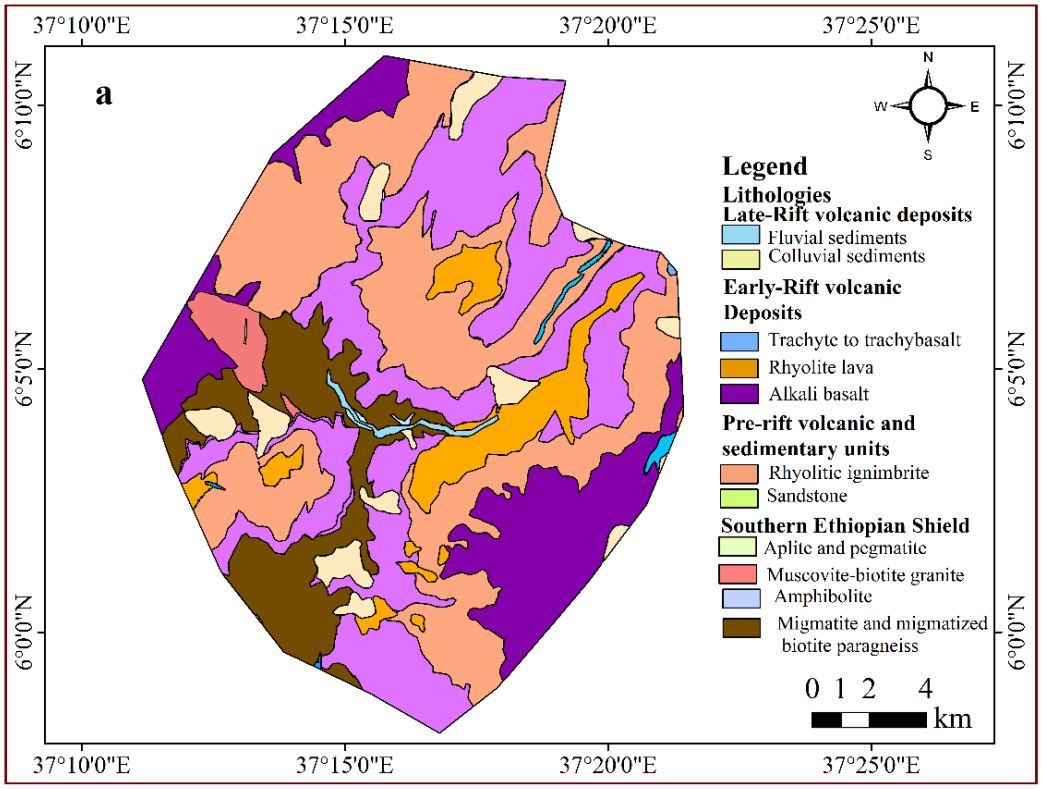

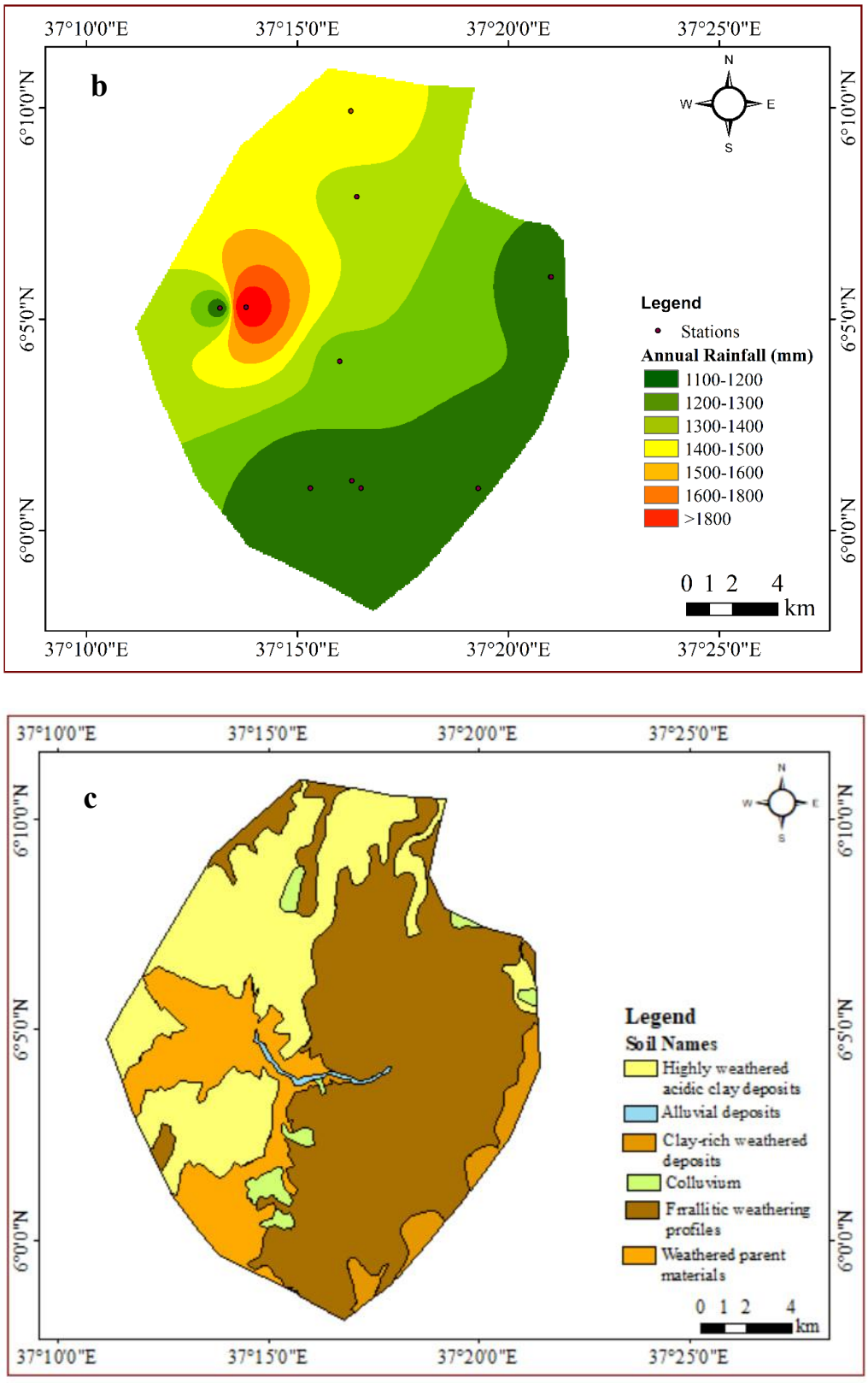

Figure 14: Landslide causative factor maps: (a) Lithology, (b) Annual Rainfall, (c) Soil Map

5.2.10 Land Use Land Cover

One of the main causes of landslides is also land use. Changes in land cover and use worldwide have a major impact on landslides caused by rainfall (Firomsa and Abay, 2018). Due to human activity, including deforestation, overgrazing, and steep slope farming, change the land's cover and use, which frequently causes slope instability (Glade, 2003). There are four types of land use types including Dense Forest, settlement, Grazing land, and agricultural land predominating in the area as shown in Figure 15.

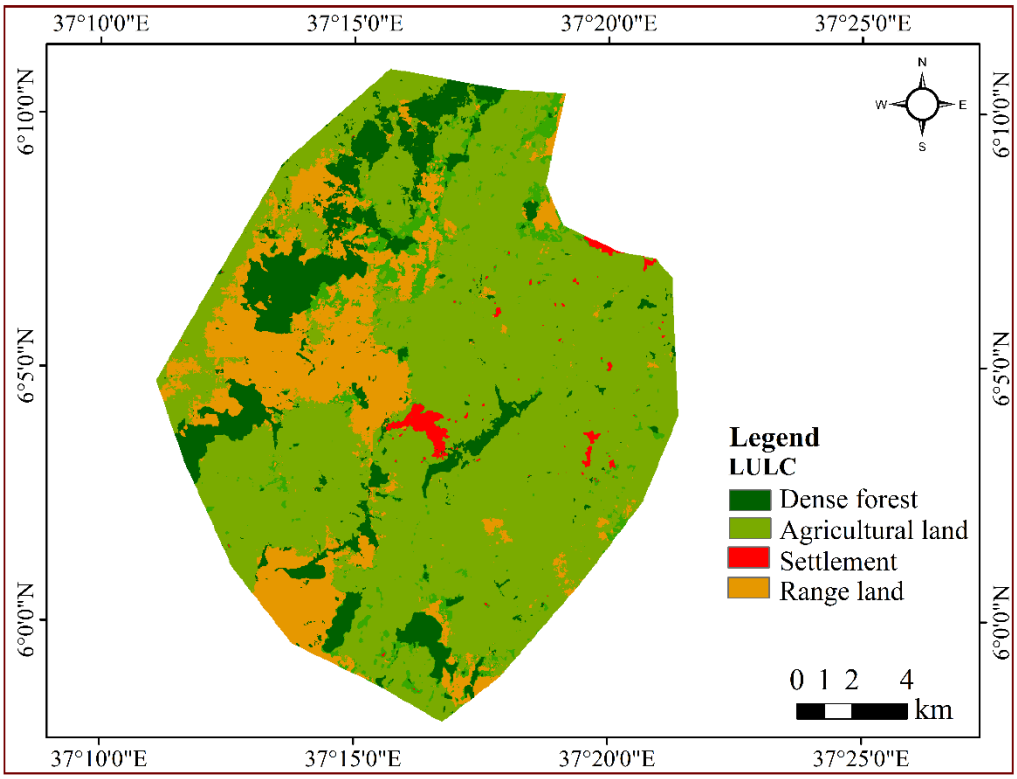

Figure 15: Landslide causative factor map: Land Use Land Cover

5.3 Multicollinearity analysis

The multicollinearity study aimed to determine whether any collinearity existed between the factors used in the landslide susceptibility analysis. Collinearity was assessed using Tolerance (TOL) and Variance Inflation Factor (VIF) values (Mallick et al., 2022). It was calculated via SPSS software, as shown in Table 3. The TOL values for all factors were above 0.4, significantly higher than the threshold of 0.1. The VIF values were below 2.2, well under the threshold of 5 or 10. These results indicate no multicollinearity among the selected factors, confirming the rationality of the evaluation index.

5.3.1 Tolerance

Multicollinearity can primarily be identified using tolerance and its reciprocal, the variance inflation factor (VIF). Tolerance represents the proportion of variance in a particular predictor that is not accounted for by the other predictors. It is mathematically defined as:

Tolerance= $1-R^2$……(eq.4)

Where R^2 is the coefficient of determination for the regression of the predictor on all the other independent variables (Senaviratna and A. Cooray, 2019). The tolerance values for the various landslide-related parameters indicate the degree of multicollinearity among the predictor variables. Most parameters exhibit high tolerance, indicating low multicollinearity. For example, Aspect and Curvature have tolerance values of 0.921 and 0.975, respectively, showing that these factors are largely independent of other predictors. Parameters such as DTL and DTS have tolerance values of 0.725 and 0.746, respectively, which suggest low multicollinearity. Geology and LULC also demonstrate low multicollinearity with tolerance values of 0.676 and 0.738, respectively. Rainfall and Slope, with tolerance values of 0.781 and 0.615, respectively, indicate some dependence on other predictors but at acceptable levels. Elevation and Soil Type show moderate multicollinearity with tolerance values of 0.475 and 0.567, respectively. Overall, the tolerance values indicate that the predictor variables are mostly independent of each other, making them suitable for regression analysis without significant multicollinearity concerns.

5.3.2 Variance Inflation Factor (VIF)

The variance inflation factor (VIF) is defined as the reciprocal of tolerance

$$VIF = \frac{1}{Tolerance} \quad \text{.....(eq.4)}$$

VIF indicates the extent to which the variance of a coefficient estimate is inflated due to multicollinearity (Senaviratna and Cooray, 2019). The Variance Inflation Factor (VIF) values for the landslide-related parameters provide insights into the degree of multicollinearity among the predictor variables. Most parameters exhibit low VIF values, indicating minimal multicollinearity. For instance, Aspect and Curvature have VIF values of 1.085 and 1.026, respectively, suggesting that these factors are largely independent of other predictors. Parameters such as DTL and DTS show low multicollinearity with VIF values of 1.380 and 1.340, respectively. Geology and LULC also exhibit low multicollinearity, with VIF values of 1.480 and 1.355, respectively. Rainfall and Slope have VIF values of 1.279 and 1.625, respectively, indicating some dependence on other predictors but at acceptable levels. Elevation and Soil Type show moderate multicollinearity with VIF values of 2.106 and 1.762, respectively, suggesting a fair amount of dependence on other predictors. Overall, the VIF values indicate that the predictor variables are mostly independent of each other, making them suitable for regression analysis without significant multicollinearity concerns.

Table 3: Collinearity diagnostic results of influence factors

	Parameters	Data type	Collinearity statistics	
			Tolerance	VIF
1	Aspect	Continuous	0.921389	1.085318
2	Curvature	Continuous	0.975065	1.025572
3	DTL	Continuous	0.724833	1.379627
4	DTS	Continuous	0.746446	1.339682
5	Elevation	Continuous	0.474805	2.106129
6	Geology	Discrete	0.675593	1.480181
7	LULC	Discrete	0.738081	1.354865
8	Rainfall	Continuous	0.781403	1.27975
9	Slope	Continuous	0.615386	1.624995
10	Soil type	Discrete	0.567397	1.762435

5.4 Rating Landslide Factors Using Information Value Method

5.4.1 Information value

A bivariate statistical technique called the information value model is used to forecast the spatial link between landslides and landslide factor classes. Yin and Yan created this technique, and then Sarkar et al. modified it. This method has the benefit of evaluating landslip susceptibility objectively. Applying the information value method, determine the weight of every factor layer class by comparing the landslip density in each class to the total area of landslide density (Du et al., 2017; Wubalem and Meten, 2020). In this study, the information value (IV) method is utilized to assess how the conditioning factor classes are related to the likelihood of landslide occurrences. A higher IV indicates a stronger connection between the probability of landslides and the conditioning factor class. The IVs are determined for each class of the factor map based on the presence of landslides within a given map unit. This calculated information value helps

in understanding the significance of each factor class in relation to landslide occurrence. All factor maps were converted into raster format with a uniform coordinate system (Adindan UTM zone 37 N) and pixel size (30m × 30m), and were reclassified into different classes. The information value for a specific factor class was computed using the logarithm of the ratio of conditional probability to prior probability. The causative factors were divided into sixty-four classes, with Table 4 showing the weights assigned to each class by the IV model. These weights demonstrate the spatial relationship between each class of causative factors and the occurrence of landslides.

Table 4: Rating of factor classes from a spatial relationship between each factor class and landslide using information value model

	Parameter	**Class**	**No of pixels in class**	**% pixel**	**No of landslide**	**% of landslide**	**Information value**
1	Aspect	Flat	50775	15.52619	37	12.25166	-0.10287
		North	20596	6.297932	18	5.960265	-0.02393
		Northeast	23033	7.043128	6	1.986755	-0.54962
		East	29585	9.046626	18	5.960265	-0.18122
		Southeast	30275	9.257617	32	10.59603	0.058644
		South	29735	9.092494	28	9.271523	0.008468
		Southwest	43547	13.31599	58	19.2053	0.159048
		West	52170	15.95276	65	21.52318	0.130071
		Northwest	47312	14.46726	40	13.24503	-0.03833
2	Curvature	Concave	88879	27.01489	90	29.80132	0.042632
		Flat	153209	46.56809	112	37.08609	-0.09888
		Convex	86912	26.41702	100	33.11258	0.098109
3	Distance to Lineament	0-380	133368	40.52137	79	26.15894	-0.19006
		380-834	97651	29.66943	87	28.80795	-0.0128
		834-1400	55725	16.931	53	17.54967	0.015586
		1400-2300	29167	8.861848	48	15.89404	0.25371
		>2300	13219	4.016346	35	11.5894	0.46023
4	Distance to stream	0-240	101498	30.83827	82	27.15232	-0.05528
		240-510	88029	26.74597	111	36.75497	0.138058
		520-810	72361	21.98554	75	24.83444	0.052917
		820-1200	47723	14.49974	27	8.940397	-0.21
		>1300	19519	5.930483	7	2.317881	-0.408
5	Elevation	1600-1900	18822	5.720973	47	15.56291	0.434621

		1900-2200	21998	6.686322	71	23.50993	0.546064
		2200-2300	25127	7.637386	64	21.19205	0.443228
		2300-2500	39111	11.88784	46	15.23179	0.107648
		2500-2700	51862	15.76353	31	10.2649	-0.1863
		2700-2800	50580	15.37386	13	4.304636	-0.55285
		2800-3000	43097	13.09939	15	4.966887	-0.42117
		3000-3100	49777	15.12979	4	1.324503	-1.05778
		>3100	28626	8.700912	11	3.642384	-0.37818
6	Lithology	Alkali basalt	8408	3.136167	89	29.4702	0.972984
		Muscovite-biotite granite	6065	2.262232	13	4.304636	0.279399
		Migmatite and migmatized biotite paragneiss	35737	13.32983	12	3.97351	-0.52565
		Rhyolite lava	22281	8.310767	62	20.5298	0.392744
		Aplite and pegmatite	68	0.025364	13	4.304636	2.229721
		Trachyte to trachybasalt	88826	33.13191	14	4.635762	-0.85413
		Alkali basalt	38535	14.37348	19	6.291391	-0.35882
		Colluvial sediments	578	0.215593	77	25.49669	2.07285
		Amphibolite	389	0.145096	1	0.331126	0.358337
		Fluvial sediments	1480	0.552037	1	0.331126	-0.22198
		Rhyolitic ignimbrite	65731	24.51753	1	0.331126	-1.86948
7	Landuse Landcover	Dense forest	39063	11.86802	48	15.89404	0.126856
		Agricultural land	217106	65.96059	102	33.77483	-0.29069
		Settlement	2995	0.909933	0	0	0
		Range land	69981	21.26145	152	50.33113	0.374244
8	Slope	0-10	68204	20.85571	18	5.960265	-0.54396
		10--17	105351	32.21467	45	14.90066	-0.33485
		17-24	82939	25.36144	91	30.13245	0.074861
		24-32	51535	15.75859	92	30.46358	0.286264
		>32	18999	5.809594	56	18.54305	0.504035
9	Soil	Nitisols	168706	51.27312	144	47.68212	-0.03153
		Alisols	93823	28.51468	45	14.90066	-0.28186
		Regosols	6624	2.013166	101	33.44371	1.220435

		Cambisols	46907	14.25597	7	2.317881	-0.78891
		Luvisols	11464	3.484138	5	1.655629	-0.32313
		Fluvisols	1510	0.458919	0	0	0
10	Rainfall	1100-1200	108767	33.04923	37	12.25166	-0.43097
		1200-1300	69195	21.02514	61	20.19868	-0.01742
		1300-1400	71086	21.59973	55	18.21192	-0.07409
		1400-1500	61106	18.56727	40	13.24503	-0.1467
		1500-1600	11435	3.474564	34	11.25828	0.510572
		1600-1800	5134	1.559984	39	12.91391	0.917938
		> 1800	2383	0.724083	36	11.92053	1.216507

The mean information values obtained from the data were arranged in descending order. Parameters with higher mean values were regarded as having a greater impact, whereas those with lower or negative values were seen as having less influence. Among these, Rainfall had the highest mean information value at 0.282264, and Lithology had the second highest at 0.225090 as shown on table 5.

Table 5: Factors influencing rank based on their mean information values

Parameters	Mean information values	Rank
Rainfall	0.282264	High influence
Lithology	0.225090	High influence
DTL	0.105333	Moderate influence
LULC	0.070136	Moderate influence
Curvature	0.013955	Low influence
Slope	-0.002730	Low influence
Soil	-0.041000	Low influence
Aspect	-0.059972	Low influence
DTS	-0.096462	Low influence
Elevation	-0.118301	Low influence

5.5 Relationship between landslide and causative factor

In this study, the relationships between ten potential causes of landslides were analyzed using the statistical information value (IV) method (appendix 4). The study explored the connection between landslides and various classes of factors, including slope, aspect, curvature, distance to streams, distance to lineaments, rainfall, lithology, and land use/land cover. The results are depicted in Figure 16.

The analysis of the landslide causative factors reveals that landslides are most common on west-facing slopes, flat or convex terrains, and at moderate elevations (1900-2220 meters). Proximity to lineaments (380-840 meters) and streams (240-510 meters) significantly increases landslide susceptibility, indicating the importance of geological fractures and water influence. Lithologically, Alkali basalt and colluvial sediments are the most vulnerable, while land use patterns show that rangeland and agricultural land are more prone to landslides compared to dense forests. Slopes between 17-32° are particularly susceptible, and soils like Nitosols and Alisols have the highest occurrence rates, likely due to their physical properties. Moderate annual rainfall (1300-1400 mm) also correlates with higher landslide frequencies, underscoring the intricate interplay between topography, geology, land use, and climatic factors in landslide occurrences. This comprehensive understanding is crucial for targeted mitigation efforts.

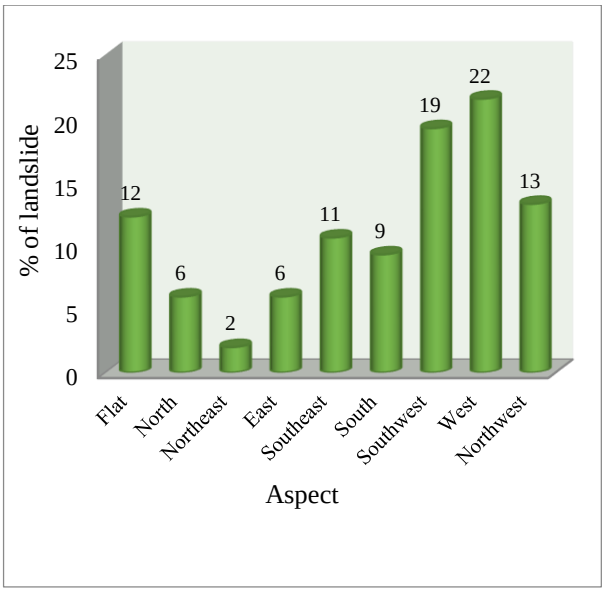
% of landslide
25
20
15
10
5
0
12
6
2
6
11
9
19
22
13
Flat
North
Northeast
East
Southeast
South
Southwest
West
Northwest
Aspect

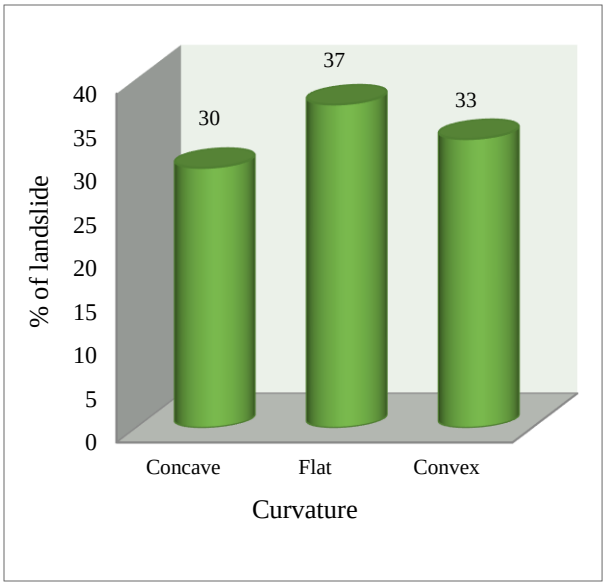
% of landslide
40
35
30
25
20
15
10
5
0
30
37
33
Concave
Flat
Convex
Curvature

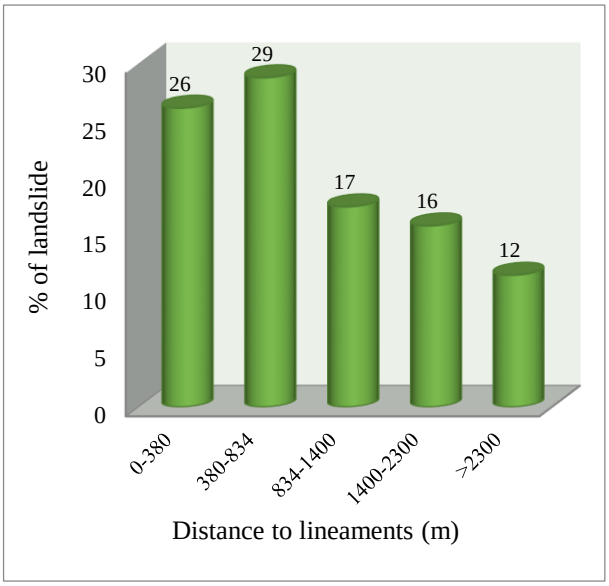
% of landslide
30
25
20
15
10
5
0
26
29
17
16
12
0-380
380-834
834-1400
1400-2300
>2300
Distance to lineaments (m)

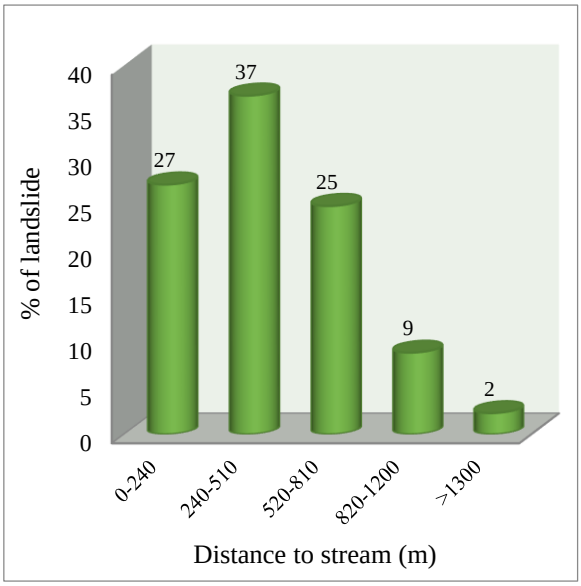
% of landslide
40
35
30
25
20
15
10
5
0
27
37
25
9
2
0-240
240-510
520-810
820-1200
>1300
Distance to stream (m)

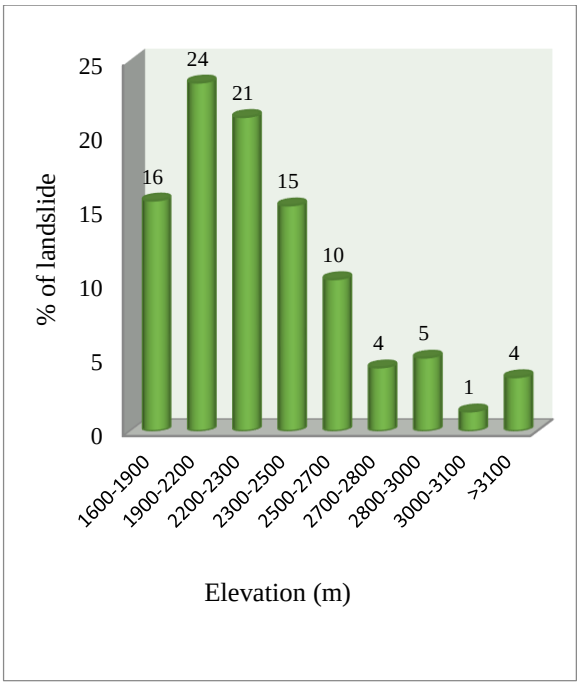
% of landslide
25
20
15
10
5
0
16
24
21
15
10
4
5
1
4
1600-1900
1900-2200
2200-2300
2300-2500
2500-2700
2700-2800
2800-3000
3000-3100
>3100
Elevation (m)

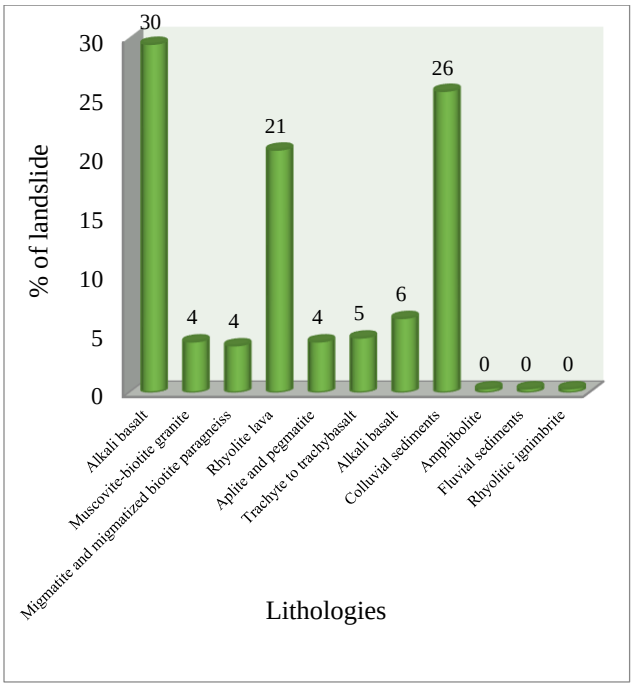
% of landslide
30
25
20
15
10
5
0
30
4
4
21
4
5
6
26
0
0
0
Alkali basalt
Muscovite-biotite granite
Migmatite and migmatized biotite paragneiss
Rhyolite lava
Aplite and pegmatite
Trachyte to trachybasalt
Alkali basalt
Colluvial sediments
Amphibolite
Fluvial sediments
Rhyolitic ignimbrite
Lithologies

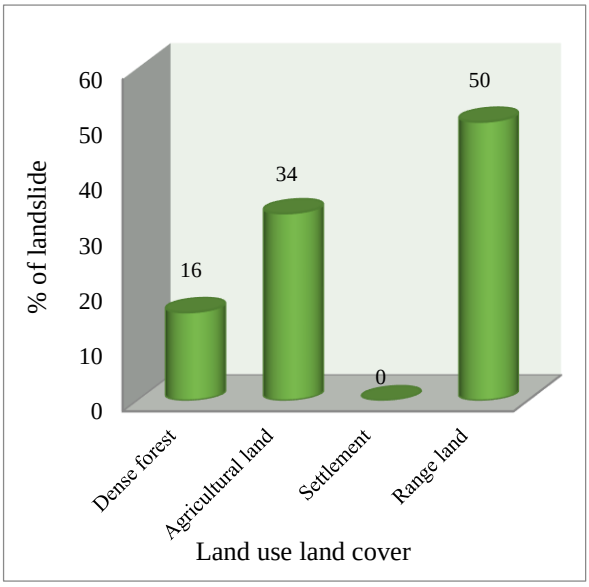
% of landslide
60
50
40
30
20
10
0
16
34
0
50
Dense forest
Agricultural land
Settlement
Range land
Land use land cover

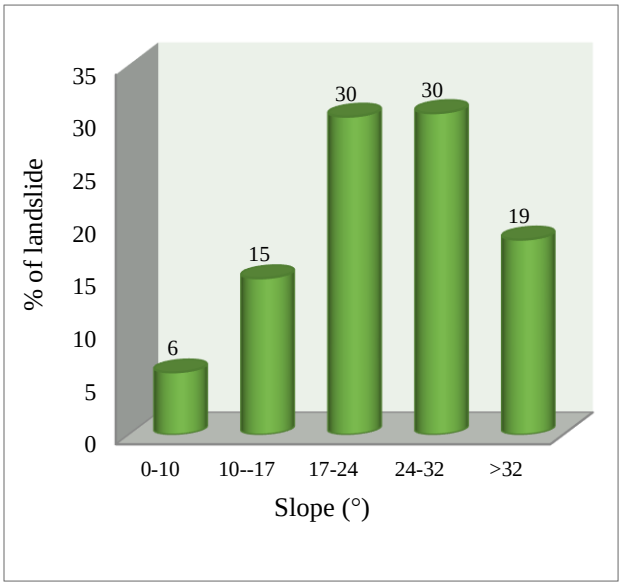
% of landslide
35
30
25
20
15
10
5
0
6
15
30
30
19
0-10
10--17
17-24
24-32
>32
Slope (°)

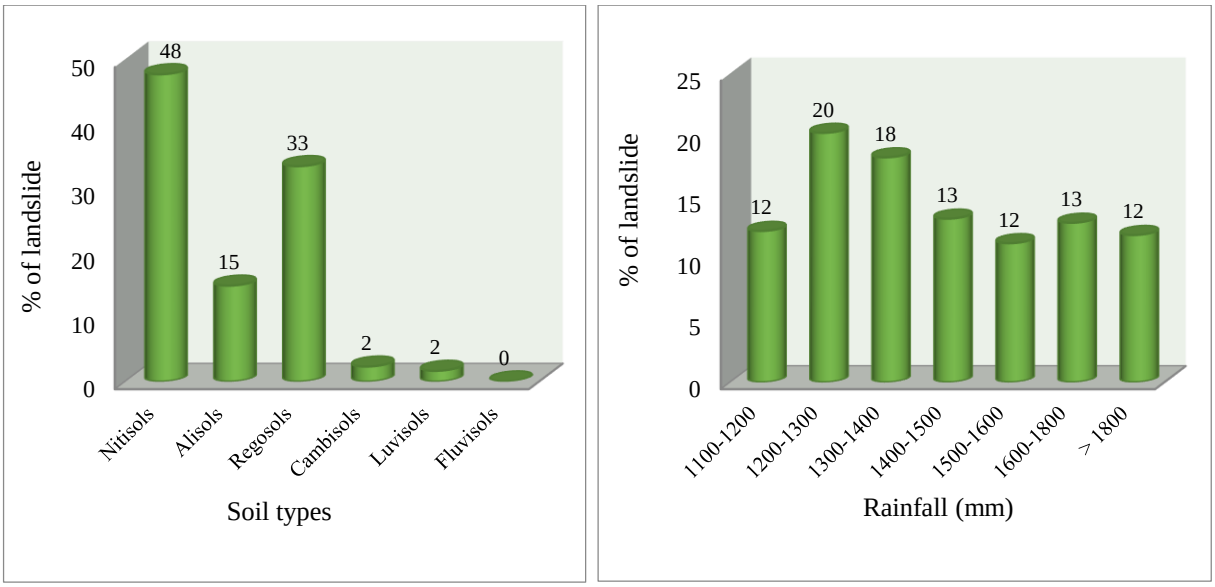

Figure 16: Relationship of landslide occurrence with the causative factors

5.6 Landslide Susceptibility Mapping

Mapping the susceptibility to landslides is an essential technique for evaluating and reducing the hazards of landslides. To identify places prone to landslides, a variety of characteristics will be analyzed, including geological, morphological, hydrological, vegetation cover, land use, and historical landslide occurrences (Ayalew and Yamagishi, 2005). All of these elements work together to cause slope instability and raise the risk of landslides. These parameters are statistically evaluated and combined to create susceptibility maps using remote sensing, geographic information systems (GIS), statistical modeling, and machine learning techniques (Van Den Eeckhaut et al., 2012). Susceptibility maps provide important information for managing catastrophe risk, planning land use, and putting mitigation plans in place to lessen the effects of landslides on infrastructure and communities (Lee et al., 2004). Decision-makers can allocate resources more wisely and create focused remedies to landslide threats by identifying locations highly susceptible to natural disasters.

The application of machine learning algorithms, including Random Forest (RF) and Support Vector Machines (SVM), has transformed the mapping of landslide susceptibility and has several advantages over more conventional methods. Machine learning algorithms like SVM and RF can handle complicated spatial relationships and non-linear patterns associated with

landslide susceptibility factors, unlike traditional methods that rely on simplified statistical approaches or deterministic models (Pradhan et al., 2011). The complex interdependencies between different factors may be difficult for traditional methodologies to capture, which could result in less accurate susceptibility estimates. By combining several predictor variables at once and adaptively learning from training data, SVM and RF, on the other hand, are excellent at modeling such complexities and provide more trustworthy and durable susceptibility maps (Bui et al., 2016). These algorithms improve land use planning choices and disaster risk management strategies by using the power of machine learning to increase the precision and efficiency of landslide susceptibility mapping.

5.6.1 Landslide Susceptibility Mapping Using SVM

The susceptibility map was classified using the natural breaks approach, dividing the landslide susceptibility into five categories. The SVM map of landslide susceptibility values was segmented into five areas: very low, low, moderate, high, and very high as shown in Figure 17. According to the model-generated map, the areas are distributed among the five susceptibility classes as follows: 16% are classified as "very low," 15% as "low," 19% as "moderate," 21% as "high," and 29% as "very high" (Table 6). This indicates that approximately 27% of the study area is categorized as "high" and "very high" susceptibility, suggesting a substantial risk of landslides in these regions.

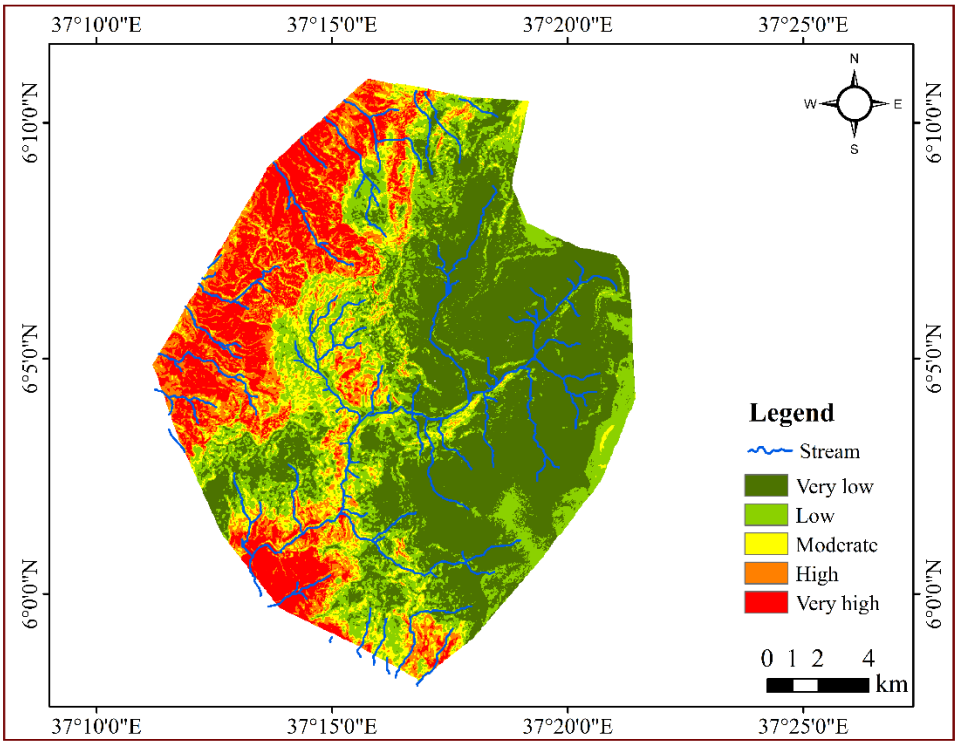

Figure 17: Landslide susceptibility map using SVM

5.6.2 Landslide Susceptibility Mapping Using RF

The susceptibility map was classified using the natural breaks approach, dividing the landslide susceptibility into five categories. The SVM map of landslide susceptibility values was segmented into five areas: very low, low, moderate, high, and very high as shown in Figure 18. The model-generated map shows the distribution of areas among the five susceptibility classes as follows: 11% are "very low," 14% are "low," 17% are "moderate," 23% are "high," and 35% are "very high" (Table 6). This means that about 58% of the study area falls into the "high" and "very high" categories, indicating a significant risk of landslides in these regions.

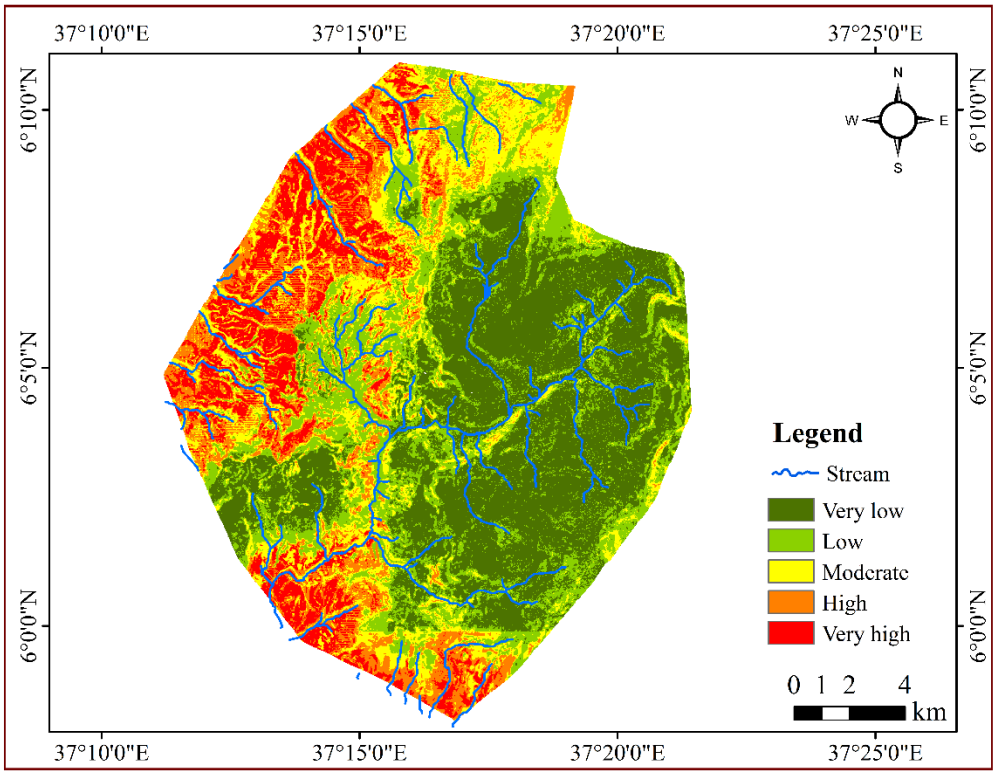

Figure 18: Landslide susceptibility map using RF

Table 6: Landslide susceptibility classes of SVM and RF model

SVM				RF			
Susceptibility classes	pixels	Area (km^2)	Area (%)	Susceptibility classes	Pixels	Area (km^2)	Area (%)
Very low	134231	32.75476	16	Very low	112223	31.58435	11
Low	69552	33.89868	15	Low	74839	42.08995	14
Moderate	47038	42.64595	19	Moderate	56583	50.54071	17
High	38068	62.50237	21	High	47017	66.37081	23
Very high	36843	121.0033	29	Very high	35070	102.2035	35

5.7 Validation of the models

The combination of landslide susceptibility and inventory maps is commonly used to evaluate the quality of a landslide susceptibility model. In this research, out of 302 identified landslides and an equal number of 302 non-landslide locations, 423 (70%) were used to create the susceptibility maps, while 181 (30%) were used for model testing. The SVM and RF algorithms were employed to assess landslide susceptibility. For validation, the area under the curve (AUC) was utilized to measure both predictive and success rates using the 30% validation landslides in the susceptibility maps. The success rate was estimated by comparing the training dataset with the susceptibility classes, and the predictive rate was calculated by comparing the validation dataset with the susceptibility classes.

5.8 Area under the Curve (AUC)

5.8.1 Success and Predictive Rate Curve

The results indicated that both SVM and RF models exhibit strong performance. Specifically, the SVM model achieved a success rate of 0.816 and a predictive rate of 0.809, while the Random Forest (RF) model demonstrated slightly better performance with a success rate of 0.821 and a predictive rate of 0.811. As illustrated in Figure 19, these results suggest that both models demonstrate commendable effectiveness.

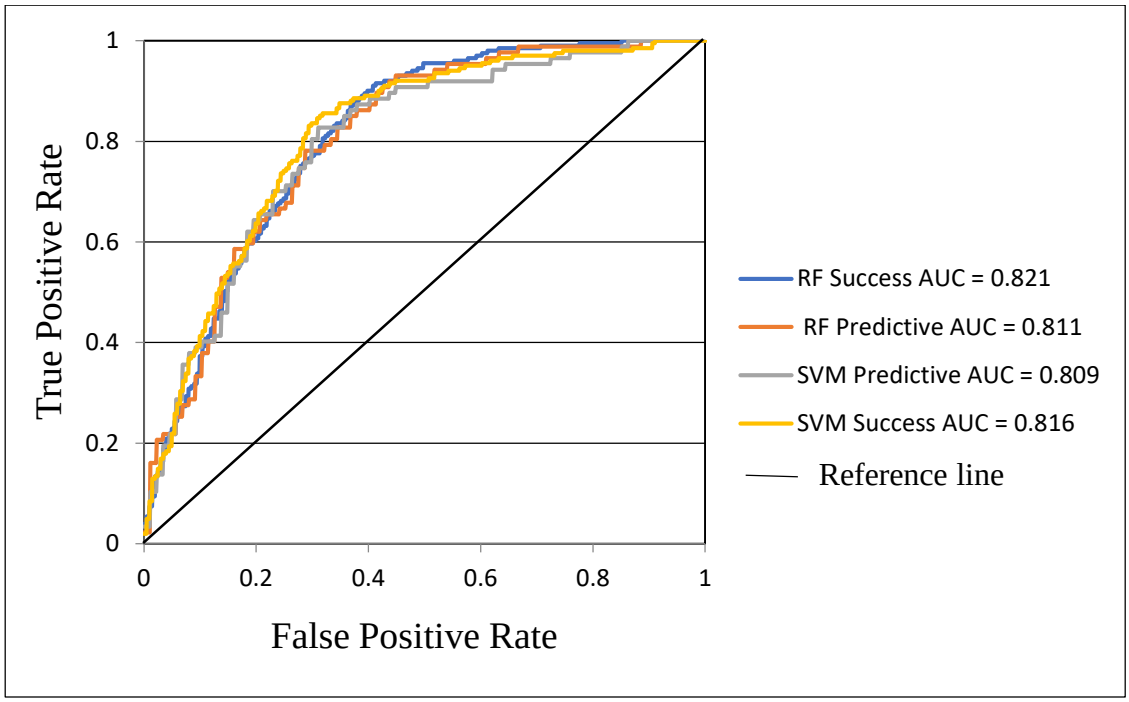

Figure 19: Success and predictive rate of SVM and RF

CHAPTER SIX

6. CONCLUSIONS AND RECOMMENDATION

6.1 Conclusions

landslide susceptibility mapping was conducted for the Halila catchment in the Gamo Zone of Southern Ethiopia using machine learning algorithms, specifically Support Vector Machine (SVM) and Random Forest (RF), integrated with GIS techniques. Key environmental factors contributing to landslides, such as slope, elevation, aspect, curvature, lithology, soil type, proximity to lineaments, distance to streams, rainfall, and land use/cover, were analyzed to understand their influence on slope instability. Heavy rainfall was identified as the primary trigger of landslides in the area, compounded by the region's steep slopes, weak geological formations, and human activities such as agriculture and construction on vulnerable slopes.

The SVM and RF models were trained on a landslide inventory compiled from historical and recent data, with 70% of the data used for training and 30% for validation. The Random Forest model achieved higher accuracy than the RF, with an Area Under the Curve (AUC) success rate of 0.821 and a predictive rate of 0.811, slightly outperforming the SVM model, which recorded an AUC success rate of 0.816 and a predictive rate of 0.809. These results indicate that both models effectively capture the complex relationships between the causative factors and landslide occurrences, with Random Forest providing a marginally better fit for susceptibility mapping in this context.

The resulting landslide susceptibility maps classify the study area into five susceptibility classes: very low, low, moderate, high, and very high, providing a clear spatial representation of landslide-prone zones. These maps serve as valuable tools for land-use planning and hazard mitigation, enabling decision-makers to prioritize interventions in high-risk areas.

6.2 Recommendations

- **Land-Use Zoning and Regulations**: It is recommended that strict land-use zoning and regulations be implemented in the Halila catchment, as human activities particularly agriculture and construction on steep slopes have been identified as factors that exacerbate landslide risks.

High-susceptibility zones where agricultural expansion and road construction have contributed to previous landslide incidents would particularly benefit from these regulations, reducing the potential for soil destabilization.

- **Vegetative and Structural Slope Stabilization**: The unstable, weathered basalts and ignimbrites of the Halila catchment, as highlighted in the study, make the area prone to landslides. To address this, deep-rooted vegetation should be planted on vulnerable slopes, and critical areas should be reinforced with retaining walls, terracing, or other structural support. Past slope failures due to weak geological formations could be mitigated through these stabilization efforts.

- **Enhanced Drainage and Water Management Systems**: Heavy rainfall has been established as a primary trigger for landslides in the Gamo Zone, with incidents often occurring during the wet season. Improved drainage systems should be installed on susceptible slopes to manage water flow effectively, reduce soil saturation, and alleviate one of the region's key landslide triggers.

- **Early Warning and Monitoring Systems**: The study's machine learning models demonstrate the potential for real-time monitoring and early warning systems to predict landslide susceptibility. Considering the frequent, severe landslides due to heavy rainfall in the Gamo Zone, it is advised that early warning systems based on susceptibility predictions and real-time weather data be deployed, providing residents critical time for evacuation or precautionary measures.

- **Public Awareness and Preparedness Programs**: Given the area's history of severe landslides and associated loss of life and infrastructure, public awareness and preparedness programs should be conducted. Communities in landslide-prone zones would benefit from training on evacuation procedures and safety measures, improving resilience and readiness for future landslide events.

REFERENCE

Abdi, A. (2016). Three types of machine learning algorithms. Research Gate, November(November), 1–27. https://doi.org/10.13140/RG.2.2.26209.10088

Abebe, B., Dramis, F., Fubelli, G., Umer, M., & Asrat, A. (2010). Landslides in the Ethiopian highlands and the Rift margins. Journal of African Earth Sciences, 56(4–5), 131–138. https://doi.org/10.1016/j.jafrearsci.2009.06.006

Addis, A. (2023). GIS-Based Landslide Susceptibility Mapping Using Frequency Ratio and Shannon Entropy Models in Dejen District, Northwestern Ethiopia. Journal of Engineering (United Kingdom), 2023, 25–29. https://doi.org/10.1155/2023/1062388

Agrawal, N., & Dixit, J. (2023). GIS-based landslide susceptibility mapping of the Meghalaya-Shillong Plateau region using machine learning algorithms. Bulletin of Engineering Geology and the Environment, 82(5), 1–19. https://doi.org/10.1007/s10064-023-03188-2

Ajayi, E. O., Akin-Idowu, P. E., Aderibigbe, O. R., Ibitoye, D. O., Afolayan, G., Adewale, O. M., Adesegun, E. A., & Ubi, B. E. (2016). We are IntechOpen , the world ' s leading publisher of Open Access books Built by scientists , for scientists TOP 1 %. Intech, 11(tourism), 13. https://www.intechopen.com/books/advanced-biometric-technologies/liveness-detection-in-biometrics

Amare, K., Mebrahtu, G., & Gebremiceal, A. (2018). Landslide characterization and distribution in northern Ethiopia: a case study from the Adishu area. Bulletin of Engineering Geology and the Environment, 77(2), 581–593. https://doi.org/10.1007/s10064-017-1064-x

Anbalagan, R., Kumar, R., Lakshmanan, K., Parida, S., & Neethu, S. (2015). Landslide hazard zonation mapping using frequency ratio and fuzzy logic approach, a case study of Lachung Valley, Sikkim. Geoenvironmental Disasters, 2(1). https://doi.org/10.1186/s40677-014-0009-y

Ayalew, L. (1999). The effect of seasonal rainfall on landslides in the highlands of Ethiopia. Bulletin of Engineering Geology and the Environment, 58(1), 9–19. https://doi.org/10.1007/s100640050065

Chen, W., Xie, X., Wang, J., Pradhan, B., Hong, H., Bui, D. T., Duan, Z., & Ma, J. (2017). A comparative study of logistic model tree, random forest, and classification and

regression tree models for spatial prediction of landslide susceptibility. Catena, 151, 147–160. https://doi.org/10.1016/j.catena.2016.11.032

Chen, Z., & Wang, J. (2007). Landslide hazard mapping using logistic regression model in Mackenzie Valley, Canada. Natural Hazards, 42(1), 75–89. https://doi.org/10.1007/s11069-006-9061-6

Cruden, D. M., & Varnes, D. J. (1996). Landslide types and processes. Special Report - National Research Council, Transportation Research Board, 247(February), 36–75.

Csc, D. (2012). Machin learnning.pdf.

Du, G. liang, Zhang, Y. shuang, Iqbal, J., Yang, Z. hua, & Yao, X. (2017). Landslide susceptibility mapping using an integrated model of information value method and logistic regression in the Bailongjiang watershed, Gansu Province, China. Journal of Mountain Science, 14(2), 249–268. https://doi.org/10.1007/s11629-016-4126-9

Firomsa, M., & Abay, A. (2018). Landslide assessment and hazard zonation in ebantu district of oromia regional state western ethiopia. Advances in Science, Technology and Innovation, 1861–1863. https://doi.org/10.1007/978-3-319-70548-4_538

Fisiche, S., & Laterina, V. (2018). Version of Record: https://www.sciencedirect.com/science/article/pii/S1464343X18303868.

Food and Agriculture Organization of the United Nations. (1986). Ethiopian Highlands Reclamation Study, Final Report Vol. 1.

Getachew, N., & Meten, M. (2021). Weights of evidence modeling for landslide susceptibility mapping of Kabi-Gebro locality, Gundomeskel area, Central Ethiopia. Geoenvironmental Disasters, 8(1). https://doi.org/10.1186/s40677-021-00177-z

Hammad Khaliq, A., Basharat, M., Talha Riaz, M., Tayyib Riaz, M., Wani, S., Al-Ansari, N., Ba Le, L., & Thi Thuy Linh, N. (2023). Spatiotemporal landslide susceptibility mapping using machine learning models: A case study from district Hattian Bala, NW Himalaya, Pakistan. Ain Shams Engineering Journal, 14(3), 101907. https://doi.org/10.1016/j.asej.2022.101907

Highland, L. M., & Bobrowsky, P. (2008). The landslide Handbook - A guide to understanding landslides. US Geological Survey Circular, 1325, 1–147.

Honavar, V., & De La Higuera, C. (2001). Machine learning: Introduction. Machine Learning, 44(1–2), 5–7. https://doi.org/10.1023/A:1010812817165

Hussain, M. A., Chen, Z., Kalsoom, I., Asghar, A., & Shoaib, M. (2022). Landslide Susceptibility Mapping Using Machine Learning Algorithm: A Case Study Along Karakoram Highway (KKH), Pakistan. Journal of the Indian Society of Remote Sensing, 50(5), 849–866. https://doi.org/10.1007/s12524-021-01451-1

Ismail, E. H., Rogers, J. D., Ahmed, M. F., Usery, E. L., & Abdelsalam, M. G. (2018). Landslide susceptibility mapping of Blue Nile and Tekeze River Basins using oblique rainfall-aspect rasters. Bulletin of Engineering Geology and the Environment, 77(4), 1311–1329. https://doi.org/10.1007/s10064-017-1033-4

Jin, Z., Shang, J., Zhu, Q., Ling, C., Xie, W., & Qiang, B. (2020). RFRSF: Employee Turnover Prediction Based on Random Forests and Survival Analysis. Lecture Notes in Computer Science (Including Subseries Lecture Notes in Artificial Intelligence and Lecture Notes in Bioinformatics), 12343 LNCS, 503–515. https://doi.org/10.1007/978-3-030-62008-0_35

Kanungo, D. P., Sarkar, S., & Sharma, S. (2011). Combining neural network with fuzzy, certainty factor and likelihood ratio concepts for spatial prediction of landslides. Natural Hazards, 59(3), 1491–1512. https://doi.org/10.1007/s11069-011-9847-z

Mahesh, B. (2019). Machine Learning Algorithms - A Review | Enhanced Reader. October. https://doi.org/10.21275/ART20203995

Mallick, J., Alqadhi, S., Talukdar, S., Sarkar, S. K., Roy, S. K., & Ahmed, M. (2022). Modelling and mapping of landslide susceptibility regulating potential ecosystem service loss: an experimental research in Saudi Arabia. Geocarto International, 37(25), 10170–10198. https://doi.org/10.1080/10106049.2022.2032393

Manderso, D. A. (2021). Landslide Hazard Zonation and Evaluation Around Debre Markos Town , NW Ethiopia — A GIS-Based.

Martínek, K., Verner, K., Hroch, T., Megerssa, L. A., Buriánek, D., Muluneh, A., Kalinová, R., & Yakob, M. (2021). Main Ethiopian Rift landslides formed in contrasting geological. January. https://doi.org/10.5194/nhess-2020-420

Martínek, K., Verner, K., Hroch, T., Megerssa, L. A., Kopačková, V., Buriánek, D., Muluneh, A., Kalinová, R., Yakob, M., & Kassa, M. (2021). Main Ethiopian Rift landslides formed in contrasting geological settings and climatic conditions. Natural Hazards and Earth System Sciences, 21(11), 3465–3487. https://doi.org/10.5194/nhess-21-3465-2021

Makonyo, M., & Zahor, Z. (2023). GIS-based analysis of landslides susceptibility mapping: a case study of Lushoto district, north-eastern Tanzania. In Natural Hazards (Vol. 118, Issue 2). Springer Netherlands. https://doi.org/10.1007/s11069-023-06038-2

Mebrahtu, T. K., Banning, A., Girmay, E. H., & Wohnlich, S. (2021). The effect of hydrogeological and hydrochemical dynamics on landslide triggering in the central highlands of Ethiopia. Hydrogeology Journal, 29(3), 1239–1260. https://doi.org/10.1007/s10040-020-02288-7

Merghadi, A., Yunus, A. P., Dou, J., Whiteley, J., ThaiPham, B., Bui, D. T., Avtar, R., & Abderrahmane, B. (2020). Machine learning methods for landslide susceptibility studies: A comparative overview of algorithm performance. Earth-Science Reviews, 207(June), 103225. https://doi.org/10.1016/j.earscirev.2020.103225

Meten, M., PrakashBhandary, N., & Yatabe, R. (2015). Effect of Landslide Factor Combinations on the Prediction Accuracy of Landslide Susceptibility Maps in the Blue Nile Gorge of Central Ethiopia. Geoenvironmental Disasters, 2(1). https://doi.org/10.1186/s40677-015-0016-7

Nikparvar, B., & Thill, J. C. (2021). Machine learning of spatial data. ISPRS International Journal of Geo-Information, 10(9), 1–32. https://doi.org/10.3390/ijgi10090600

OCHA, N. (2020). Ethiopia: 2020 kiremt weather outlook, Floods Update No.3 as Of 18 August 2020 . 3, 1–5.

Oladipupo, T. (2010). Types of Machine Learning Algorithms. New Advances in Machine Learning, February 2010. https://doi.org/10.5772/9385

Parra, F., González, J., Chacón, M., & Marín, M. (2023). Modeling and evaluation of the susceptibility to landslide events using machine learning algorithms in the province of Chañaral , Atacama region , Chile. June.

Popescu, M. E. (2002). Landslide causal factors and landslide remediatial options. 3rd International Conference on Landslides, Slope Stability and Safety of Infra-Structures, 1–21.

Raghuvanshi, T. K., Ibrahim, J., & Ayalew, D. (2014). Slope stability susceptibility evaluation parameter (SSEP) rating scheme - An approach for landslide hazard zonation. Journal of African Earth Sciences, 99(PA2), 595–612. https://doi.org/10.1016/j.jafrearsci.2014.05.004

Sci, I. J., Valley, R., Oyda, Y., Berhane, G., & Regasa, H. (2023). Landslide Threat Evaluation and Zoning in Birbir Mariam District , Gamo. 47–67.

Senaviratna, N. A. M. R., & A. Cooray, T. M. J. (2019). Diagnosing Multicollinearity of Logistic Regression Model. Asian Journal of Probability and Statistics, 5(2), 1–9. https://doi.org/10.9734/ajpas/2019/v5i230132

Shanthamallu, U. S., & Spanias, A. (2022). Introduction to Machine Learning. Synthesis Lectures on Signal Processing, 1–8. https://doi.org/10.1007/978-3-031-03758-0_1

Sharma, L. P., Patel, N., Debnath, P., & Ghose, M. K. (2012). Assessing landslide vulnerability from soil characteristics-a GIS-based analysis. Arabian Journal of Geosciences, 5(4), 789–796. https://doi.org/10.1007/s12517-010-0272-5

Shahzad, N., Ding, X., & Abbas, S. (2022). A Comparative Assessment of Machine Learning Models for Landslide Susceptibility Mapping in the Rugged Terrain of Northern Pakistan. Applied Sciences (Switzerland), 12(5). https://doi.org/10.3390/app12052280

Shano, L., Raghuvanshi, T. K., & Meten, M. (2021). Landslide susceptibility mapping using frequency ratio model: the case of Gamo highland, South Ethiopia. Arabian Journal of Geosciences, 14(7). https://doi.org/10.1007/s12517-021-06995-7

Survey, C. G. (n.d.). Geology , Soil Environment and Hydrogeology of the Sidama Region , Ethiopia.

Thiruvengadam, K., Watson, B., Chinnaiyan, P., & Krishnan, R. (2022). A Review of Statistical Modelling and Machine Learning in Analytical Problems. International Journal of Applied Engineering Research, 17(05), 506–510. https://doi.org/10.37622/ijaer/17.5.2022.506-510

Vařilová, Z., Kropáček, J., Zvelebil, J., Šťastný, M., & Vilímek, V. (2015). Reactivation of mass movements in Dessie graben, the example of an active landslide area in the Ethiopian Highlands. Landslides, 12(5), 985–996. https://doi.org/10.1007/s10346-015-0613-2

Varnes1978_.pdf.fdmdownload. (n.d.).

Wahsington State Dept of Natural Resources. (2017). What are landslides and how do they occur? Washington Geological Survey. https://www.dnr.wa.gov/geology

Woldearegay, K. (2013). Review of the occurrences and influencing factors of landslides in the highlands of Ethiopia: With implications for infrastructural development. Momona Ethiopian Journal of Science, 5(1), 3. https://doi.org/10.4314/mejs.v5i1.85329

Woldearegay, K., Schubert, W., Klima, K., & Mogessie, A. (2006). Failure Mechanisms and Influencing Factors of Landslides Triggered by Heavy Rainfalls in Adishu Area , Northern Ethiopia Properties of rocks and soils. Disaster Mitigation of Debris Flows, Slope Failures and Landslides, 65–71.

Woldearegay, W. (2014). Landslide Related Road Failures in Ethiopia. 1–36.

Wubalem, A., & Meten, M. (2020). Landslide susceptibility mapping using information value and logistic regression models in Goncha Siso Eneses area, northwestern Ethiopia. SN Applied Sciences, 2(5), 1–19. https://doi.org/10.1007/s42452-020-2563-0

Yuan, X., Liu, C., Nie, R., Yang, Z., Li, W., Dai, X., Cheng, J., Zhang, J., Ma, L., Fu, X., Tang, M., Xu, Y., & Lu, H. (2022). A Comparative Analysis of Certainty Factor-Based Machine Learning Methods for Collapse and Landslide Susceptibility Mapping in Wenchuan County, China. Remote Sensing, 14(14). https://doi.org/10.3390/rs14143259

APPENDIX

Appendix 1: A literature review from different Articles

No	Author name	Title of the paper	Area of the study	Influencing factors	ML techniques/ Algorithms
1	(Naeem et al., 2022)	A Comparative Assessment of Machine Learning Models for Landslide Susceptibility Mapping in the Rugged Terrain of Northern Pakistan	Northern Pakistan	Elevation Slope Aspect TWI TPI Distance to drainage Distance to fault NDVI Rainfall Land use land cover Geological layer	RF SVM maxent GBM LR
2	(Israr et al., 2022)	An Integrated Approach of Machine Learning, Remote Sensing, and GIS Data for the Landslide Susceptibility Mapping	Pakistan	Aspect Curvature Elevation Lithology NDVI NDWI TRI Plane Curvature Profile Curvature Slope Fault Roads Soil LCCS	LR Linear regression SVM
3	(Agrawa & JDixit, 2023)	GIS-based landslide susceptibility mapping of the Meghalaya-Shillong Plateau region using machine learning algorithms	India	Aspect Curvature Distance from fault Distance from river	ANN XGBoost KNN RF

				Distance from roads Elevation Geomorphology LULC NDVI Rainfall Slope SPI Soil texture TWI	SVM
4	(Jamali., 2020)	Landslide hazard risk modeling in north-west of Iran using optimized machine learning models	north-west of Iran	Elevation Slope Aspect Curvature Rainfall Distance to stream Lithology Distance to fault LULC Distance to road	RF XGBoost SSAMLP MVOMLP
5	(Muhammad et al., 2022)	Landslide Susceptibility Mapping Using Machine Learning Algorithm:	Pakistan	Slope Elevation Aspect TWI Curvature Roughness Distance to river Lithology NDVI Landcover	RF XGBoost KNN
6	(Francisco et al., 2023)	Modeling and evaluation of the susceptibility to landslide events using machine learning algorithms	Chile	Aspect Elevation Hillshade Slope Planar curvature	SVM RF LR XGBoost

				Ruggedness TRI TPI Slope length Melton Convergence index VD LS Geomorphons TWI NDVI GNDVI EVI NDMI NDGI NBRI	
7	(Xinyue et al., 2022)	A Comparative Analysis of Certainty Factor-Based Machine Learning Methods for Collapse and Landslide Susceptibility Mapping	China	Slope Aspect Curvature Terrain relief TWI Lithology Soil type Distance to fault Rainfall Distance to river PGA NDVI Land use	LR SVR RF
8	(Ahmad et al., 2022)	Spatiotemporal landslide susceptibility mapping using machine learning models	Pakistan	LULC NDVI Slope Aspect Elevation Curvature	LR RF

				Profile curvature Plain curvature TWI Lithology Faults Distance to road Distance to stream	
9	(Nhu et al., 2019)	Landslide Susceptibility Mapping Using Machine Learning Algorithms and Remote Sensing Data	Cameron	Slope Aspect Elevation Curvature Profile curvature Distance to river River density TWI SPI Lithology distance to fault NDVI Land cover Distance to road Road density Soil Rainfall	AdaBoost (AB), alternating decision tree (ADTree)
10	(Lee et al., 2016)	A Support Vector Machine for Landslide Susceptibility Mapping	Korea	Elevation Slope gradient Slope aspect Profile curvature Plan curvature Topographic wetness index	SVM

				Elevation Slope gradient Slope aspect Profile curvature Plan curvature Topographic wetness index Elevation Slope gradient Slope aspect Profile curvature Plan curvature Topographic wetness index Land cover	
11	(Napoli et al., 2020)	Machine Learning ensemble modelling as a tool to improve landslide susceptibility mapping reliability	Northern Italy	Rainfall Topography Geology Land Cover/Land Use Soil Landform Distance to Roads Distance to Rivers/Streams Distance to Fault Lines Land Transformation Previous Landslides Aspect Elevation	Ensemble of Artificial Neural Network Generalized Boosting Model Maximum Entropy Machine Learning Algorithms
12	(Zhou et al., 2018)	Landslide susceptibility modeling applying machine learning methods	China	Altitude (Elevation) Distance to Rivers Lithology (Interbeds of mudstone and sandstone) Distance to Roads	SVM ANN LR

				Slope Rainfall Land Use and Urbanization Monsoon Season	
13	(Pham et al., 2016)	A comparative study of different machine learning methods for landslide susceptibility assessment	India	Slope Angle Slope Aspect Elevation Curvature Plan Curvature Profile Curvature Soil Type Land Cover Mean Annual Rainfall Distance to Lineaments Distance to Roads Distance to Rivers Lineament Density Road Density River Density	SVM LR Fisher's Linear Discriminant Analysis (FLDA) Bayesian Network (BN) NB
14	(Bui et al., 2019)	Spatial prediction of shallow landslide using Bat algorithm optimized machine learning approach	Vietnam	Slope Angle Slope Length Slope Aspect Curvature Elevation Topographic Wetness Index Stream Power Index Sediment Transport Index Valley Depth Distance to Rivers Distance to Roads Distance to Faults Land Use	Relevance Vector Machine ANN LR SVM

				Soil Type	
15	(Zhu et al., 2017)	Comparison of two optimized machine learning models for predicting displacement of rainfall-induced landslide	China	Rainfall Geological Settings Hydrological Conditions Slope Surface Angle	SVM Double Exponential Smoothing (DES)
16	(Hu et al., 2020)	Machine learning and fractal theory models for landslide susceptibility mapping	China	Elevation slope aspect SOA SOS geological lithology distance to faults land use precipitation NDVI curvature	SVM) Naïve Bayes (NB) model
17	(Nguyen et al., 2020)	Hybrid Machine Learning Approaches for Landslide Susceptibility Modeling	northeast Vietnam	Slope Distance to Faults Curvature Slope Aspect Map Slope Length Distance to Rivers Elevation Distance to Roads Lithology Valley Depth Topographic Wetness Index (TWI) Terrain Roughness Index (TRI)	Neuro Fuzzy Inference System Artificial Neural Networks) Decision Trees
18	(Yao et al., 2008)	Landslide susceptibility mapping based on Support Vector Machine	China	Slope Angle Slope Aspect Elevation Profile Curvature of Slope	SVM

				Lithology Vegetation Cover Topographic Wetness Index (TWI)	
19	(Ageenko et al., 2022)	Landslide Susceptibility Mapping Using Machine Learning	Eastern Denmark	Elevation Terrain Roughness Index (TRI) Standard Deviation of Slope Distance from the Coast Distances from Roads Distances from Railroads Distances from Quarries	RF SVM LR
20	(YAO & DAI, 2006)	Support vector machine modeling of landslide susceptibility using a GIS: A case study	Hong Kong	Slope Aspect Elevation Slope Gradient Profile of Slope Plan of Slope Curve of Slope Vegetation Cover Lithology	SVM

Appendix 2A: Annual rainfall data of each station

Stations	2013	2014	2015	2016	2017	2018	2019	2020	2021	2022
Arbaminch	1061.1	866.2	1121.3	795.1	752.6	787.2	1866.9	1241	860.35	502.2
Arfaide	628.1	976.1	1065	636.5	890.75	980.2	933.95	1391.7	887.35	528.4
Laska	1734.5	1100.4	865.4	934.6	623.4	413.5	723.6	345	435	234.3
Kemba	869.35	1498.9	1576.7	1108.4	1694.35	2160.4	1501.5	1806.6	1392.05	1432.3
Beza	1123.3	1078.5	912.5	1020.7	1653.6	1654.4	1132.2	1321.2	721.2	623.2
Garassee	1318.35	1207.63	1513.48	1139.06	1165.42	1207.6	1434.37	2030.26	1416.54	1104.32
Arguba	1722.7	914.2	983.4	774.6	907.8	959.95	845.7	832.65	358.55	408.6

Appendix 2B: Maximum rainy months rainfall data of each station

Months	**Arbaminch**	**Arfaide**	**Laska**	**Kemba**	**Beza**	**Garassee**	**Arguba**
Jun	142.11	44.05	65.695	119.85	91.6	74.89	101.254
Jul	169.64	183.6	89.16875	286.735	201.805	282.886	176.68
Aug	145.42	98.51	167.44	256.975	130.73	213.845	113.955
Sep	67.86	89.28	63.935	182.7111	181.65	92.957	76.09375
Oct	151.33	100.43	111.55	176.4889	147.5	186.27	107

Appendix 3: Landslide inventory data of the Study area

No	Easting	Northing	Mode of failure
1.	37.23462994330	6.13826400173	Earth slide
2.	37.26324555660	6.00312870849	Earth slide
3.	37.25305135710	6.05714663886	Earth slide
4.	37.25525043290	6.08138170942	Debris slide
5.	37.23077423950	6.02204704979	Earth slide
6.	37.26197311090	6.12230494753	Rock slide
7.	37.23236779620	5.99984286509	Earth slide
8.	37.23096194570	6.00248580835	Earth slide
9.	37.22911554830	6.00261951391	Earth slide
10.	37.22987898680	5.99805369127	Earth slide
11.	37.22068022350	6.01291310970	Earth slide
12.	37.23901471370	6.00810456616	Earth slide
13.	37.23705331880	6.00882327167	Earth slide
14.	37.24039749360	6.00705551360	Earth slide
15.	37.24248800510	6.00543375050	Earth slide
16.	37.24231224710	5.98938586601	Rock slide
17.	37.24555767720	6.00986317918	Earth slide
18.	37.23564420990	6.00669371081	Earth slide
19.	37.23119235990	5.99927493476	Earth slide
20.	37.22613592970	6.01574523287	Earth slide
21.	37.22146901750	6.01755254126	Debris flow
22.	37.22410650410	6.01815236669	Earth slide
23.	37.24758107330	6.13798685781	Earth slide
24.	37.24919136160	6.13662329414	Earth slide
25.	37.21862050490	6.01152272873	Earth slide
26.	37.24691844590	6.12787272344	Debris flow
27.	37.24717304900	6.13241009677	Earth slide
28.	37.24788243400	6.13037282201	Earth slide
29.	37.24198777250	6.13780565829	Debris flow
30.	37.24261599040	6.14114154278	Earth slide
31.	37.24397436760	6.14506041336	Earth slide
32.	37.23369811250	6.15232201143	Earth slide
33.	37.24645286690	6.14079795327	Debris flow
34.	37.24465607650	6.13761448857	Earth slide
35.	37.26903148030	6.09572245810	Earth slide
36.	37.26416499100	6.11516484619	Earth slide
37.	37.26760508800	6.17190001155	Earth slide
38.	37.26374407590	6.17208472154	Earth slide
39.	37.23782543500	6.15528416817	Earth slide

40.	37.24088681850	6.15836012675	Earth slide
41.	37.20658607590	6.05775333223	Earth slide
42.	37.20064658700	6.07721412544	Earth slide
43.	37.20862388950	6.11104793070	Earth slide
44.	37.23026910800	6.14907736121	Earth slide
45.	37.26453365900	6.16296763661	Earth slide
46.	37.26279648490	6.16773883620	Earth slide
47.	37.26058531250	6.16508629239	Earth slide
48.	37.27116744410	6.16400906403	Earth slide
49.	37.27478252710	6.16984040615	Earth slide
50.	37.24629494970	6.16237142196	Earth slide
51.	37.25204396540	6.16876213216	Transitional slide
52.	37.24986074750	6.16659879277	Earth slide
53.	37.23959021050	6.01270040404	Earth slide
54.	37.24253374560	6.01163291949	Rock slide
55.	37.23535026000	6.01212133409	Earth slide
56.	37.23645855050	6.03186388274	Earth slide
57.	37.23816200290	6.03213816776	Earth slide
58.	37.23575055980	5.99463253551	Earth flow
59.	37.25494455540	6.01008729574	Debris flow
60.	37.24953974010	6.01320454774	Debris flow
61.	37.24686572050	6.03040351128	Earth slide
62.	37.24176603100	6.02833035608	Earth slide
63.	37.22096547720	6.00774029097	Earth slide
64.	37.24582465920	6.00063702206	Earth slide
65.	37.20115185110	6.08718048882	Earth slide
66.	37.19125575840	6.07545163715	Earth slide
67.	37.22850983180	6.11880668960	Rock slide
68.	37.23541076670	6.12083995775	Earth slide
69.	37.22482709480	6.12017542087	Rock slide
70.	37.26256524650	5.98058190652	Earth slide
71.	37.27907856740	5.97329027643	Debris flow
72.	37.29158262300	5.98067645181	Earth slide
73.	37.26083489740	6.12577597218	Earth slide
74.	37.25169903890	6.13433749229	Earth slide
75.	37.26356320840	6.11947289459	Rock slide
76.	37.25536091150	6.11488387492	Earth slide
77.	37.24504748470	6.10789210400	Earth slide
78.	37.24956849800	6.10856665861	Earth slide
79.	37.24398498190	6.09858253856	Earth slide
80.	37.24591680050	6.10132265854	Earth slide

81.	37.23483101090	6.10488449897	Earth slide
82.	37.21380527930	6.11479242238	Earth slide
83.	37.22102522270	6.11097681433	Earth slide
84.	37.21292440100	6.10755737340	Earth slide
85.	37.21072635820	6.10326739086	Earth slide
86.	37.20558159690	6.09863908449	Earth slide
87.	37.20669371550	6.09693770142	Transitional slide
88.	37.21035294150	6.09933820577	Transitional slide
89.	37.21224690760	6.09762730122	Earth slide
90.	37.22052475260	6.10413204458	Rock slide
91.	37.26947715470	6.10024163817	Earth slide
92.	37.26584456700	6.09973896977	Rock slide
93.	37.26270567810	6.17521927636	Debris slide
94.	37.26700170620	6.16888853087	Debris slide
95.	37.26578314390	6.17863257466	Earth slide
96.	37.27122356740	5.97539372012	Earth slide
97.	37.26632210060	5.97882853271	Earth slide
98.	37.27467895930	6.01650747994	Earth slide
99.	37.26453728710	6.10704491779	Earth slide
100.	37.28670351780	6.12805944400	Transitional slide
101.	37.30190168120	6.15234152713	Earth slide
102.	37.27255675210	6.16054286595	Earth slide
103.	37.28526599630	5.97540934906	Earth slide
104.	37.28295633700	5.97394760940	Earth slide
105.	37.28897072490	5.97707330130	Earth slide
106.	37.23671953980	6.02258175071	Rock slide
107.	37.24043381400	6.02052074830	Rock slide
108.	37.24344115570	6.01917200624	Earth slide
109.	37.24287263070	6.02311619344	Earth slide
110.	37.24591795550	6.02212767980	Rock slide
111.	37.24805346190	6.02458672498	Earth slide
112.	37.24841912230	6.01990077806	Earth slide
113.	37.25221431480	6.02132992798	Earth slide
114.	37.26196999660	6.01853716859	Transitional slide
115.	37.24835010250	6.05493876125	Transitional slide
116.	37.24433968570	6.05263073493	Earth slide
117.	37.24974833960	6.03825890579	Earth slide
118.	37.25149697240	6.04936233239	Earth slide
119.	37.29184837920	6.15730959652	Earth slide
120.	37.28040692630	6.17592473197	Earth slide
121.	37.30460015430	6.16942479191	Earth slide

122.	37.31414898550	6.16604478802	Earth slide
123.	37.30895066650	6.14493969524	Earth slide
124.	37.30762402080	6.16108656408	Earth slide
125.	37.31163437860	6.15526525806	Earth slide
126.	37.30032233590	6.13622456202	Earth slide
127.	37.31968982500	6.09697513885	Earth slide
128.	37.32452822900	6.09509165616	Rock slide
129.	37.25098661780	6.10373804403	Earth slide
130.	37.32443128370	6.12365048809	Earth slide
131.	37.20828900890	6.08450490323	Earth slide
132.	37.19758574120	6.08535738796	Rock slide
133.	37.20201898670	6.08469703647	Earth slide
134.	37.20380261440	6.08696838211	Earth slide
135.	37.20562306550	6.07409241001	Earth slide
136.	37.19862407320	6.07169256319	Earth slide
137.	37.20397750160	6.06702806802	Earth slide
138.	37.24343796180	6.12295792828	Transitional slide
139.	37.31080459460	6.13270599718	Earth slide
140.	37.24494749260	6.13024732433	Earth slide
141.	37.24812433980	6.12010750487	Earth slide
142.	37.24594382860	6.12063977627	Earth slide
143.	37.23090908410	6.01444659156	Earth slide
144.	37.22967784110	6.01868464498	Earth slide
145.	37.26020423220	6.02825967741	Debris slide
146.	37.26285349850	6.02682457482	Debris slide
147.	37.22620324830	6.07193339690	Earth slide
148.	37.25379196390	6.10702041617	Rock slide
149.	37.20858076070	6.09461119783	Earth slide
150.	37.23122065880	6.09925302396	Earth slide
151.	37.26192961140	6.15609058747	Earth slide
152.	37.20775097710	6.08076650157	Rock slide
153.	37.30636318880	6.13328548681	Earth slide
154.	37.28277261310	5.99352509935	Earth slide
155.	37.20513759680	6.07816071621	Earth slide
156.	37.19440708680	6.07900206024	Earth slide
157.	37.20973237750	6.09131758443	Earth slide
158.	37.26522306730	6.17347955513	Rock slide
159.	37.22725518370	6.01254273834	Earth slide
160.	37.22891968470	6.01038994773	Earth slide
161.	37.24903389170	6.06540664379	Earth slide
162.	37.23360427420	6.00167574551	Earth slide

163.	37.22523562590	6.00679186282	Earth slide
164.	37.23516245580	6.00338408449	Earth slide
165.	37.22651114650	6.00462415328	Earth slide
166.	37.23175658960	6.00703224917	Earth slide
167.	37.22891690250	6.00685499248	Rock slide
168.	37.22697674620	6.00102155944	Debris flow
169.	37.25321023840	5.98438313893	Earth slide
170.	37.25217127080	5.98662233167	Earth slide
171.	37.25136004750	5.98849580540	Rock slide
172.	37.24619273860	5.98836713736	Earth slide
173.	37.24552821950	5.98660735018	Earth slide
174.	37.24838699050	5.98715982592	Earth slide
175.	37.28073870530	5.99663526487	Earth slide
176.	37.28339376640	5.99748483810	Earth slide
177.	37.28567897010	5.99771581120	Transitional slide
178.	37.28791568530	5.99766979829	Earth slide
179.	37.28985567210	5.99695344370	Earth slide
180.	37.28359446660	5.98975827817	Earth slide
181.	37.28363206630	5.98327395887	Earth slide
182.	37.29438384360	6.17252422003	Debris slide
183.	37.29793491970	5.98733196295	Earth slide
184.	37.29653582620	5.98329457592	Earth slide
185.	37.25001460310	5.98984316203	Earth slide
186.	37.22489766440	6.02028546896	Earth slide
187.	37.22102275740	6.01978571226	Rock slide
188.	37.25557613090	6.06927433822	Earth slide
189.	37.25512804920	6.07110282242	Earth slide
190.	37.25636226700	6.07428223438	Earth slide
191.	37.25361234600	6.07642604916	Debris flow
192.	37.25571100400	6.07754349607	Earth slide
193.	37.25670879600	6.07806932458	Earth slide
194.	37.25861314310	6.07828631533	Transitional slide
195.	37.25888397380	6.08085761454	Earth slide
196.	37.26091780940	6.08358072971	Earth slide
197.	37.25429931110	6.12390015734	Earth slide
198.	37.25490347810	6.12582956435	Rock slide
199.	37.25883690040	6.11906491586	Rock slide
200.	37.25647364420	6.12011753348	Earth slide
201.	37.25361612080	6.12074117233	Earth slide
202.	37.25305002470	6.12919627878	Earth slide
203.	37.25375679250	6.12716428957	Earth slide

204.	37.22566867580	6.09127000188	Earth slide
205.	37.22544286390	6.08852362233	Earth slide
206.	37.22433791940	6.08539968058	Earth slide
207.	37.22637773930	6.08391347208	Earth slide
208.	37.22603247680	6.08213470103	Earth slide
209.	37.22154936530	6.07889047938	Earth slide
210.	37.22718818110	6.09408023799	Earth slide
211.	37.22188008250	6.09344446513	Earth slide
212.	37.22180587640	6.09499100004	Earth slide
213.	37.21871095430	6.09443319943	Earth slide
214.	37.21984687710	6.09056407919	Earth slide
215.	37.22318895530	6.06216457803	Earth slide
216.	37.22733564200	6.06058826865	Earth slide
217.	37.22556856440	6.05651574761	Earth slide
218.	37.23218386170	6.06166432663	Earth slide
219.	37.20610370510	6.10155267102	Earth slide
220.	37.20270978650	6.10217273183	Earth slide
221.	37.27348368560	6.14382878852	Earth slide
222.	37.27382166820	6.15266764318	Transitional slide
223.	37.27522894480	6.14014810133	Earth slide
224.	37.27088334330	6.13683810459	Earth slide
225.	37.25314273640	6.14852942663	Earth slide
226.	37.25296205870	6.14502634344	Earth slide
227.	37.25062988840	6.15113188693	Earth slide
228.	37.24830180920	6.15428692810	Rock slide
229.	37.24430403860	6.15736245949	Earth slide
230.	37.24277402500	6.15928584271	Earth slide
231.	37.24604931050	6.15567301249	Debris slide
232.	37.24796471990	6.15538947716	Earth slide
233.	37.23751694490	6.14490168233	Earth slide
234.	37.23917767220	6.14133656233	Earth slide
235.	37.23989150590	6.14329816198	Earth slide
236.	37.23760382000	6.14908412888	Earth slide
237.	37.23905667060	6.14709608722	Earth slide
238.	37.25287809300	6.15169966829	Transitional slide
239.	37.26097002140	6.15939294133	Earth slide
240.	37.25855246150	6.16292362781	Earth slide
241.	37.28819548120	6.13394597761	Earth slide
242.	37.29046614120	6.13757562308	Earth slide
243.	37.28086035070	6.14616732833	Earth slide
244.	37.28538516190	6.14341829671	Earth slide

245.	37.29020980640	6.14847357636	Earth slide
246.	37.19778189890	6.06791394523	Earth slide
247.	37.19213110750	6.06892123783	Earth slide
248.	37.19721487920	6.06366164060	Earth slide
249.	37.19774967590	6.05452509110	Earth slide
250.	37.21698408080	6.13132869159	Earth slide
251.	37.21749890320	6.12677655410	Earth slide
252.	37.21621895630	6.12124678217	Transitional slide
253.	37.22797075930	6.14450601659	Earth slide
254.	37.22605434120	6.14001088321	Earth slide
255.	37.22344455260	6.13661917336	Rock slide
256.	37.22204119840	6.13248637980	Earth slide
257.	37.22296621110	6.12880584377	Earth slide
258.	37.24354476220	6.13298719539	Transitional slide
259.	37.24296488220	6.15397382354	Earth slide
260.	37.24578646930	6.15032219164	Earth slide
261.	37.25029785890	6.14509897987	Earth slide
262.	37.24989039060	6.14222544116	Earth slide
263.	37.22863133390	6.12662463018	Earth slide
264.	37.23175258850	6.13922293818	Earth slide
265.	37.23105879300	6.13616728032	Earth slide
266.	37.23023159950	6.13222010621	Transitional slide
267.	37.23380842320	6.14191138868	Earth slide
268.	37.23348574170	6.14513987366	Earth slide
269.	37.25552176270	6.15560301522	Earth slide
270.	37.21476485560	6.09082597918	Earth slide
271.	37.21575267540	6.09523215511	Earth slide
272.	37.21273192580	6.09439301781	Rock slide
273.	37.20658883620	6.09498121952	Earth slide
274.	37.22593240180	6.02322514447	Earth slide
275.	37.22888375670	6.02107254593	Earth slide
276.	37.22830691750	6.02503322718	Earth slide
277.	37.22238452150	6.02325504904	Rock slide
278.	37.22310115760	6.01180293078	Earth slide
279.	37.22486956900	6.00875509832	Earth slide
280.	37.22374200630	6.00958628427	Earth slide
281.	37.21109726790	6.06996730752	Transitional slide
282.	37.20666949520	6.07088845138	Earth slide
283.	37.20337214170	6.07180212763	Earth slide
284.	37.22165796280	6.08234355953	Earth slide
285.	37.22436029910	6.07764917705	Earth slide

286.	37.27108179990	6.17400554163	Earth slide
287.	37.25962195010	6.15554135797	Earth slide
288.	37.25880077490	6.15922222241	Earth slide
289.	37.25528081030	6.16410540865	Earth slide
290.	37.25691137500	6.16184804855	Earth slide
291.	37.23209937030	6.06762290716	Transitional slide
292.	37.25831899550	6.14945271418	Earth slide
293.	37.25681878050	6.14384197225	Earth slide
294.	37.25611014440	6.13894234518	Rock slide
295.	37.23690067080	6.13696319102	Earth slide
296.	37.24038289360	6.12611147586	Earth slide
297.	37.23817760990	6.13043443000	Debris slide
298.	37.23462446630	6.13169876416	Earth slide
299.	37.20605056870	6.09103792269	Earth slide
300.	37.20889673300	6.08885423789	Transitional slide
301.	37.21147348700	6.08708432081	Earth slide
302.	37.20351315300	6.09228663996	Rock slide

Appendix 4: Photographs showing landslide-affected areas (source from dame tekalegn's thesis)

Debris slide landslide type

Earth flow type of landslide

Rock slide type of slide

Appendix 5: Spatial relationship between conditioning factors and landslide using the information value method

Parameter	Class	ncpix	% ncpix	nslpix	nslpix %	con prob	prior prob	cp/pp	Iv
Aspect	Flat	50775	15.52619	37	12.25166	0.000729	0.000923	0.789096	-0.10287
	North	20596	6.297932	18	5.960265	0.000874	0.000923	0.946384	-0.02393
	Northeast	23033	7.043128	6	1.986755	0.00026	0.000923	0.282084	-0.54962
	East	29585	9.046626	18	5.960265	0.000608	0.000923	0.658838	-0.18122
	Southeast	30275	9.257617	32	10.59603	0.001057	0.000923	1.144574	0.058644
	South	29735	9.092494	28	9.271523	0.000942	0.000923	1.01969	0.008468
	Southwest	43547	13.31599	58	19.2053	0.001332	0.000923	1.442274	0.159048
	West	52170	15.95276	65	21.52318	0.001246	0.000923	1.349182	0.130071
	Northwest	47312	14.46726	40	13.24503	0.000845	0.000923	0.915518	-0.03833
Curvature	Concave	88879	27.01489	90	29.80132	0.001013	0.000918	1.103144	0.042632
	Flat	153209	46.56809	112	37.08609	0.000731	0.000918	0.796384	-0.09888
	Convex	86912	26.41702	100	33.11258	0.001151	0.000918	1.253456	0.098109
DTL	0-380	133368	40.52137	79	26.15894	0.000592	0.000918	0.645559	-0.19006
	380-834	97651	29.66943	87	28.80795	0.000891	0.000918	0.970964	-0.0128
	834-1400	55725	16.931	53	17.54967	0.000951	0.000918	1.036541	0.015586
	1400-2300	29167	8.861848	48	15.89404	0.001646	0.000918	1.793536	0.25371
	>2300	13219	4.016346	35	11.5894	0.002648	0.000918	2.885559	0.46023

DTS	0-240	101498	30.83827	82	27.15232	0.000808	0.000918	0.880475	-0.05528
	240-510	88029	26.74597	111	36.75497	0.001261	0.000918	1.374225	0.138058
	520-810	72361	21.98554	75	24.83444	0.001036	0.000918	1.129581	0.052917
	820-1200	47723	14.49974	27	8.940397	0.000566	0.000918	0.61659	-0.21
	>1300	19519	5.930483	7	2.317881	0.000359	0.000918	0.390842	-0.408
Elevation	1600-1900	18822	5.720973	47	15.56291	0.002497	0.000918	2.720327	0.434621
	1900-2200	21998	6.686322	71	23.50993	0.003228	0.000918	3.516123	0.546064
	2200-2300	25127	7.637386	64	21.19205	0.002547	0.000918	2.774778	0.443228
	2300-2500	39111	11.88784	46	15.23179	0.001176	0.000918	1.281291	0.107648
	2500-2700	51862	15.76353	31	10.2649	0.000598	0.000918	0.651181	-0.1863
	2700-2800	50580	15.37386	13	4.304636	0.000257	0.000918	0.279997	-0.55285
	2800-3000	43097	13.09939	15	4.966887	0.000348	0.000918	0.379169	-0.42117
	3000-3100	49777	15.12979	4	1.324503	8.04E-05	0.000918	0.087543	-1.05778
	>3100	28626	8.700912	11	3.642384	0.000384	0.000918	0.418621	-0.37818
Lithology	Alkali basalt	8408	3.136167	89	29.4702	0.010585	0.001126	9.396885	0.972984
	Muscovite-biotite granite	6065	2.262232	13	4.304636	0.002143	0.001126	1.902826	0.279399
	Migmatite and migmatized biotite paragneiss	35737	13.32983	12	3.97351	0.000336	0.001126	0.298092	-0.52565
	Rhyolite lava	22281	8.310767	62	20.5298	0.002783	0.001126	2.470266	0.392744

	Aplite and pegmatite	68	0.025364	13	4.304636	0.191176	0.001126	169.7153	2.229721
	Trachyte to trachybasalt	88826	33.13191	14	4.635762	0.000158	0.001126	0.139918	-0.85413
	Alkali basalt	38535	14.37348	19	6.291391	0.000493	0.001126	0.437708	-0.35882
	Colluvial sediments	578	0.215593	77	25.49669	0.133218	0.001126	118.2632	2.07285
	Amphibolite	389	0.145096	1	0.331126	0.002571	0.001126	2.282112	0.358337
	Fluvial sediments	1480	0.552037	1	0.331126	0.000676	0.001126	0.599825	-0.22198
	Rhyolitic ignimbrite	65731	24.51753	1	0.331126	1.52E-05	0.001126	0.013506	-1.86948
LULC	Dense forest	39063	11.86802	48	15.89404	0.001229	0.000918	1.339232	0.126856
	Agricultural land	217106	65.96059	102	33.77483	0.00047	0.000918	0.512046	-0.29069
	Settlement	2995	0.909933	0	0	0	0.000918	0	0
	Range land	69981	21.26145	152	50.33113	0.002172	0.000918	2.367248	0.374244
Slope	0-10	68204	20.85571	18	5.960265	0.000264	0.000923	0.285786	-0.54396
	10--17	105351	32.21467	45	14.90066	0.000427	0.000923	0.462543	-0.33485
	17-24	82939	25.36144	91	30.13245	0.001097	0.000923	1.188121	0.074861
	24-32	51535	15.75859	92	30.46358	0.001785	0.000923	1.933141	0.286264
	>32	18999	5.809594	56	18.54305	0.002948	0.000923	3.191797	0.504035
Soil	Nitisols	168706	51.27312	144	47.68212	0.000854	0.000918	0.929963	-0.03153

	Alisols	93823	28.51468	45	14.90066	0.00048	0.000918	0.522561	-0.28186
	Regosols	6624	2.013166	101	33.44371	0.015248	0.000918	16.6125	1.220435
	Cambisols	46907	14.25597	7	2.317881	0.000149	0.000918	0.16259	-0.78891
	Luvisols	11464	3.484138	5	1.655629	0.000436	0.000918	0.47519	-0.32313
	Fluvisols	1510	0.458919	0	0	0	0.000918	0	0
Rainfall	1100-1200	108767	33.04923	37	12.25166	0.00034	0.000918	0.370709	-0.43097
	1200-1300	69195	21.02514	61	20.19868	0.000882	0.000918	0.960692	-0.01742
	1300-1400	71086	21.59973	55	18.21192	0.000774	0.000918	0.843155	-0.07409
	1400-1500	61106	18.56727	40	13.24503	0.000655	0.000918	0.713354	-0.1467
	1500-1600	11435	3.474564	34	11.25828	0.002973	0.000918	3.240198	0.510572
	1600-1800	5134	1.559984	39	12.91391	0.007596	0.000918	8.278232	0.917938
	> 1800	2383	0.724083	36	11.92053	0.015107	0.000918	16.46294	1.216507